学位論文

MEG study on the prediction of motion trajectory

(脳磁図を用いた運動軌道予測に関する研究)

東京大学　大学院新領域創成科学研究科

複雑理工学専攻

斉　亮

Contents

Abstract

Motion is one of the most important ways for humans to communicate with environments, that is, with other people and objects. However, there are patients have a clear consciousness but are not able to move their body because of injuries to their peripheral motor nerves or voluntary muscles. In these cases, Brain Computer Interface (BCI) can bypass the injured parts, directly link brain activity to artificial devices, and enable paralyzed patients to move as healthy people.

In recent years, many researchers have focused on BCI with invasive measurements such as implanted microelectrode arrays or electrocorticography (ECoG). These methods directly record brain activities from the brain surface, thus they are accurate but not safe and reliable. On the other hand, non-invasive methods such as electroencephalography (EEG) and magnetoencephalography (MEG) can record brain activity from outside the head and thus are safer and more convenient. However, non-invasive methods are easily contaminated by environmental noise and thus making it difficult to extract motion patterns. Therefore, current non-invasive studies can not provide an efficient prediction and the motion related features in continuous motion are yet to be revealed.

The two most important problems in motion trajectory prediction are noise reduction and feature selection because the prediction will not be efficient and robust if the features used have too much noise. Therefore in this thesis, both noise reduction method and feature selection strategy are discussed to perform an efficient continuous motion prediction.

To perform accurate prediction of motion trajectory from single trials data, a new effective noise reduction method with almost no brain activity loss is introduced. Firstly, the original spatiotemporal signal space separation (tSSS) method developed by Dr. Samu Taulu in Helsinki University of Technology is applied to our system and the signal loss problem in tSSS method is discussed. Then an innovative improvement on tSSS method, a compensation process which suppresses noise and preserves brain signals simultaneously, is introduced. With the compensation process, our method shows very good noise reduction performance for both simulation of and the application to real MEG data. It should be noted that our method can be applied to all kinds of MEG systems, whereas the original method can be applied only to the MEG system with both gradiometers and magnetometers.

A study on 1-D continuous motion using a tool bar is then presented and compensation tSSS method is applied to the recorded MEG data to reduce noise. It was found out that MEG signal spectrums of certain frequency bands closely resemble motion parameters and thus these spectrums are used to predict motion trajectory. Thus, in this study, the correlations averaged across all subjects between

brain activity spectrum and motion parameters are investigated, and several motion-related features that have relatively high correlation values are extracted out. Moreover, different channel selection models and time-windows are adopted, and proper features that enable us to improve predictions are determined by multivariate linear regression prediction. With spectral, spatial, and temporal feature selection, an effective motion trajectory prediction with relatively high correlation coefficients (average value across all subjects is 0.59, $p < 0.001$) is achieved on the 5 epoch averaged data preprocessed by compensation tSSS method.

To further improve the prediction performance and provide an acceptable single trial motion prediction, differences in brain mechanism between subjects are considered and a more robust frequency feature selection model is proposed. In this study, motion related frequency features ranged from μ (8-16Hz) and β rhythm (18-24Hz) to low frequency δ rhythm (5-7Hz) and some part of high frequency γ bands (30-50Hz, 60-70Hz) are determined for each subject. By combining these selected subject-dependent frequency features, the prediction performance is further improved and this improvement is significant for most subjects. From the prediction performance of all subjects, it is concluded that using the correlation based feature selection method, single-trial MEG data could also predict continuous motion well ($R = 0.46$) with few features (less than 100).

Moreover, two other tasks are performed and the robustness of our feature selection method on different motion cycles and external devices is proven. In task 1, similar motion using a different device (trackball) is performed and the prediction results confirm that our feature selection method worked equally well on different devices which indicates a robustness in different devices. In task 2, a different motion cycle without visual guidance is considered, and the efficiency of our feature selection method on different motion cycle, which showed a robustness in different motion, is confirmed. As there is no visual guidance, the selected features are verified to be from motion brain activities. From further contour map and source estimation studies, it is also confirmed that the sources of frequency features selected by our method is really located in the contralateral motor cortex and sensorimotor cortex, and thus motion related features.

Our study reveals detailed characteristics of motion related activities which are consistent with ECoG and EEG studies. It also provides a guidance to select features and achieves a successful single trial motion trajectory prediction. The high quality prediction demonstrates that non-invasive measurement can predict motion comparably well as invasive measurement such as ECoG. Also, the prediction of continuous motion trajectory in our study provides a possibility of controlling external prosthetic devices.

Chapter 1 Introduction

Chapter 1 provides the purpose of our thesis, and briefly reviews each chapter. Then we introduce the background of motor system and its pathway, as well as that of brain computer interface (BCI), which is a direct communication pathway between a brain and an external device. Current BCI researches and techniques are reviewed, and existing problems are discussed. Moreover, we introduce magnetoencephalography (MEG), which is a non-invasive measurement employed in the current study, noise conditions and data analysis method adopted in our research.

1.1 Brief review

Brain computer interface (BCI) is a technology to directly connect brain and an external device. BCIs can be used for assisting paralyzed patient achieving certain motion, remote surgery or controlling robotic arms. However, current BCI studies mainly use invasive recording method or focus on discrete motion, which are not suitable for BCI real application. In our study, we discuss continuous motion using non-invasive recording method and propose a possible solution for future BCI application.

The main purpose of this thesis is to develop a BCI that accurately predicts motion trajectory from brain signals non-invasively recorded with MEG. Specifically, we provide an efficient feature selection method that enables real-time prediction of motion trajectory. For an accurate prediction of motion trajectory from single-trial MEG data, extracting brain signal from environmental noise is vital. Therefore in chapter 2, we propose a new noise reduction method called compensation tSSS, which cope with the signal loss problem in a previous method (Taulu et al., 2006). We prove the effectiveness of our method from simulation data. In chapter 3, we present an MEG experiment to record brain activity when subjects moved their arm following a cyclic motion of visual target, and investigate temporal, spectral and spatial characteristics of motion related activities. We then talk about motion related feature characteristics and present an effective motion prediction. By using this feature selection protocol, we find that motion related μ-rhythm is the most important feature to achieve a good prediction. In chapter 4, we further consider a possibility for a subject-dependent frequency band selection, which includes δ-wave, β-wave, γ-band in addition to μ-rhythm. This is proven to be efficient in the prediction from single trial data. This is a great progress in non-invasive motion prediction. Finally in chapter 5, we discuss the features used for the motion prediction in sensor domain as well as in source domain. Both analyses provide the evidence that selected features are motion-related activities originating from motor cortex, not artifacts such as visual response. From these results, we propose that our subject-dependent feature selection method, in combination with noise-reduction method called compensation tSSS, is suitable for non-invasive BCI studies.

In the following, we first introduce the background of our study which includes motor system, BCI, MEG recording and data analysis.

1.2 Motor System

Motion is one of the most important ways for human to communicate with environments such as other people or objects. During the motion procedure, many different parts of our body need to collaborate together and take charge in the

generation and control of voluntary and reflex movements. These parts comprise motor system. Motor system is a hierarchy and can be simply divided into low level, mediate level subcortical motor structures and high level motor cortex. As is shown in Figure 1 - 1, motor control is a complicated and distributed process. Low level of motor system includes muscles and spinal cords, and it mainly takes charge in transferring motor commands and translating motor command into motion. Muscle is the executor who executes all forms of movement by extension or contraction. Mediate level, or subcortical motor structures, contains cerebellum, basal ganglia and brainstem. These parts mainly combine and translate high level motor commands into detailed low level motor command. High level, or motor cortex, is the most important part which can generate motion commands and regulate low level structures directly or indirectly.

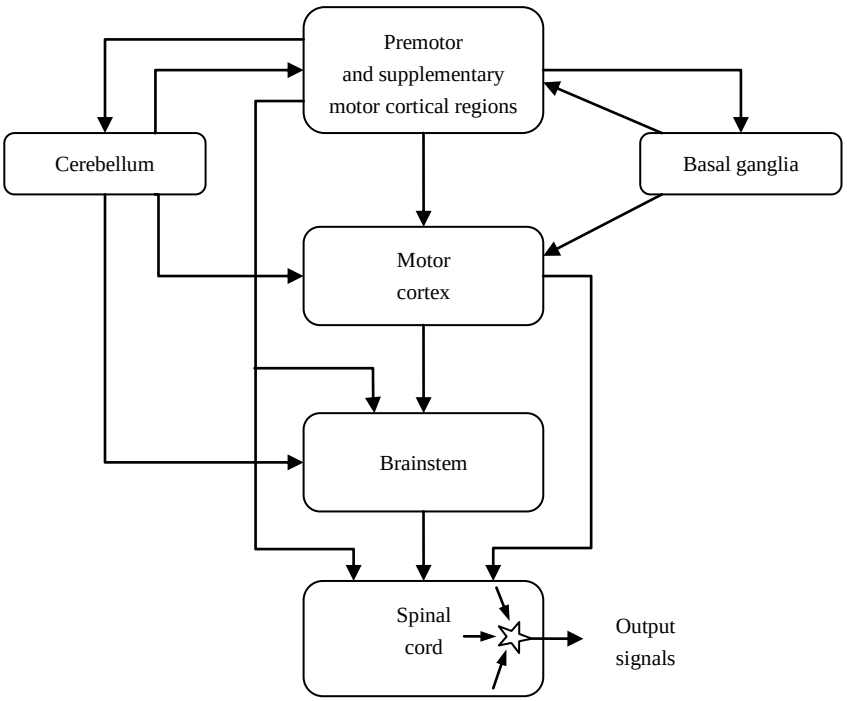

Figure 1 - 1 Schematic diagram of the major components of the vertebrate motor systems (Gazzaniga et al., 2002).

Arrows indicate the main neural connections between regions.

The motor cortex is an area occupies part of the frontal lobe and parietal lobe which is involved of the planning, control, and execution of voluntary motor functions. Motor cortex is divided into several regions by Brodmann and Matelli (Brodmann, 1909; Matelli et al., 1985, 1991). These regions are mainly the primary motor cortex

(MI) and secondary motor cortices, including posterior parietal cortex, premotor cortex (PMC) and supplementary motor area (SMA). Primary motor cortex is anterior to the central sulcus, the anatomical division separating the frontal and parietal cortex. Primary motor cortex is responsible for generating the neural impulses controlling execution of movement and is the most prominent part in motor cortex. Different body parts are controlled by distinct areas of primary motor cortex, lined up along the central sulcus, as is shown in Figure 1 - 2. Posterior parietal cortex, premotor cortex and supplementary motor area are also responsible for some motion related functions and it is confirmed that these parts worked together and form a complex brain cortical networks (Luppino et al., 1990; He et al., 1993, 1995; Picard and Strick, 1996; Ikeda et al., 1999; Geyer et al., 2000; Picard and Strick, 2001; Matsumoto et al., 2003; Paxinos and Mai, 2004; Matsumoto et al., 2007). However, motor system is a distributed system and other parts illustrated in Figure 1 - 3 also take part in motion control procedure.

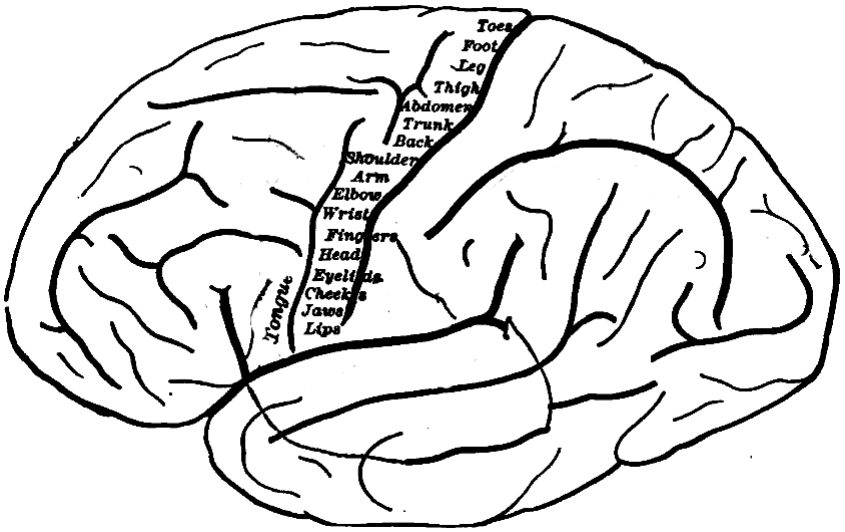

Figure 1 - 2 Human motor cortex topography (Ranson, 1920).

Different body parts are represented by distinct areas, lined up along the central sulcus.

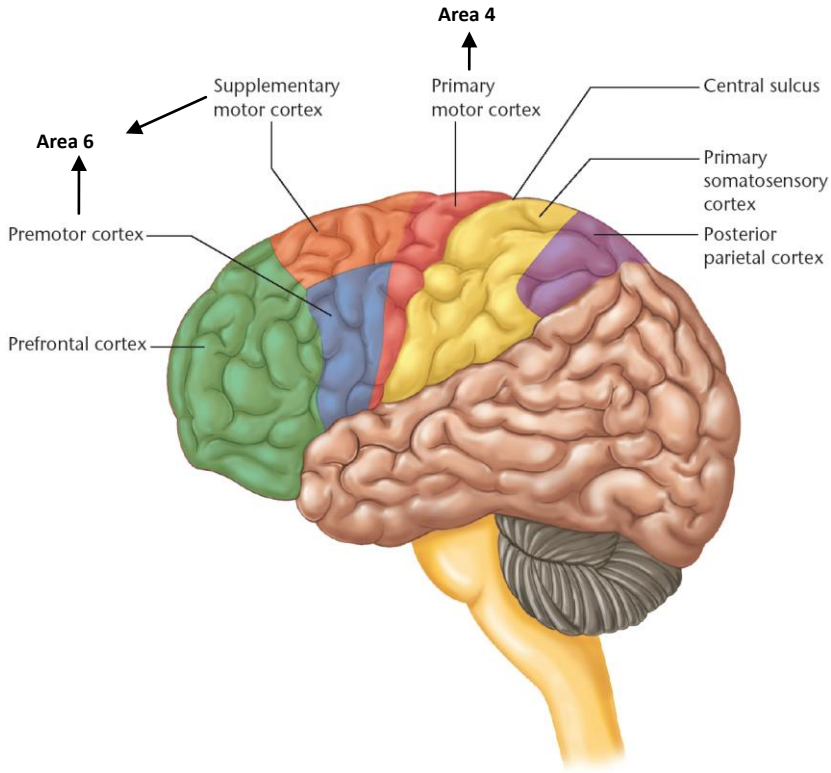

Figure 1 - 3 The motor related areas of the cerebral cortex.

Area 4 is the primary motor cortex. Area 6 on the medial surface is referred to as supplementary area (SMA) and on the lateral surface as the premotor cortex (PMC). Prefrontal cortex includes the frontal eye fields. Lesions in many posterior areas also can produce severe problems in coordination.

1.3 Brain computer interface (BCI)

1.3.1 History of BCI

In motor system, the motor cortex is obviously the essential part while other two are important as well. There are cases that patients who have clear conscious are not able to move their body, because of the injuries of their peripheral motor nerves or the muscles for execution. In these cases, BCI is a possible solution.

A brain-computer-interface is a communication system in which the brain does not use nerves to transmit orders to the body or to the world outside. For paralyzed patients, it can replace the injured motor pathway and provide the patients with an alternative way for acting on the world, such as controlling a wheel chair to move. While for healthy people, BCI is an artificial extension of the brain in order to control computer cursor, cars or even the artificial robot arm.

The first study on BCIs was done in the 1970s at the University of California Los

Angeles (UCLA) under a grant from the National Science Foundation, followed by a contract from DARPA (Vidal, 1973, 1977). And since then, BCI technology has developed exponentially. Early BCI researches briefly use invasive techniques such as implanted electrodes which is highly risky. Thus early researches mainly focus on animals such as rats or monkeys (Fetz, 1969; Schmidt et al., 1978). These researches reported that animals could perform simple tasks using only mind, such as moving a cursor on a monitor, or controlling a robotic arm. However, very few researches results on human are also reported during this period. In the 1980s, Apostolos Georgopoulos at Johns Hopkins University discovered a key mathematical correlation between the electrical responses of individual motor-cortex neurons in rhesus macaque monkeys and the direction that they moved their arms (Georgopoulos et al., 1989). Since the mid-1990s, several groups have been able to capture complex brain motor cortex signals using recordings from groups of neurons and use these to control external devices, and BCI comes to a rapid developing period (Serruya and Donoghue; Stanley et al., 1999; Wessberg et al., 2000; Serruya et al., 2002; Taylor et al., 2002; Carmena et al., 2003; Musallam et al., 2004; Lebedev et al., 2005; Santucci et al., 2005; Lebedev and Nicolelis, 2006; Huber et al., 2008).

1.3.2 Procedures of BCI

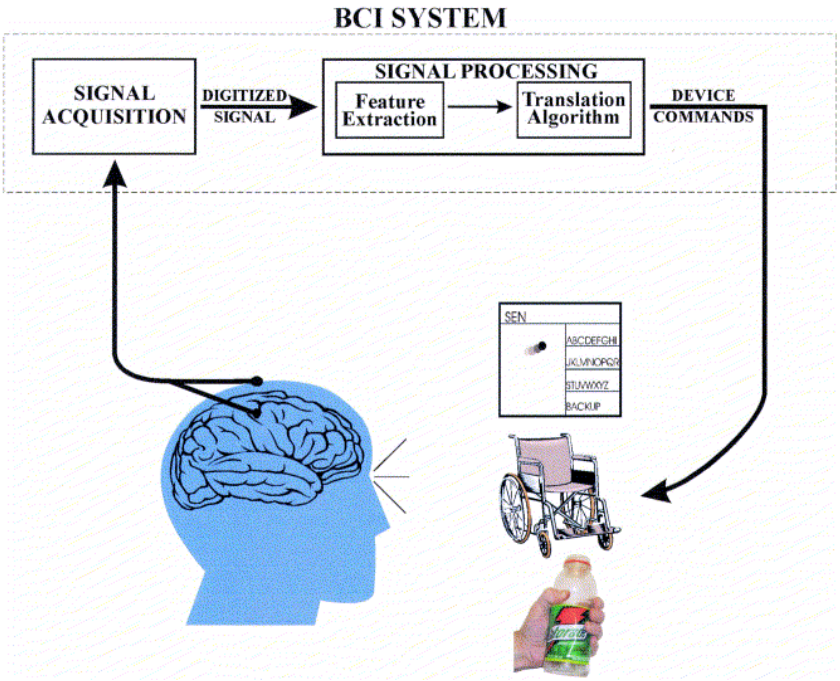

Figure 1 - 4 Schematic illustration of the 4 major BCI components: signal acquisition, signal processing, output device, and operating protocol (Wolpaw et al., 2002).

A common BCI procedure includes four major components: signal acquisition, signal processing, output device, and operating protocol. Signal acquisition, or recording technique, is the basis of all BCI system. From the technique which is adopted in brain activity recording, BCIs fall into two categories: invasive and non-invasive ones (Schwartz et al., 2006). Invasive BCIs record the brain activity directly from the grey matter of the brain or inside the skull. These techniques are implanted electrode or electrode array (Kennedy and Bakay, 1998; Hochberg et al., 2006) and Electrocorticography (ECoG) (Pistohl et al., 2008). As they rest in the grey matter or attach to brain cortex, invasive devices produce the highest quality signals of BCI devices. However, they are not stable and the signal will become weaker or even lost as the body reacts to a foreign object in the brain. On the other hand, non-invasive BCIs record the brain activity from outside of the skull. These techniques are Electroencephalography (EEG) (Taheri et al., 1994; Bogdan et al., 2003), Magnetoencephalography (MEG) and functional magnetic resonance imaging (fMRI) (Sitaram et al., 2007; Miyawaki et al., 2008). Non-invasive devices are safe and easy to wear, but they produce poor signal resolution because the skull disperses and blurs the electromagnetic waves created by the neurons. This makes it difficult to

determine the specific area of the brain which creates them or the actions of individual neurons. Therefore, motion related features are not completely revealed in current non-invasive studies and the predictions are not as accurate and believable as invasive studies. In our study, we concentrate on non-invasive MEG recording and try to extract useful features.

Signal processing includes mainly feature extraction and translation algorithm. By using these methods, motion related features of interest are extracted and then translated into motion commands for the output device. An ideal BCI would respond to initial characteristics of user's brain waveform features, adjust to its changes, and update as the user adapted to the system. Thus it is mainly about the algorithm and models used in the BCI prediction. Moreover, for non-invasive studies, data preprocessing, especially noise reduction method is very important, because high signal to noise ratio (SNR) could make the following process much easier. These parts are discussed in section 1.4.

Output device implements the messages or commands conveyed by the translation algorithm. Based on the type of motion, BCI is divided into two categories: continuous and discrete BCI. In discrete BCI, only very limited motion commands are produced and the motion is discrete, such as moving left, right, forward and backward in a wheel chair control. The most common discrete BCI output device is a computer monitor on which user could input alphabets simply by thinking, or a wheel chair controlled by paralyzed patients. Although this kind of BCI devices provides some convenient ways to interact with environmental surroundings, it is very limited and not so natural because it is very different to most motions we performed in our daily life. For example in a lifting process, our arm gradually and slowly moves from the starting position to the end position, but not unexpectedly disappears at the starting position and suddenly reappears at the ending position. Therefore, continuous BCI providing continuous motion commands can achieve more complicated motion control such as computer cursor control, robotic arms and mobile robots.

Operating protocol reflects how the user and the BCI interact. Signal acquisition and output device are hardware; signal processing is software, whereas the operating protocol is spirit of the design of BCI. Considering operating protocol, BCIs fall into two categories: dependent and independent. A dependent BCI needs an at least partially intact peripheral system. A dependent BCI could flash letters on a screen. A user could then choose the letters by gazing at them, while brain activity is recorded above the particular part of the brain that is active when gazing. From certain brain reaction, dependent BCI could recognize and send motion commands. An independent BCI, in contrary, works with signals that are totally independent of external cues. The flashing letters in the former example would be chosen not by the user brain activity of gazing but by "thinking". Although dependent BCIs are easier to make, they are not convenient and some severely paralyzed patients could not use them. In our study, we

focus on the independent BCI. Although we use visual cues, it is not for arouse cue-depend patterns and the successful prediction in task without visual cues also confirms this fact.

1.3.3 Current status of BCI

Current BCI researches are on discrete or continuous motions with invasive or non-invasive signal acquisition methods. In invasive researches, both discrete and continuous BCI are well studied, as the invasive techniques could provide clear signal with high spatial and temporal resolutions. Motion-related cosine tuning model is well studied and therefore perfect predictions are easily achieved. On the other hand, non-invasive researches are mainly focused on discrete motion and only very few studies discussed continuous motion prediction. This is because the SNR and the spatial resolution are rather poor in non-invasive measurements. Although non-invasive measurements have large quantities of data, the useful information is limited and difficult to be extracted, thus the prediction is inefficient.

Table 1 - 1 listed current representative studies on continuous motion. The first three studies using invasive methods show relatively high prediction performance with fewer feature number than non-invasive cases (Georgopoulos et al., 2005; Bradberry et al., 2009; Bradberry et al., 2010; Toda et al., 2011). In non-invasive studies, two studies provide high prediction performance (Georgopoulos et al., 2005; Toda et al., 2011) but use an extremely large feature number. Considering the training procedure in prediction, the large feature number will lead to a geometric progression of calculation cost, which includes calculation time and computer hardware requirements. What is more important, the large feature number in prediction always causes overfitting problem. With too many features, not only the motion information, but also noises and vibrations during motion are considered and precisely described by the prediction model. Thus it is highly possible that the model under this condition will not work well in other conditions. Considering this fact, selecting efficient features is important. In Schalk's ECoG research, they added a frequency selection and achieved a relatively high prediction performance with about only 10 features. Even in invasive researches, this feature number is an amazingly small one. This is because of its effective feature selection method which considers features in all temporal, spatial and spectral aspects. In non-invasive MEG studies, this feature selection method is expected to provide similar high prediction performance with small feature number and this is testified in this thesis.

Table 1 - 1 Representative studies on continuous motion

* Prediction performance (*r*) is the correlation between actual and predicted motion positions.

	Neural data	**Task**	**Feature selection**	**Feature number**	**Average *r* ***
Wessberg et al.,2000	Microelectrode array	1D; Fetching	Time	Less than 100	0.66
Wessberg et al.,2000	Microelectrode array	3D; Fetching	Time	Less than 100	0.53
Schalk et al., 2007	ECoG	2D; Drawing circle	Frequency, Channel, Time	About 10	0.5
Bradberry et al.,2009	MEG	2D; Center-out	Channel, Time	1240	0.4
Georgopoulos et al.,2005	MEG	2D; Darwing Pentagon	Time	4960	0.7
Bradberry et al.,2010	EEG	3D; Center-out	Channel, Time	340	0.29
Toda et al., 2011	MEG + fMRI	2D; Center-out	Source, Time	16500	0.77

1.4 Magnetoencephalography (MEG) recording

As all recordings in our experiment are done using magnetoencephalography (MEG), the characteristics of brain magnetic fields and recording method is introduced in this section.

Magnetic field of brain activity is induced by synchronized neural currents. To generate a MEG signal that is detectable, approximately 50,000 active neurons must keep their synchronous and spatially parallel activity for a few milliseconds (Okada, 1983). In macro scale, these neuronal currents with similar orientations can be thought as electric dipoles or electric currents. According to Maxwell's equations, any electrical current will produce an orthogonally oriented magnetic field, as is shown in Figure 1 - 5. The brain magnetic field which is about several tens or several hundreds femtotesla (fT) is considerably smaller than the ambient magnetic noise in an urban environment, which is at the level of 10^8 fT or 10 μT. Thus the essential problem of MEG measurement is the weakness of the signal relative to the sensitivity of the detectors, and to the environmental noise.

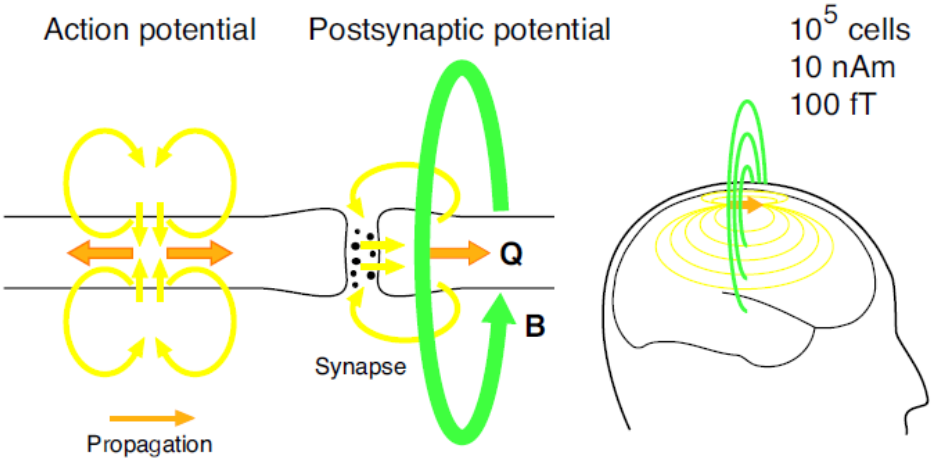

Figure 1 - 5 Schematic illustration of idealized magnetic field generated by postsynaptic current.

The current is represented as a dipole moment with strength typically on the order of 10 nAm. This generates a magnetic field of about 100 fT at the distance of the MEG sensors (Taulu, 2008).

MEG signals were first measured in 1968 by David Cohen who is a physicist in University of Illinois, using a copper induction coil as the detector (Cohen, 1968). To reduce the magnetic background noise, the measurements is made in a magnetically shielded room. The coil detector is barely sensitive enough, resulting in poor, noisy MEG measurements that are difficult to use. Later, Cohen built a better shielded room at MIT, and used one of the first superconducting quantum interference device (SQUID) detectors, which is developed by James E. Zimmerman (Zimmerma.Je et al., 1970), to again measure MEG signals (Cohen, 1972). This time the signals are almost as clear as those of EEG. This stimulates the interest of physicists who had been looking for uses of SQUIDs. Subsequently, various types of spontaneous and evoked MEGs began to be measured.

At first, single SQUID detector is used to measure the magnetic field at a number of points around the subject's head. In the 1980s, MEG manufacturers begin to arrange multiple sensors into arrays to cover a larger area of the head. Nowadays, MEG arrays are set in helmet-shaped dewar that typically contain several hundreds of sensors, covering most of the head. Currently, we use MEG system containing 440 SQUID gradiometer sensors, which is the most advanced MEG system in the world. In this way, MEGs of a subject or patient can be accumulated rapidly and efficiently.

Nowadays, most MEG systems adopt SQUID as the detector because of SQUID's

sensitivity. SQUIDs are sensitive enough to measure fields as low as 5 aT (5×10^{-18} T) within a few days of averaged measurements with a noise levels of 3 fT $Hz^{-½}$ (Drung et al., 2007). There are two main types of SQUID considering the number of weak links (Jesephon junction) in the SQUID ring: direct current (DC) and radio frequency (RF), as is shown in Figure 1 - 6. DC SQUIDs work with two Josephson junction which is more stable and sensitive, while RF SQUIDs can work with only one Josephson junction, which might make them cheaper to produce, but are less sensitive. Considering the stableness and sensitivity of SQUID, most MEG systems are DC SQUID type.

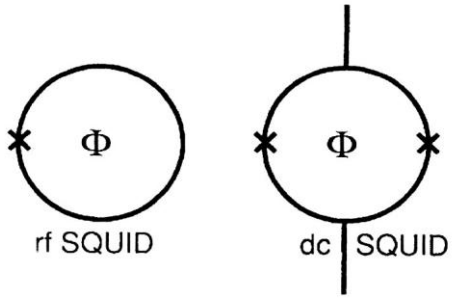

Figure 1 - 6 Schematic illustration of an rf and dc SQUID (Hamalainen et al., 1993).

The Josephson junctions are indicated by crosses. The magnetic flux Φ threads the superconducting loop of the SQUID, changing the impedance around (rf SQUID) or across (dc SQUID) the loop.

As is mentioned, the environmental noises such as terrestrial magnetism or ones generated by electric devices, vehicles or elevator in real world are much higher than brain magnetic fields. Therefore, we have to adopt several techniques to suppress noises. One way is to use gradiometer. To minimize the outer noises, the coil which can measure the spatial gradient of magnetic fields is designed. This coil is one-order gradiometer and is usually called gradiometer. Gradiometer is categorized in to axial type and planer type, as is shown in Figure 1 - 7. Axial gradiometer consists of two magnetometers placed in series and the result coming from the device is the difference in magnetic flux at that point in space ($\partial B_z/\partial z$), while planar gradiometer consists of two magnetometers placed next to each other and the result coming from the device is the difference in flux between the two loops ($\partial B_x/\partial z$ or $\partial B_y/\partial z$). Sometimes we talked about vector gradiometer ($\partial B_x/\partial z$, $\partial B_y/\partial z$ and $\partial B_z/\partial z$), which consists of two planar and one axial gradiometer located at the same position and orthogonal to

each other.

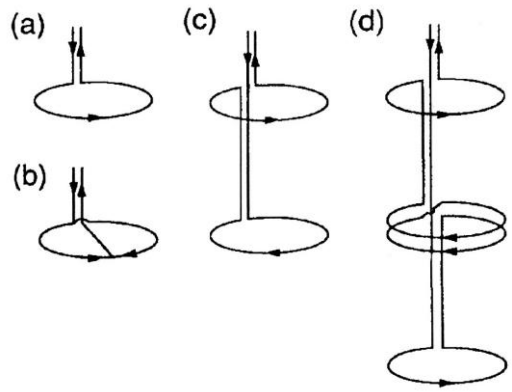

Figure 1 - 7 Various types of flux transformers (Hamalainen et al., 1993).
(a) Magnetometer; (b) (first-order parallel) planer gradiometer; (c) (first-order symmetric series) axial gradiometer; (d) second-order axial gradiometer.

Another noise suppression method is using magnetically shielded room (MSR). A MSR consists of several layers which is made of a pure aluminium layer, plus a high permeability ferromagnetic layer, similar in composition to molybdenum permalloy. This helps eliminate radio frequency radiation and magnetic fields at frequencies greater than 1 Hz.

In our whole-head 440-channel MEG system (MEG version: PQ2440R, Yokogawa Electric Co., Tokyo, Japan), both MSR and gradiometer techniques are used and thus data with relatively high SNR can be easily obtained.

1.5 Data analysis in MEG

1.5.1 Noise reduction

In the former section, noise suppression methods using gradiometers and magnetically shielded room are discussed. These two kinds of method are based on hardware and can to some extent degrade the effect of environmental noises. However, in real application, only by using these methods is not enough to perfectly protect MEG signals from outer noises, therefore further software noise reduction methods are necessary.

Many noise reduction methods have been applied on MEG data (de Cheveigné and Simon, 2007). Among them, some of the methods employ the reference sensors that measure environmental fields (Adachi et al., 2001; Vrba and Robinson, 2001;

Volegov et al., 2004; Ahmar and Simon, 2005). As reference sensors are distinct to brain sources, only noises are recorded and noise effect could be rejected by reconstructing noise sources. However a larger number of reference sensors are necessary, therefore it is not suitable for some MEG systems without reference sensors. Spectral filter focuses on environmental noise which is typically dominated by slowly varying magnetic fields from elevators, vehicles, etc., and by power line components at 50 Hz or 60 Hz and multiples. This method is simple and effective, therefore is widely adopted in MEG studies. Another category is spatial filtering in which linear combinations of sensor signals are formed to suppress noise and/or enhance brain activity. Examples are the Laplacian (Kayser and Tenke, 2006), Principal Component Analysis (PCA) (Ahissar et al., 2001; Spencer et al., 2001; Kayser and Tenke, 2003, 2006), Independent Component Analysis (ICA) (Makeig et al., 1996; Vigário et al., 1998; Barbati et al., 2004), Signal Space Projection (SSP) (Tesche et al., 1995; Uusitalo and Ilmoniemi, 1997), Signal Space Separation (SSS) (Taulu and Kajola, 2005; Taulu et al., 2005), Spatiotemporal Signal Space Separation (tSSS), beamforming (Sekihara et al., 2001; Sekihara et al., 2006; Taulu and Simola, 2006) and other linear techniques (Parra et al., 2005).

1.5.2 Feature extraction

Motion related features contain information of motion, therefore motion related feature extraction is essential for the efficiency of motion prediction. Before prediction, most researches perform different kinds of feature selections, ranging from spatial selection, time-window selection as well as frequency feature selection. In invasive studies, spatial selection is done by directly placing electrodes on the related motor cortex, while in non-invasive studies this is done by selecting channels over motor cortex. By considering different channel selection and evaluating the prediction performance, complicated channel selection method could be achieved. In most researches, the time-window is fixed from several seconds to several hundred of milliseconds before the motion moment. There are very few BCI studies focus on frequency selection. The only example is an invasive ECoG study. In this ECoG study, the selected frequency ranges mainly based on the experience of former discrete motion researches and distributed in low frequency band of 2-5 Hz, μ-rhythm , β rhythm, some part of γ bands in non-invasive studies and even high-γ bands over 100 Hz. Further selection method called correlation-based feature selector (CFS) is used, which could automatically reduce feature number and select features from a large feature set by evaluating the prediction performances. This method is a little time-consuming, but provides more efficient prediction which indicates a successful feature selection strategy.

1.5.3 Prediction method

Prediction method is used for transforming motion related features into actual motion parameters. Continuous motion predictions are always performed by artificial neural network (ANN) or the linear model. ANN is performed in some invasive researches of predicting monkey hand position. ANN is a mathematical model that is inspired by the structure aspects of biological neural networks. A neural network consists of an interconnected group of artificial neurons, and it processes information using a connectionist approach to computation. In most cases an ANN is an adaptive system and changes its structure based on external or internal information that flows through the network during the learning procedure. As this method can adjust its structure automatically, it is usually used to suitable to model complex relationships between features and real parameters.

Linear regression is an approach to modeling the relationship between a scalar variable y and one or more variables denoted X. In linear regression, models of the unknown parameters are estimated from the data using linear functions. Linear regression procedure is usually divided into a train session and a test session. In the train session, the relationship between y and X is qualified by the training data set which includes a number of y and corresponding X. This is also called a fit procedure. Linear regression models are often fitted using the least squares approach, but they may also be fitted in other ways, such as by maximizing the correlation value between actual and predicted y. After train session, linear regression can be used to predict y using X. As algorithm of linear regression is simple and the train procedure is fast, it is more popular than other methods and is widely adopted by almost all invasive and non-invasive studies.

1.5.4 Mapping and source estimation

Modern MEG system contains several hundreds of channels which cover most area of our head. Therefore, the MEG measurement can provide us the map on the sensor space, which is called contour map. We can investigate task related patterns of the brain regions and recognize where the patterns are from. These contour maps provide us a chance to understand the meanings of measured signals easily.

From contour map, we could briefly recognize the interested patterns' source location such as motor cortex or visual cortex. However, this recognition depends on head position in MEG helmet and the anatomical structure of the head, and further detailed recognition, such as finger or arm motion patterns in motor area, cannot be determined by contour map. Thus we need source estimation method which can transform MEG signals into sources in the brain. One approach is to perform source localization by fitting an equivalent current dipole (Scherg, 1990). This assumes only

one active current dipole in the brain at one time, thus is adopted only in some simple brain activities. However, brain activity is always complicated and contains many current dipoles distributed in all the brain. In this case, we consider a more sophisticated approach, which is called beamformer. For different kinds of data, there exists several beamformer methods, such as minimum-norm estimates (MNE) , low resolution brain electromagnetic tomography (LORETA) (Pascual-Marqui, 1999), linearly constrained minimum variance method (LCMV) (Van Veen et al., 1997) and dynamic imaging of coherent sources (DICS) (Gross et al., 2001), which are different in the calculation algorithm.

Chapter 2 Noise reduction - compensation tSSS

In this chapter, we propose an effective noise reduction method with hardly any brain activity loss, which is vital for the accurate prediction of motion trajectory from single trials data. We first described the algorithm of the original spatiotemporal signal space separation (tSSS) method developed by Dr. Taulu. Then we discussed the signal loss problem in the original method, and proposed an improvement on the method. We newly introduced a compensation process which could suppress noises and preserve brain signals simultaneously. This method showed very good noise reduction performances for both simulation and the application to the real MEG data. It should be noted that our method can be applied to all kinds of MEG system, while the original method can only be applied to the MEG system with both gradiometers and magnetometers.

2.1 Introduction

Magnetoencephalography (MEG) is a non-invasive method to measure the magnetic fields of ionic current distributions produced by the brain. Because the MEG signal generated by brain neuron activities and attenuated with the inverse square law as distance increased, these magnetic fields which usually recorded at 3-5 cm far from the origins are very weak (about 10^{-15}T). Thus, these brain magnetic fields are always contaminated by external interference electromagnetic noise as well as some biosignals such as heart beat or eye movements. In the single-trial analysis, this problem is more serious because we focused on the variety of signals and could not reduce the noise by averaging. In this case the noise reduction is very important.

In order to remove the interference noises, several noise reduction methods including hardware and software ways are developed. By using either hardware method or software method or by using the combination of them, the interference noises can be greatly suppressed. The most widely used hardware methods are magnetically shielded rooms (MSR), gradiometers and reference channels. Some of the popular software methods are signal space projection (SSP), principal component analysis (PCA), independent component analysis (ICA) and spatiotemporal signal space separation (tSSS).

In our case, the hardware method of MSR and gradiometers are combined. The MSR can dramatically reduce external interference outside the room, while gradiometers can remove homogeneous magnetic fields generated by electric devices inside the shield room. Thus, the residuals of interference noises contain electromagnetic fields generated by sources near the sensors, such as the noise of MEG device and biomagnetic signals of subject. Usually, these kinds of noises can be greatly reduced by the average of amount of repeated task. However, in some case single-trial variety is important and thus other noise reduction method is necessary. SSP bases on the predefined pattern of noise and thus may be affected by the changes between the noises before and during the experiment. PCA and ICA aim to extract the temporal patterns of interested biosignals and the interference noises. Then, these patterns have to be discriminated manually based on prior knowledge. This discrimination process is really a challenging work even for expertise researchers and thus the quality of the noise reduction varies according to the discrimination criterions. Among them, tSSS is a more robust and reliable interference suppression method based on spatial filters. This method bases on signal space separation (SSS) which consideres the geometry of the sensors and separates biosignals from interference noises using the characteristics of magnetic field. After SSS process, temporal patterns are further considered for noise removal and clean brain activities are reconstructing using the coefficient of signal space basis. The results of tSSS do not depend on the prior conditions or users experience and thus tSSS is the ideal noise reduction method

in our measurement condition.

TSSS is originally developed for Elekta system which contains both magnetometer and gradiometer type sensors. Currently, most applications of tSSS method are done under the Elekta system (Song et al., 2008; Medvedovsky et al., 2009; Taulu and Hari, 2009), while the application on other systems with only gradiometer type sensors is still not fully tested. In our study, we first implemented tSSS algorithm on Matlab and applied it to our system (Yokogawa PQ2440R). However, the tSSS results did not present a good result on our system. Signal leakage problem occurred and brain activities reduced to 1/3~1/2 after using tSSS method. Therefore, we carefully considered the leakage problem of tSSS under gradiometer only system and tried to fix it.

We first introduced the algorithm of SSS and tSSS developed by Dr. Taulu, and discussed the possible reasons for the signal leakage. Then we provided a solution utilizing a compensation process. By this process, our "compensation tSSS" can not only effectively remove the environmental noise, but also well preserve useful brain signals with our gradiometer system. Our compensation tSSS should work well not only on MEG systems with only gradiometers or magnetometers such as Yokogawa system but also on MEG systems with magnetometers and gradiometers such as Elekta system. In the future, our method can also be used on other types MEG system. And this is a great improvement compared to the original tSSS method.

2.2 Method

As SSS and tSSS algorithms developed by Dr. Taulu are the basis of our compensation tSSS method, in this section, SSS and tSSS methods are firstly reviewed in 2.2.1 and 2.2.2. Then the signal leakage problem is discussed and the algorithm of compensation tSSS method made by ourselves is proposed in 2.2.3.

2.2.1 SSS algorithm

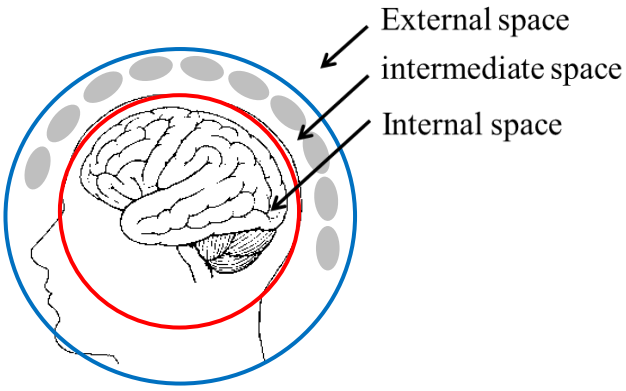

Figure 2 - 1 Illustration of internal, intermediate and external spaces.
The gray area indicates the position of MEG sensors.

SSS is a method to separate internal signals and external signals. A geometric model of MEG measurement is shown in Figure 2 - 1. In this figure, the red line presents a sphere covering the whole brain while the blue line presents a sphere covering both the whole brain and sensor space. Here the red and blue spheres have the same origin. In this model, the neural activity arouses in the red sphere and thus this space is regarded as 'Internal Space'. All MEG sensors locate in the space between the red and blue sphere and this space is called 'Intermediate space' or 'Sensor space'. Interference electromagnetic noises occur outside the blue sphere and thus this space is regarded as 'External space'.

As it is known, the magnetic field $\boldsymbol{B}$ in the sensor space sacrifices the quasistatic Maxwell equation:

$$\nabla \times \boldsymbol{B} = \mu_0 \boldsymbol{J} \ , \qquad \nabla \cdot \boldsymbol{B} = 0 \ , \tag{2 - 1}$$

where μ_0 is the magnetic permeability of vacuum. As the sensors of MEG system locate in a source-free volume, the current density $\boldsymbol{J} = 0$. We can get $\nabla \times \boldsymbol{B} = 0$. This curl-free magnetic field $\boldsymbol{B}$ thus can be expressed as a gradient of a scalar potential

$$\boldsymbol{B} = -\mu_0 \nabla \boldsymbol{\Phi} \ . \tag{2 - 2}$$

Considering equation 2 - 1, the $\boldsymbol{\Phi}$ has to satisfy Laplace's equation $\nabla^2 \boldsymbol{\Phi} = 0$. In

a spherical coordinates(r, θ, φ), the solution of Laplace's equation can be expanded in spherical harmonics :

$$\boldsymbol{\Phi}(r,\theta,\varphi) = \sum_{l=0}^{\infty}\sum_{m=-l}^{l}\frac{1}{r^{l+1}}\alpha_l^m Y_l^m(\theta,\varphi) + \sum_{l=0}^{\infty}\sum_{m=-l}^{l} r^l \beta_l^m Y_l^m(\theta,\varphi)$$
$$= \boldsymbol{\Phi}_{in} + \boldsymbol{\Phi}_{out} \ , \qquad 2 - 3$$

where $Y_l^m(\theta,\varphi)$ is the spherical harmonic function.

When equation 2 - 3 is substituted into equation 2 - 2, the magnetic field can be expressed as

$$\boldsymbol{B}(r,\theta,\varphi) = -\mu_0\sum_{l=0}^{\infty}\sum_{m=-l}^{l}\alpha_l^m \nabla\left(\frac{Y_l^m(\theta,\varphi)}{r^{l+1}}\right) - \mu_0\sum_{l=0}^{\infty}\sum_{m=-l}^{l}\beta_l^m \nabla\left(r^l Y_l^m(\theta,\varphi)\right)$$
$$= \boldsymbol{B}_{in} + \boldsymbol{B}_{out} \ . \qquad 2 - 4$$

With infinitive number of *l*, the numbers of internal and external basis are infinitive and thus this expansion reconstructed magnetic field exactly. However, in real case, the magnetic field $\boldsymbol{B}$ is expressed approximately with a finite number of *l*, thus the internal and external basis as well as the coefficients could be written as the form of matrices.

With the spherical harmonic basis, the MEG recordings $\boldsymbol{B}$ can be expressed as follows:

$$\boldsymbol{B} = \boldsymbol{x}_{in}\boldsymbol{S}_{in} + \boldsymbol{x}_{out}\boldsymbol{S}_{out} \ , \qquad 2 - 5$$

where $\boldsymbol{S}_{in}$ and $\boldsymbol{S}_{out}$ are matrices containing gradient of spherical harmonic functions in equation 2 - 4, $\boldsymbol{x}_{in}$ and $\boldsymbol{x}_{out}$ are the matrices containing the coefficient α_l^m and β_l^m. Equation 2 - 5 can also be written as a compact form as

$$\boldsymbol{B} = [\boldsymbol{x}_{in} \quad \boldsymbol{x}_{out}]\begin{bmatrix}\boldsymbol{S}_{in}\\ \boldsymbol{S}_{out}\end{bmatrix} = \boldsymbol{X}\boldsymbol{S} \ . \qquad 2 - 6$$

Here, the SSS basis $\boldsymbol{S}$ can be divided into separate subspaces $\boldsymbol{S}_{in}$ and $\boldsymbol{S}_{out}$ which are related to the internal biomagnetic and external interference signals respectively, while $\boldsymbol{x}_{in}$ and $\boldsymbol{x}_{out}$ indicated coefficients of the internal and external basis.

From formula 2 - 6, the coefficients $\boldsymbol{x}_{in}$ and $\boldsymbol{x}_{out}$ can be calculated from the pseudoinverse matrix of $\boldsymbol{S}$, as the following :

$$[\hat{\boldsymbol{x}}_{in} \quad \hat{\boldsymbol{x}}_{out}] = \boldsymbol{S}^{\dagger}\boldsymbol{B} = (\boldsymbol{S}^{T}\boldsymbol{S})^{-1}\boldsymbol{S}^{T}\boldsymbol{B} \ . \qquad 2\text{ - }7$$

By using the internal basis $\boldsymbol{S}_{in}$ and estimated coefficient $\hat{\boldsymbol{x}}_{in}$, the estimated biomagnetic field can be reconstructed as

$$\boldsymbol{B}_{in} = \hat{\boldsymbol{x}}_{in}\boldsymbol{S}_{in} \ . \qquad 2\text{ - }8$$

2.2.2 tSSS

Two kinds of errors which may affect the accuracy of SSS reconstruction are the MEG sensor calibration error and the truncation error. The reconstruction errors can be presented as

$$\hat{\boldsymbol{x}}_{in,\epsilon} = \hat{\boldsymbol{x}}_{in,c} + \hat{\boldsymbol{x}}_{in,t} \ , \qquad 2\text{ - }9$$

$$\hat{\boldsymbol{x}}_{out,\epsilon} = \hat{\boldsymbol{x}}_{out,c} + \hat{\boldsymbol{x}}_{out,t} \ , \qquad 2\text{ - }10$$

where the suffixes 'ϵ', 'c' and 't' indicate total error, calibration error and truncation error respectively.

In SSS method, accurate calibration and proper sensor configuration are necessary for optimal operation (Taulu et al., 2005). In practice, with modern multichannel devices using thin-film sensor technology, a calibration accuracy of about 0.1% can be achieve in sensitivity, location, orientation, gradiometer balance and cross-talk between the channels (Taulu and Simola, 2006). Thus the calibration error is not a serious problem. The truncation error related to the termination of the harmonic expansions, but it is a insignificantly small error with the assumption that no sources of magnetic field in the 'intermediate space'. However, intermediate interference sources exist unfortunately in practice and do not fall completely on $\boldsymbol{S}_{in}$ or $\boldsymbol{S}_{out}$. This leads to leakage of the interference contribution into both internal and external spaces and the spatial SSS model with finite truncation orders make this problem more serious. That is not only sources located in sensor space but also sources near sensor space cause such truncation error.

In order to remove the intermediate interference sources, the common temporal components of $\hat{\boldsymbol{x}}_{in}$ and $\hat{\boldsymbol{x}}_{out}$ are extracted and recognized as the intermediate interference noises. Because signals of brain activities do not leak to the external basis in Electa Nueromag System case, these common patterns do not contain brain activities. Thus, the extracted common components can be projected out from the SSS reconstructed signals without any loss of useful biosignals. The common temporal

patterns can be extracted by calculating the intersection of internal and external subspace matrices, as :

$$\boldsymbol{L} = \boldsymbol{X}_{in} \cap \boldsymbol{X}_{out} \quad , \qquad 2 - 11$$

where $\boldsymbol{X}_{in}$ and $\boldsymbol{X}_{out}$ are the subspace spanned by coefficient $\hat{\boldsymbol{x}}_{in}$ or $\hat{\boldsymbol{x}}_{out}$ respectively and $\boldsymbol{L}$ is the common subspace of $\boldsymbol{X}_{in}$ and $\boldsymbol{X}_{out}$. The calculation of $\boldsymbol{L}$ is referred to 'Matrix Computations' (Golub and Van Loan, 1996).

In the calculation of $\boldsymbol{L}$, two vectors in $\boldsymbol{X}_{in}$ and $\boldsymbol{X}_{out}$ respectively are considered identical when the angle θ between them scarifies $\cos\theta > 1 - \delta$. Here δ is the parameter to control the risk of selection. If δ is too small, only interferences with highest amplitudes will be rejected, while for a relatively large δ, the risk of removing brain signals will increase. In practice, the selection of δ dependes on the noise level of the MEG data.

In the calculation of $\boldsymbol{L}$, time-window length is also an important factor. Here, the time-window length T is related to the number n of sample points of MEG data segment for calculation. With finite number n, the angle between two random signals is less than $90°$. On the other hand, random noise in the MEG data creates the uncertainty in the direction of signal vector, and we have to choose a time window length T long enough that the angle between the deviation and the orthogonality condition is smaller than the noise uncertainty. With longer time-window length, the orthogonality is better and the common temporal patterns $\boldsymbol{L}$ is easy to be extracted correctly, while a small time-window always lead to loss of useful biosignals.

With proper calculated $\boldsymbol{L}$, the intermediate interferences can be removed by projecting the signals into the orthogonal subspace of $\boldsymbol{L}$ in time domain. When $\boldsymbol{L}$ is orthonormalized, the corrected coefficient are calculated as :

$$\hat{\boldsymbol{x}}_{in,p} = \left[(\boldsymbol{I} - \boldsymbol{L}\boldsymbol{L}^T)\hat{\boldsymbol{x}}_{in}{}^T\right]^T \quad . \qquad 2 - 12$$

With the corrected coefficient, the accurate estimated brain activity signals can be given as

$$\boldsymbol{B}_{in} = \hat{\boldsymbol{x}}_{in,p}\boldsymbol{S}_{in} = \left[(\boldsymbol{I} - \boldsymbol{L}\boldsymbol{L}^T)\hat{\boldsymbol{x}}_{in}{}^T\right]^T \boldsymbol{S}_{in} \quad . \qquad 2 - 13$$

2.2.3 Compensation tSSS

In section 2.2.2, we explained the fact that error of reconstruction coefficient

mainly comes from the truncation error, because the calibration error can be restricted into an insignificant level. As Dr. Taulu have said, this truncation error briefly relates to the leakage of intermediate interferences, because the leakage of internal and external sources is very small in their Elekta Neuromag System, which contains both magnetometer and gradiometer type sensors. In our case, Yokogawa 440ch MEG System contains only the gradiometer type sensors and thus the changes of sensor condition greatly affect the reconstruction error.

Considering the working principals of the sensors, magnetometer records much more information of large external interference noise signals than small internal biosignals, while gradiometer picks out signals of near internal source of brain activities better than signals of external source far away from sensors. In the algorithm view, basis vectors contained in $\boldsymbol{S}_{out}$ bases are predominantly along the magnetometer dimensions of the signal space, whereas in the $\boldsymbol{S}_{in}$ bases, the gradiometric dimensions dominate.

Our Yokogawa system contains only gradiometer type sensors, thus angle between external interference sources and external bases $\boldsymbol{S}_{out}$ is bigger in our gradiometer only system than in magnetometer plus gradiometer type system. Meanwhile, the angle between internal sources and external bases $\boldsymbol{S}_{out}$ is smaller than magnetometer plus gradiometer type system. This fact leads to serious problem of signal leakage of internal signals falling into external space and external signals falling into internal space. This is just similar to problem of intermediate interference sources. As finite truncation orders is used in the SSS model, the total error of coefficients is the truncation error in our system which comes from three parts, as is shown in the following :

$$\hat{\boldsymbol{x}}_{in,\epsilon} = \hat{\boldsymbol{x}}_{in,t} = \hat{\boldsymbol{x}}_{in,internal} + \hat{\boldsymbol{x}}_{in,external} + \hat{\boldsymbol{x}}_{in,intermediate} \quad , \qquad 2 - 14$$

$$\hat{\boldsymbol{x}}_{out,\epsilon} = \hat{\boldsymbol{x}}_{out,t} = \hat{\boldsymbol{x}}_{out,internal} + \hat{\boldsymbol{x}}_{out,external} + \hat{\boldsymbol{x}}_{out,intermediate} \quad , \qquad 2 - 15$$

where the suffixes ‘internal’, ‘external’ and ‘intermediate’ indicated error of coefficient come from the leakage of internal, external and intermediate sources respectively. Thus the SSS separation results are

$$\hat{\boldsymbol{x}}_{in} = \hat{\boldsymbol{x}}_{in,0} + \hat{\boldsymbol{x}}_{in,\epsilon} = \hat{\boldsymbol{x}}_{in,0} - \hat{\boldsymbol{x}}_{in,internal} + \hat{\boldsymbol{x}}_{in,external} + \hat{\boldsymbol{x}}_{in,intermediate} \quad , \qquad 2 - 16$$

$$\hat{\boldsymbol{x}}_{out} = \hat{\boldsymbol{x}}_{out,0} + \hat{\boldsymbol{x}}_{out,\epsilon} = \hat{\boldsymbol{x}}_{out,0} + \hat{\boldsymbol{x}}_{out,internal} - \hat{\boldsymbol{x}}_{out,external} + \hat{\boldsymbol{x}}_{out,intermediate} \quad , \qquad 2 - 17$$

where the suffix '0' indicates undistorted coefficient, the operator '-' means signal loss and operator '+' indicates the interference part. Among these coefficients, the undistorted coefficients $\widehat{\boldsymbol{x}}_{in,0}$ and $\widehat{\boldsymbol{x}}_{out,0}$ are obvious uncorrelated because they contain only internal or external temporal patterns respectively. For other coefficients, the suffix indicates the source space of the temporal components which the coefficients contain. Thus the common components in our case are much more complicated and it can be written as

$$\boldsymbol{L} = \boldsymbol{X}_{in} \cap \boldsymbol{X}_{out} = \{\boldsymbol{L}_{internal}, \boldsymbol{L}_{external}, \boldsymbol{L}_{intermediate}\} . \quad 2 - 18$$

where $\boldsymbol{L}_{internal}$, $\boldsymbol{L}_{external}$ and $\boldsymbol{L}_{intermediate}$ are common components containing internal, external and intermediate temporal patterns. Among them, $\boldsymbol{L}_{internal}$ is the part to be preserved while $\boldsymbol{L}_{external}$ and $\boldsymbol{L}_{intermediate}$ are the parts to be removed. If the original tSSS method is used as equation 2 - 12, not only the intermediate interference components, but also the internal components will be removed. This is the problem of biosignal loss occurred in gradiometer only system. Thus further analysis to discriminate the internal components from external and intermediate components is needed.

Here, a simple method by comparing the amplitude of magnetic field fallen in $\boldsymbol{S}_{in}$ and $\boldsymbol{S}_{out}$ is applied. For each vector $\boldsymbol{l}$ in the common components $\boldsymbol{L}$, magnetic field of temporal pattern $\boldsymbol{l}$ in internal space and external space can be extracted, by the formula

$$\boldsymbol{B}_{in,l} = (\boldsymbol{l}\boldsymbol{l}^T\widehat{\boldsymbol{x}}_{in})^T\boldsymbol{S}_{in} , \quad 2 - 19$$

$$\boldsymbol{B}_{out,l} = (\boldsymbol{l}\boldsymbol{l}^T\widehat{\boldsymbol{x}}_{out})^T\boldsymbol{S}_{out} , \quad 2 - 20$$

where $\boldsymbol{B}_{in,l}$ indicates magnetic field containing temporal pattern $\boldsymbol{l}$ and being reconstructed by internal bases, $\boldsymbol{B}_{out,l}$ indicates magnetic field containing temporal pattern $\boldsymbol{l}$ and being reconstructed by external bases. If $\boldsymbol{l}$ is an internal temporal pattern, then $\boldsymbol{B}_{in,l}$ should be much larger than $\boldsymbol{B}_{out,l}$ as $\boldsymbol{B}_{out,l}$ is the leakage part of internal source. On the other hand, if $\boldsymbol{l}$ is an external temporal pattern, then $\boldsymbol{B}_{in,l}$ should be much smaller than $\boldsymbol{B}_{out,l}$ as $\boldsymbol{B}_{in,l}$ is the leakage part of external source. And if $\boldsymbol{l}$ is an intermediate temporal pattern, then $\boldsymbol{B}_{in,l}$ should be comparable with $\boldsymbol{B}_{out,l}$ as both of $\boldsymbol{B}_{in,l}$ and $\boldsymbol{B}_{out,l}$ are the leakage parts of intermediate source. With this knowledge, statistics of the amplitudes of $\boldsymbol{B}_{in,l}$ and $\boldsymbol{B}_{out,l}$ can be used to determine whether $\boldsymbol{l}$ is internal or external or intermediate components. We firstly calculate the absolute amplitude of $\boldsymbol{B}_{in,l}$ and $\boldsymbol{B}_{out,l}$, and average them across time domain and channels and written as $\boldsymbol{B}_{in,l}$ and $\boldsymbol{B}_{out,l}$. Then, a ratio for source space judgment is given as

$$r = \frac{\boldsymbol{B}_{in,l}}{\boldsymbol{B}_{ou,l}} \ . \qquad 2 - 21$$

For internal component ***l***, r should be much smaller than 1, while in other cases *r* should be much greater or about the value of 1. From the value of r, the source space of vector ***l*** can be easily determined and $\boldsymbol{L}$ can be discriminated as $\boldsymbol{L}_{internal}$, $\boldsymbol{L}_{external}$ and $\boldsymbol{L}_{intermediate}$.

Then, similar to original tSSS method, we can remove the external and intermediate temporal patterns in $\hat{\boldsymbol{x}}_{in}$ by the projection operator $\left(\boldsymbol{I} - \boldsymbol{L}_{interference}\ \boldsymbol{L}_{interference}^{T}\right)$ where $\boldsymbol{L}_{internal}$ is the collection of $\boldsymbol{L}_{external}$ and $\boldsymbol{L}_{intermediate}$. Then, we can extract the internal temporal patterns in $\hat{\boldsymbol{x}}_{out}$ by the projection operator $(\boldsymbol{L}_{internal}\ \boldsymbol{L}_{internal}^{T})$.

Thus, we can get coefficient containing only internal temporal patterns, in the form

$$\hat{\boldsymbol{x}}_{in,p} = \left[\left(\boldsymbol{I} - \boldsymbol{L}_{interference}\ \boldsymbol{L}_{interference}^{T}\right)\hat{\boldsymbol{x}}_{in}{}^{T}\right]^{T} =$$

$$\hat{\boldsymbol{x}}_{in}\left(\boldsymbol{I} - \boldsymbol{L}_{interference}\ \boldsymbol{L}_{interference}^{T}\right)^{T} = \hat{\boldsymbol{x}}_{in,0} - \hat{\boldsymbol{x}}_{in,internal} \ , \qquad 2 - 22$$

$$\hat{\boldsymbol{x}}_{out,p} = \left[(\boldsymbol{L}_{internal}\ \boldsymbol{L}_{internal}^{T})\hat{\boldsymbol{x}}_{in}{}^{T}\right]^{T} = \hat{\boldsymbol{x}}_{out}\,(\boldsymbol{L}_{internal}\ \boldsymbol{L}_{internal}^{T})^{T} = \hat{\boldsymbol{x}}_{out,internal} \ , \qquad 2 - 23$$

Considering the missing temporal internal patterns in internal coefficients are leaked into the external coefficients, the leakage magnetic field of internal patterns can be written as

$$\boldsymbol{B}_{leak,internal} = \hat{\boldsymbol{x}}_{in,internal}\ \boldsymbol{S}_{in} = \hat{\boldsymbol{x}}_{out,internal}\ \boldsymbol{S}_{out} \ . \qquad 2 - 24$$

Thus, a combination of $\hat{\boldsymbol{x}}_{in,p}$ and $\hat{\boldsymbol{x}}_{out,p}$ is given in the form

$$\hat{\boldsymbol{x}}_{in,p}\boldsymbol{S}_{in} + \hat{\boldsymbol{x}}_{out,p}\boldsymbol{S}_{out} = \left(\hat{\boldsymbol{x}}_{in,0} - \hat{\boldsymbol{x}}_{in,internal}\right)\boldsymbol{S}_{in} + \hat{\boldsymbol{x}}_{out,internal}\ \boldsymbol{S}_{out} = \hat{\boldsymbol{x}}_{in,0}\boldsymbol{S}_{in} \ . \qquad 2 - 25$$

This formula indicates that by combining the coefficients $\hat{\boldsymbol{x}}_{in,p}$ and $\hat{\boldsymbol{x}}_{out,p}$, internal magnetic field can be accurately reconstructed as

$$\boldsymbol{B}_{in} = \hat{\boldsymbol{x}}_{in,p}\boldsymbol{S}_{in} + \hat{\boldsymbol{x}}_{out,p}\boldsymbol{S}_{out} = \left[\left(\boldsymbol{I} - \boldsymbol{L}_{interference}\ \boldsymbol{L}_{interference}^{T}\right)\hat{\boldsymbol{x}}_{in}{}^{T}\right]^{T}\boldsymbol{S}_{in} +$$

$$\left[\left(\boldsymbol{L}_{internal}\ \boldsymbol{L}_{internal}^{T}\right)\hat{\boldsymbol{x}}_{in}{}^{T}\right]^{T}\boldsymbol{S}_{out} \quad . \qquad 2 - 26$$

Our new method first removes the leakages of external and intermediate components in internal space, which is the same process with original tSSS method. And then it extracts and recovers the leakages of internal components in external space, which can be called as a compensation process. Thus in the following sections, we call this method 'compensation tSSS' in order to discriminate it from original tSSS method.

2.2.4 Application of compensation tSSS on simulation and real MEG data

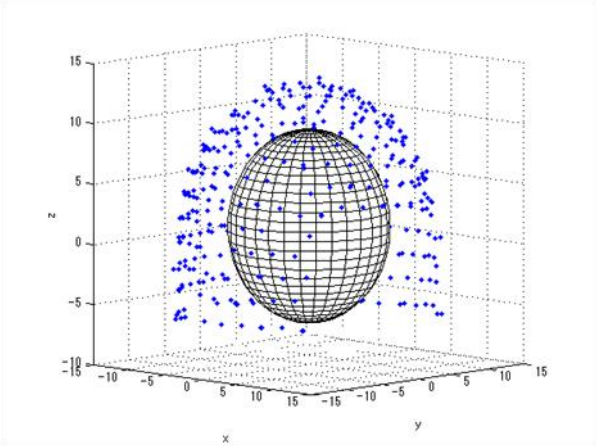

Figure 2 - 2 Position of single sphere head model and distribution of gradiometer sensors in our MEG system.

Blue dots indicate the position of MEG sensors, the sphere in the center shows the position of head model. The coordinate (x,y,z) with the unit 'cm' is Yokogawa MEG coordinate and we use this coordinate in the following dipole simulation.

To evaluate the signal/noise separation performances of compensation tSSS, we apply it on simulation data, phantom data and raw MEG data. In the simulation of this study, we adopted a simple sphere head model whose center locates at the position (0, 0, 0.02) m in the coordinate illustrated in Figure 2 - 2. The internal human brain activity is modeled by the equivalent current dipole source, which is given

$$\boldsymbol{B}(\boldsymbol{r}) = \frac{\mu_0}{4\pi \boldsymbol{F}^2}(\boldsymbol{F}\boldsymbol{Q} \times \boldsymbol{r}_0 - \boldsymbol{Q} \times \boldsymbol{r}_0 \cdot \boldsymbol{r}\nabla \boldsymbol{F}) \ , \qquad 2 - 27$$

where $\boldsymbol{F} = \boldsymbol{a}(\boldsymbol{r}\boldsymbol{a} + \boldsymbol{r}^2 - \boldsymbol{r}_0\boldsymbol{r}) \ , \qquad 2 - 28$

$$\nabla \boldsymbol{F} = (\boldsymbol{r}^{-1}\boldsymbol{a}^2 + \boldsymbol{a}^{-1}\boldsymbol{a} \cdot \boldsymbol{r} + 2\boldsymbol{a} + 2\boldsymbol{r})\boldsymbol{r} - (\boldsymbol{a} + 2\boldsymbol{r} + \boldsymbol{a}^{-1}\boldsymbol{a} \cdot \boldsymbol{r})\boldsymbol{r}_0 \ , \qquad 2 - 29$$

$$\boldsymbol{a} = \boldsymbol{r} - \boldsymbol{r}_0 \ . \qquad 2 - 30$$

Here $\boldsymbol{r}_0$ indicates the vector of internal source position, $\boldsymbol{r}$ indicates the vector of sensor position and $\boldsymbol{B}$ is the vector of magnetic field at $\boldsymbol{r}$ generated by internal source at $\boldsymbol{r}_0$.

In addition, two kinds of external interference sources were adopted: current dipole and magnetic dipole. The magnetic field generated by external current dipole can be modeled as

$$\boldsymbol{B}(r) = \frac{\mu_0}{4\pi} \frac{\boldsymbol{Q} \times (\boldsymbol{r} - \boldsymbol{r}_0)}{|\boldsymbol{r} - \boldsymbol{r}_0|^3} \ , \qquad 2 - 31$$

where $\boldsymbol{Q}$ is the moment of external current dipole. The magnetic field generated by external magnetic dipole is given as the following formula

$$\boldsymbol{B}(\boldsymbol{r}) = \frac{3(\boldsymbol{m} \cdot \boldsymbol{r})\boldsymbol{r} - \boldsymbol{m}\boldsymbol{r}^2}{|\boldsymbol{r}|^3} \ , \qquad 2 - 32$$

where $\boldsymbol{m}$ is the moment of external magnetic dipole located at $\boldsymbol{r} = 0$.

In the simulation, we adopted the sensor array configuration following Yokogawa 440-channel MEG system installed at the University of Tokyo. This system enclosed 140 planar type gradiometers and 300 axial type gradiometers with a common baseline of 5 cm. All these gradiometer sensors located in a sphere shell with a radius from 12 cm to 15 cm. The distribution of distance from the origin of coordinate to the sensors was presented in Figure 2 - 3. In the phantom and raw MEG data test process, the same system with the same configuration was used.

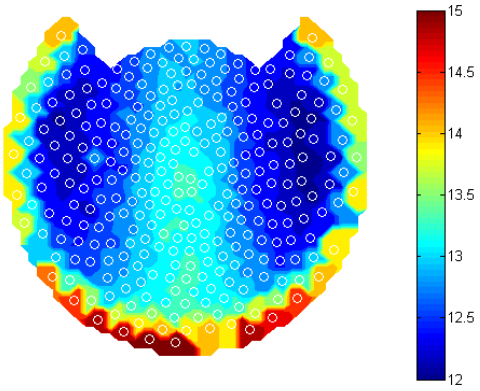

Figure 2 - 3 The distribution of distance from the origin of coordinate to the sensor.

The circles indicate the position of sensors. Colors show the distance in unit centimeter.

The quality of the compensation tSSS performance is evaluated by the value of reconstruction error, which is given

$$error = \sqrt{\frac{\sum(\boldsymbol{B}_{reconstructed} - \boldsymbol{B}_{original})^2}{\sum \boldsymbol{B}_{original}{}^2}}, \qquad 2 - 33$$

where $\boldsymbol{B}_{reconstructed}$ is the reconstructed internal magnetic field by compensation tSSS method and $\boldsymbol{B}_{original}$ is the true internal magnetic field simulated by the current dipole equation 2 - 27.

2.3 Experiments and Results

2.3.1 Parameter determination

Similar to tSSS method, compensation tSSS method also needs the reconstruct coefficient $\boldsymbol{x}_{in}$ and $\boldsymbol{x}_{out}$ separated by SSS method. In SSS method, we adopt formula 2 - 4 to separate internal and external signals. In the formula, magnetic field is expanded by infinitive bases as l is considered from 0 to positive infinity. This is the optimal case and in practice we use finite number l to make the calculation possible. This will cause truncation errors and the level of truncation error will be affected by the value of l. In the formula 2 - 4, we have two values L_{in} and L_{out} to be set, which correspond to the forward and backward l value in the equation and determine the number of vectors in internal and external bases. Please note that the parameter L_{in}

and L_{out} mentioned in this section are scalars to determine the base number, and they are different with parameter $\boldsymbol{L}$ in bold font which indicates the common temporal component matrix.

In order to determine L_{in} and L_{out}, we calculate the angle between magnetic field of random internal current dipole source and the reconstructed magnetic field , and used θ to indicate the angle. The cosine value of angle θ is proportional to the inner product of original and reconstructed magnetic field vectors of the dipole, and thus represents the similarity of these two vectors. The equation of θ is given

$$cos\,\theta = \frac{\boldsymbol{B}_{original} \cdot \boldsymbol{B}_{reconstructed}}{|\boldsymbol{B}_{original}||\boldsymbol{B}_{reconstructed}|}, \qquad 2 - 34$$

where $\boldsymbol{B}_{original}$ is the simulated magnetic field data of all the channels at a certain moment and $\boldsymbol{B}_{reconstructed}$ is reconstructed magnetic field data of all the channels at the same moment. If the reconstructed result is perfectly accurate, then $\boldsymbol{B}_{original} = \boldsymbol{B}_{reconstructed}$, and $\cos\theta = 1$. Thus $\theta = 0$ is the highest performance of SSS. Usually the angle θ varies from 0 to 90° and smaller value of angle θ presented a better SSS performance level.

In practice, a typical human brain superficial source locates around a shell from 0.07 m to 0.08 m, corresponding to distances of about 2 cm – 3 cm from the sensors to the brain activity dipoles. Thus the distances of 0.07 m – 0.08 m from head model origin to the simulated dipoles have to be considered seriously. In order to evaluate the separation performance of SSS, 100 simulated internal current dipoles were adopted to generate simulated magnetic field. These dipoles randomly located at an upper hemisphere with a radius of 7 cm and their moment was set randomly with an amplitude of 10^{-7}Am. The angles between simulated and reconstructed magnetic field under different combination of L_{in} and L_{out} were considered and illustrated in Figure 2 - 4. These results turned out that when L_{in} increases and L_{out} decreases, the angle decreases. From the criterion mentioned in the former paragraph, bigger L_{in} and smaller L_{out} turned to be better for the reconstruction. Thus we concluded $L_{in} = 10$ should be the best for SSS method in our system.

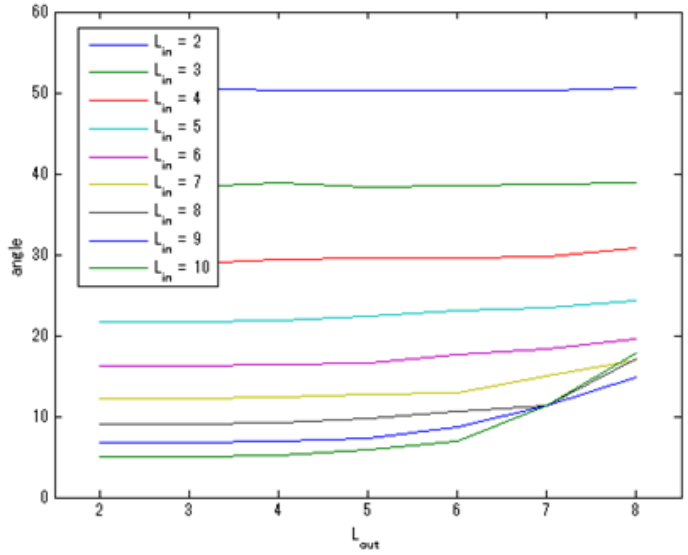

Figure 2 - 4 Angles between simulated and reconstructed magnetic field of internal dipole under different combination of L_{in} and L_{out} .

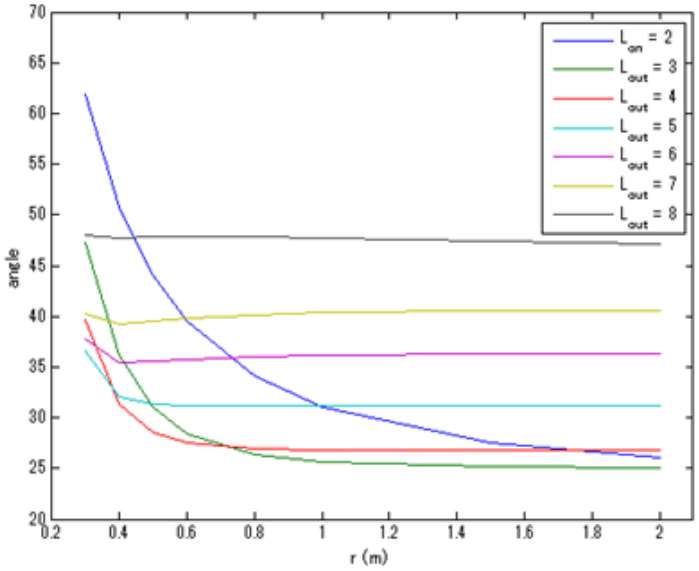

Figure 2 - 5 Angles between simulated and reconstructed magnetic field of external dipoles under different L_{out} .

As the angle hardly varies when $L_{out} < 5$, we designe further simulation for L_{out} determination. In this step, external current dipoles located at spheres with different radius were employed. At each sphere, the angle between randomly generated and reconstructed magnetic field were calculated 100 times. Here the reconstructed magnetic field was calculated by SSS method with fixed $L_{in} = 10$ and different L_{out} condition. The average results are shown in Figure 2 - 5. From this result, As

L_{out} increases, the overall performance firstly improves and then worsens, with the best performance at $L_{out} = 3$ and 4. Considering the results of dipoles far from sensors, $L_{out} = 3$ is a little better than $L_{out} = 4$. However, from the results of dipoles near to sensors, $L_{out} = 4$ performed much better than $L_{out} = 3$. In summary, condition of $L_{in} = 10$ and $L_{out} = 4$ is confirmed the best in our system and is used in the following parts.

2.3.2 Computer simulation

In the simulation, internal current dipole, external current dipole and external magnetic dipole were generated. To match the experiment cases which we were interested in, two internal current dipoles were generated as the motor and visual brain activity sources respectively which appeared in different time segments. 100 external current dipoles which located in a sphere with a radius of 0.5 m and 1 external magnetic dipole were adopted to mimic the complicated interference noise condition. Because our MEG device is gradiometer type system and locates inside a magnetically shielded room, interference noise sources with further location are not considered in our study. Finally we also added some random sensor noises with the amplitude about 40 fT to make the simulated data much similar with real experimental condition. The sensor noises are following the standard normal distribution and are generated by the Matlab function 'randn'. The location, moment amplitude and orientation are listed in Table 2 - 1.

Table 2 - 1 Location and moment information of simulated dipoles

	Number	**Location (m)**	**Amplitude (Am) or (Am^2) for current or magnetic dipole respectively**	**Orientation**	**Oscillation**
Internal current dipole	2	Visual (0, 0, 0.05) Motor (0.03, -0.05, 0.05)	1e-19 1e-19	(1, 0, 0) (1, 0, 0)	10 Hz
External current dipoles	100	In sphere with radius of 0.5 m	5e-6	random	3 Hz
External magnetic dipole	1	(0.1, 0.5, 0.2)	1e-3	(-1, -1, -1)	2 Hz

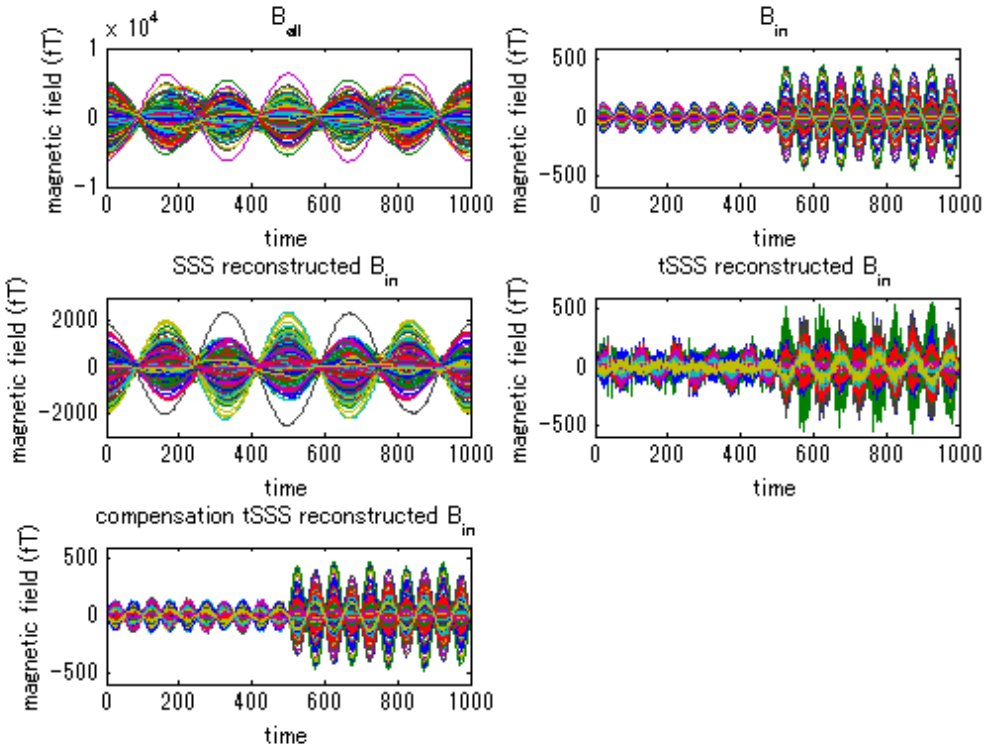

Figure 2 - 6 Time-series results of simulated dipoles reconstruction using SSS, original tSSS and compensation tSSS method.

The signal reconstruction and interference suppression effects of SSS, original tSSS and compensation tSSS method with common parameters ($L_{in} = 10,\ L_{out} = 4,$ $\delta = 0.1$ and time-window length of 1000 sample points; in compensation tSSS, the ratio *r* in equation 2 - 21 is set to 1) can be examined from time domain characteristics in Figure 2 - 6. The upper left waveform plot shows the simulated magnetic field of all the internal and external sources. The upper right waveform plot presents the simulated magnetic field of brain activity sources which appears in different time periods. From the middle left waveform, it is obviously that the interference noise from 3Hz external current dipole is suppressed to one third of the original level while the 2 Hz external magnetic dipole is suppressed much more to an invisible level. This verified that SSS method on our system has some noise reduction effects, but the effect is far not enough. The middle right waveform shows the interference suppression effect of original tSSS method and it turned out that both the external current and magnetic dipole are suppressed greatly and hardly exist anymore, however the signal is also suppressed a little bit by tSSS method. As the waveform is noisy because of the sensor noise residuals, it is difficult to evaluate the loss of internal signals. The lower left waveform plot illustrates the result of compensation

tSSS method which presents the best performance among all the results. Not only the external current and magnetic interference source, but also most of the sensor noise are suppressed greatly. Moreover, the waveform reconstructed by compensation tSSS method resembles the original signal in the upper right plot very well which revealed a high quality reconstruction. From equation 2 – 33, we calculated the relative difference, or the reconstruction error of these three kinds of method. The reconstruction error of SSS, original tSSS and compensation tSSS method are 7.0443, 0.4683, 0.1467 respectively. The smallest relative difference of compensation tSSS method also confirmed that this method had the best performance in our system.

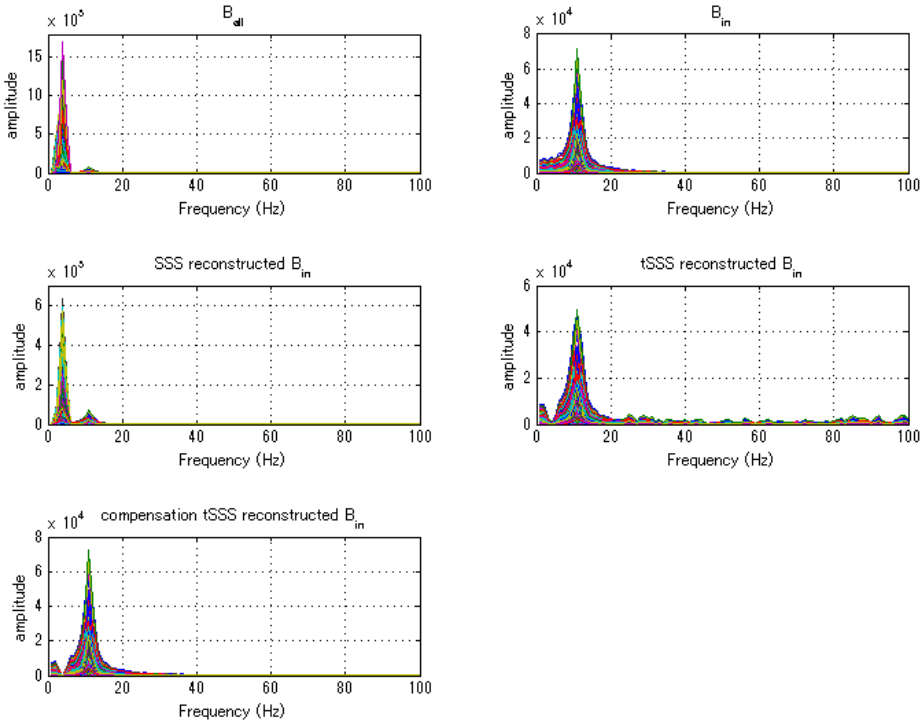

Figure 2 - 7 FFT results of simulated dipoles reconstruction using SSS, original tSSS and compensation tSSS method.

Instead of temporal patterns, frequency characteristics can indicate the loss of useful signals or the suppression of external noise much clearly. Figure 2 - 7 shows the corresponding fast furious transform (FFT) of time series presents in Figure 2 - 6. In the upper left plot, the large peak is the external signals. Because of the small sample point number and the Gibbs effect of Furious transform, two peaks at 2 Hz and 3 Hz are mixed together here. The minor peak around 10 Hz in this plot presents the internal signal which is indicated in the upper right plot. From the amplitudes in

these two plots, it is clear that the power of external signals is 20 times larger than the one of internal signal. The middle left plot illustrates the SSS reconstructed result in which the external signals is suppressed to half of original level. In the middle right plot which indicates the original tSSS reconstructed result, the external signals are removed completely, but the internal signal around 10 Hz is also suppressed from about 70000 to 50000. The lower left plot is the reconstructed results of compensation tSSS. As the former plot, external signals are removed completely. Meanwhile, the peak around 10 Hz is about the value of 70000, which is just the same with original internal signal showed in upper right plot. These FFT results also turned out that compensation tSSS method can suppress interference noise and preserve internal signal very well comparing with SSS and original tSSS method.

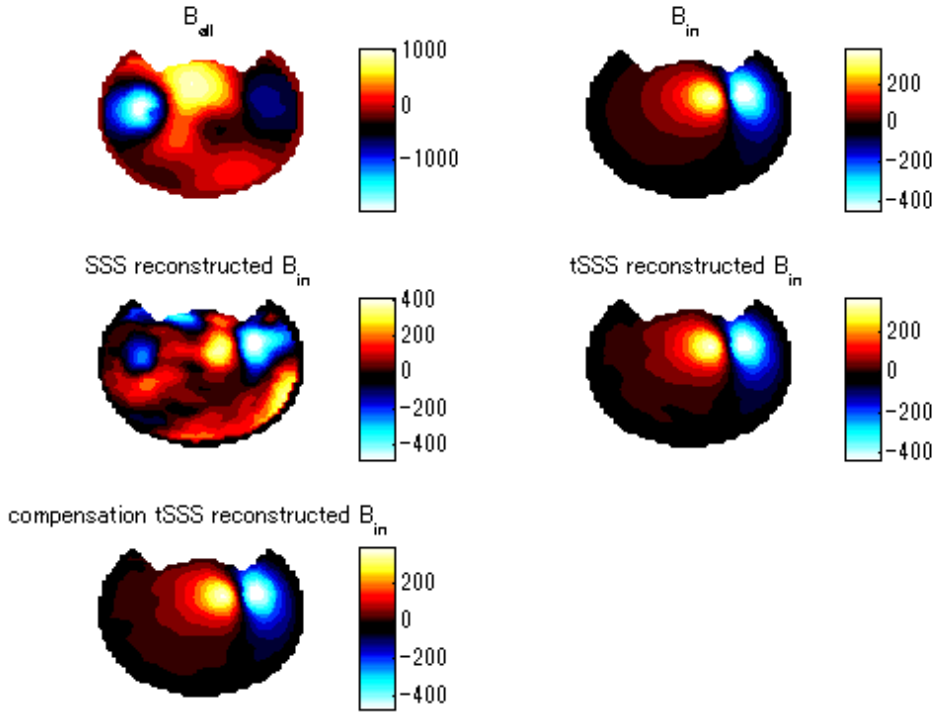

Figure 2 - 8 Contour map results of simulated dipoles reconstruction using SSS, original tSSS and compensation tSSS method.

After presenting the well reconstructed results of compensation tSSS method in temporal patterns and signal amplitudes, we continued to investigate the performance from spatial patterns. The contour map results of all the methods are compared in Figure 2 - 8. The upper right map turns out that the simulated internal dipole located around the motor cortex in the right hemisphere, with amplitude of about 200 fT.

However in the upper left map, the spatial pattern is distorted heavily by external interference noises and the spatial pattern over right motor cortex is totally concealed. In the middle left map, although it is still noisy in the contour map, two peaks over right motor cortex can be roughly recognized. Considering the performance of SSS in temporal pattern and FFT analysis, the contour map presents a surprisingly reconstruction. This is because of the principle of SSS method – spatial filter, which can remove interference noise patterns and extract useful internal patterns in spatial domain. The middle right and the lower left map shows the results of original and compensation tSSS reconstructed results respectively, which presents similar spatial patterns. These two contour maps highly resemble the original map and thus we employed dipole fitting method to compare them. In order to accomplish the dipole fitting problem, we used the Matlab toolbox 'Fieldtrip' (Scherg, 1990) which is developed by Donders Institute for Brain, Cognition and Behaviour, The Netherlands. The dipole fitting errors are 10.680, 2.516, 2.609 mm for SSS, original tSSS and compensation tSSS method respectively. This concluded that although SSS method can briefly extracted the spatial pattern of internal signal, the reconstruction is not so accurate comparing with the other two methods. Original and compensation tSSS both presented a very well reconstruction results and original tSSS performed a little bit better than the other one. However, the difference is only 0.1 mm and is negligible in most cases. Considering the preservation of useful signal, it is concluded that compensation tSSS method performed best among all these three methods. From all the aspect of time, frequency and spatial domain, compensation tSSS deeply suppresses interference noises and greatly preserved internal signals in our simulation, thus it is confirmed effective for noise reduction in our system.

2.3.3 MEG generated by phantom

In computer simulation, we generated several external dipoles as well as random sensor noises to mimic the complicated environmental noises. However, in the real application, the noise condition is much more complicated than we can imagine. In addition, imperfect calibration of MEG sensors, sensor instability and sensor noises will also affect reconstruction results greatly. To perform simulation under actual experimental condition, we used phantom dipole to imitate brain activity source and recorded raw data by our MEG system. Then, we used MEG raw data to determine the important factor r in equation 2 - 21 and testified the effectiveness in actual experimental condition.

In this experiment, signal generator was adopted to output 10 Hz sine waveform to a coil which placed inside the helmet of MEG system to imitate brain activity source. The amplitude of generated signal recorded by MEG system is recognized as about 500fT from the 1000 times averaged data. Here the common parameters in SSS,

original and compensation tSSS are $L_{in} = 10$, $L_{out} = 4$, $\delta = 0.1$ and time-window length of 8000 sample points (4s data with sample rate of 2000 Hz).

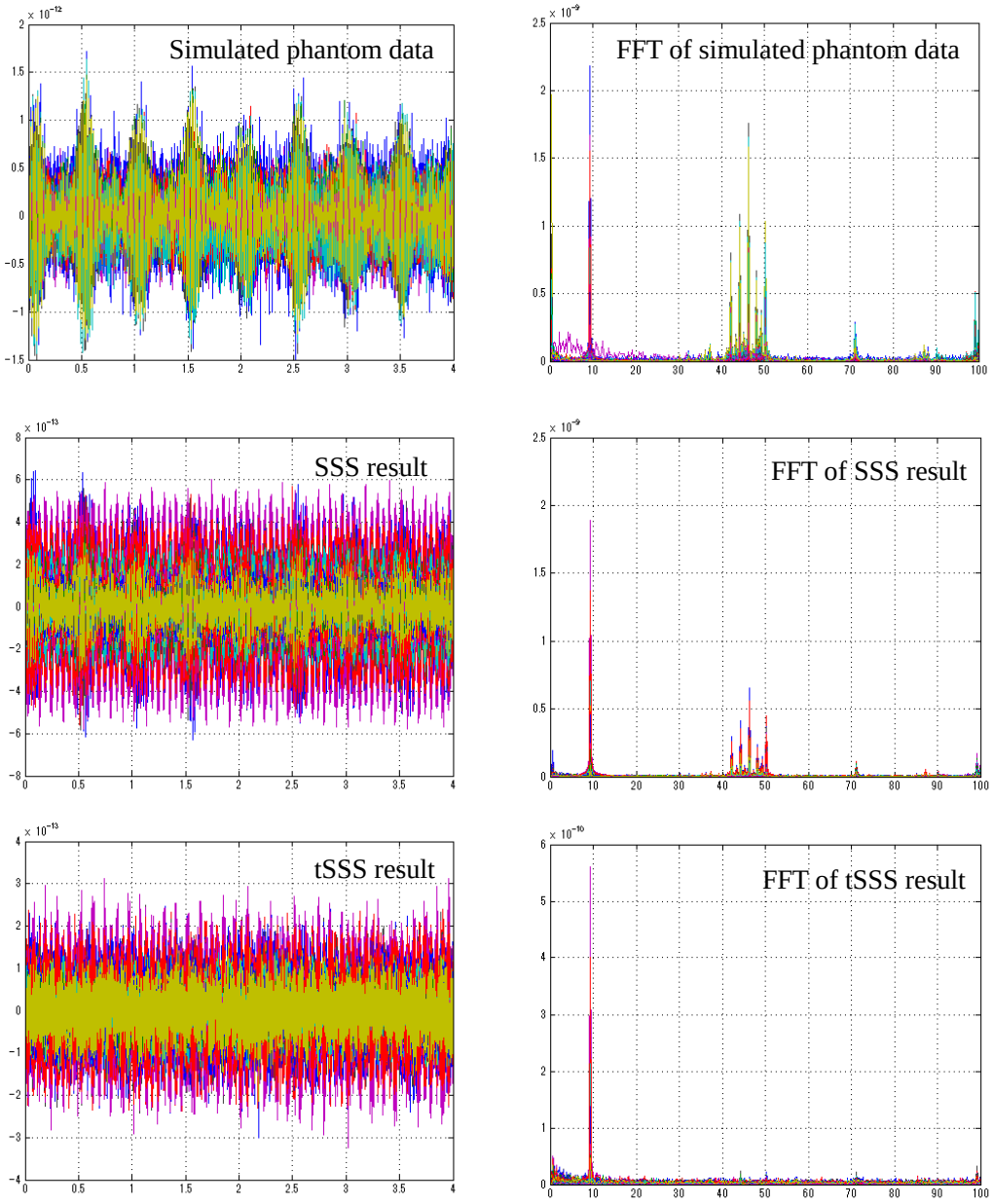

Figure 2 - 9 Time-series and FFT results of simulated phantom dipoles reconstruction using SSS and original tSSS.

The reconstructed results of SSS and original tSSS are shown in Figure 2 - 9. The upper two plots illustrate the time series and FFT of recorded MEG raw data which contain both simulated phantom data and actual environmental noises. The signal peak around 10 Hz is the phantom data and this part is what we want to preserve. Interference noises in this experiment included 50 Hz and 100 Hz which come from the power line noise, peaks from 40 to 50 Hz which are mainly from Helium

circulation system of MEG device, and low frequency noise around 1 Hz which might be the vibration of nearby devices. The middle two plots illustrate reconstruction after SSS, most of the low frequency noise is removed while other noise and useful signals are also suppressed to some extent. The lower two plots are the reconstruction results of original tSSS. All the noises as well as useful signals were suppressed in a great deal. This result is the same with computer simulation, and thus verified our theoretical analysis mentioned in section 2.2.2.

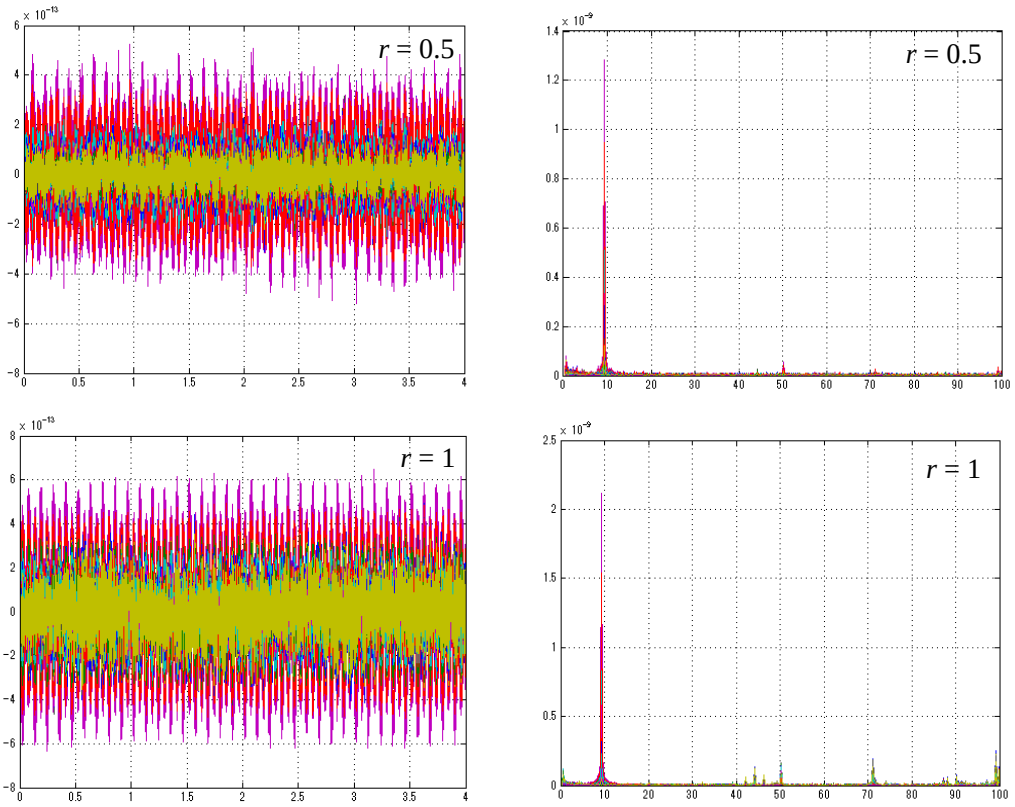

Figure 2 - 10 Time-series and FFT results of simulated phantom dipoles reconstruction using compensation tSSS with different *r* value.

In compensation tSSS method, we applied the same parameter settings with original tSSS in this experiment and considered different values of magnetic field in-to-out power ratio *r*. With different value of *r*, the recognition results of temporal patterns are different. This will affect the reconstruction results of compensation tSSS. Figure 2 - 10 shows the reconstruction results of compensation tSSS. The upper two plots are corresponding to $r = 0.5$, while lower two plots are corresponding to $r = 1$. When $r = 0.5$, the FFT results turn out clear that hardly any noise around 40 – 50 Hz existed anymore and useful signals are suppressed to near half of original amplitude, from 2.2e-9 to 1.2e-9. When $r = 1$, the FFT results indicate that there are very small

power loss of signals around 10 Hz, but interference noises are not completely remove in this case. In the lower left plot, the time series of reconstructed result presents an extremely clean temporal pattern which is just the about 10Hz sine-wave signal with an amplitude of 500 fT. These results specified that the in-to-out ratio value 1 is more proper under complicated condition of actual environmental noise.

2.3.4 MEG evoked by button press movement

The MEG raw data contains recorded MEG data while subject is asked to perform a button pushing task. In this section, the results of SSS, original tSSS and compensation tSSS method with common parameters ($L_{in} = 10,\ L_{out} = 4,\ \delta = 0.1$ and time-window length of 1000 sample points (1s data with sample rate of 1000 Hz), in-to-out ratio r = 0.5) were investigated. As it is difficult to manually recognize single trial time series patterns even in reconstructed data, we adopted 10 epochs of button pushing data. Thus in the following, 10 epochs average of each result was calculated, and the root-mean-square (RMS) values across channels were calculated and compared to evaluate the performance of them. Here, the zero second in each plot is the motion onset of button pushing. From prior experience, there should be a peak about several hundred fT around zero second.

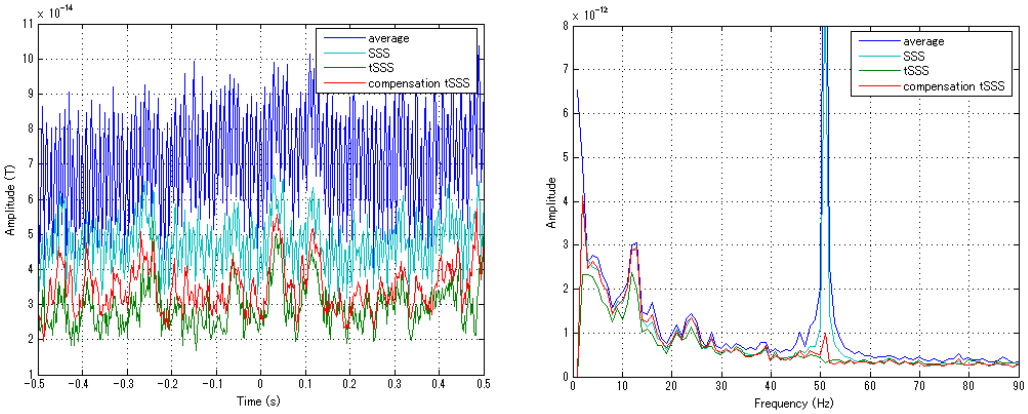

Figure 2 - 11 Time series and FFT of RMS results using SSS, original tSSS and compensation tSSS method.

The left plot in Figure 2 - 11 shows the time series of RMS results. The blue line indicates RMS of 10 epoch averaged raw MEG data. It turned out to be so noisy that the peak around motion onset is completely berried. In the green line of SSS reconstructed result, although the result is still noisy, a minor peak of motion activity was extracted. From the FFT result illustrated in the right plot, we could find out the

noise mainly come from 50 Hz power line effect and low frequency interference which might be generated by device vibration and baseline fluctuation. Considering original tSSS method in red line, the peak of motion activity in time series is obvious with very few noises. However in the FFT result, it is a pity that spectral amplitude of motion activity around 12 Hz is greatly suppressed. In result of compensation tSSS showed in light blue line, the peak is obvious and the amplitude is larger than result of original tSSS. From the right plot of FFT, it turned out that motion activity was highly preserved and interference noises around 50 Hz and below 1 Hz are greatly suppressed. These results confirmed that in actual experiment application, compensation tSSS in current settings is effective to preserve brain activity and suppress interference noises.

2.4 Discussion and Conclusion

2.4.1 Overfitting problem

Signal space separation (SSS) method focused on the separation of internal and external signals by using amount of spatial bases which is related to sensor configurations. This separation is achieved by a linear model of the expansion using spherical harmonic functions. In this model the degree L_{in} and L_{out} determine the number of spherical harmonic bases and affect the results of the method. In noise-free situation, the separation and reconstruction accuracy increase as the base number increases. However, in the real situation where noise is added to the signal, the overfitting problem occurs because the statistical model describes random error or noise instead of the underlying relationship of signals. Overfitting is a serious problem in most statistical studies and thus we should control base number to avoid this problem. In order to deal with the overfitting problem, we run a simulation.

First, we simulated common brain magnetic field including motor activity (generated by a dipole with position of (0, 5, 6) cm and amplitude of (1, -1, 0)*20e-9 Am) and visual activity (generated by a dipole with position of (-8, 0, 0) cm and amplitude of (0, 0, 1)*25e-9 Am), and added sensor noise with different noise level (peak to peak value from 30 – 80 fT which covered a common sensor noise level) on it. The coordinate used in the dipole simulation is defined in Figure 2 – 2 in section 2.2.4. We reconstructed the dipole signal by SSS method with different L_{in}. Figure 2 - 12 shows the goodness of fit (GOF) as a function of L_{in}. The GOF value is defined as following:

$$GOF = 1 - \frac{\sum_{sensor} (\boldsymbol{B}_{reconstucted} - \boldsymbol{B}_{simulated})^2}{\sum_{sensor} \boldsymbol{B}^2_{simulated}} ,$$

where $\boldsymbol{B}_{simulated}$ and $\boldsymbol{B}_{reconstucted}$ indicate simulated and reconstructed signals respectively. The suffix 'sensor' indicates a sum calculation across sensors. Considering different sensor noise levels, the GOF peaks around the basis number of 10, and overfitting is occurring when the basis number is larger than 10. Thus, we choose $L_{in} = 10$ as a proper value. Also, in the application to simulated and real recorded MEG data, $L_{in} = 10$ worked well under different dipole and noise conditions, which indicates that this value is really suitable to our experiment condition.

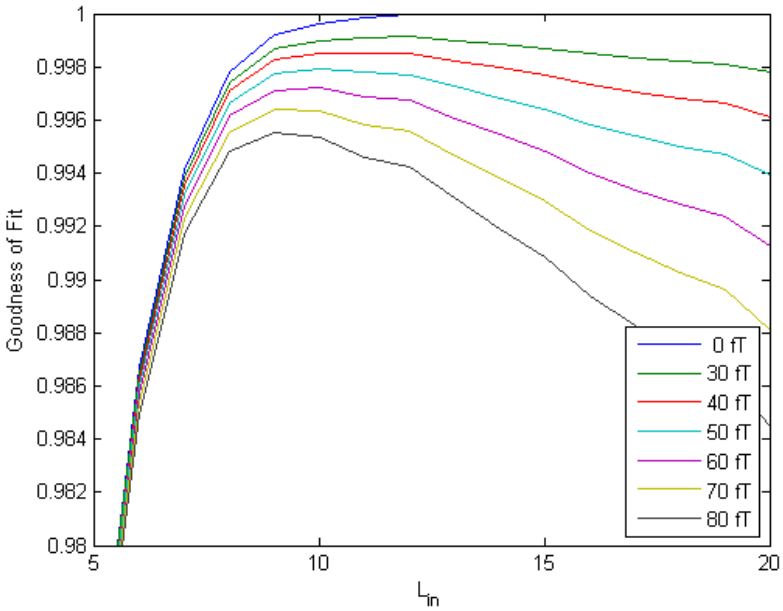

Figure 2 - 12 Goodness of fit result of reconstructed signal using SSS method with different L_{in} under different sensor noise levels.

2.4.2 Leakage problem in gradiometer system

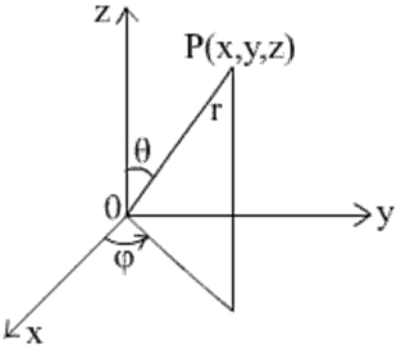

Figure 2 - 13 Relationship between spherical coordinates and rectangular coordinates.

All of SSS, tSSS and compensation tSSS method are based on the separation of internal and external space using geometry information of MEG sensors. Thus the MEG sensor configuration is the most important factor to affect the performance of signal separation. This can be explained by the properties of gradiometer and magnetometer. For magnetometer, both signals near and far from sensors can be recorded. But as a hardware method to remove environmental noise, gradiometer records the gradient of magnetic field. So interference noise which is always far away from MEG sensors is greatly suppressed by gradiometer, while internal sources which is near sensors can be preserved. Thus spherical harmonic bases corresponding to magnetometer is sensitive to both internal and external sources while gradiometer is only sensitive to internal sources. In this case, Spherical harmonic bases of gradiometer only system cannot reconstruct external signals well and this caused the leakage of signals.

The signal leakage problem can be explained more clearly by considering the angle between simulated dipoles and spherical harmonic bases $\boldsymbol{S}_{in}$ and $\boldsymbol{S}_{out}$. Here, we simulated several internal or external current dipoles with common moment $(1,1,1) * 10^{-7}\mathrm{Am}$ and different position. The internal dipoles' positions were in the same direction $(\theta = \pi/4\,, \varphi = \pi/2)$ with different r values from 0.01 m to 0.08 m with a 0.01 m interval. The external dipoles' positions were in the same direction $(\theta = \pi/4\,, \varphi = \pi/2)$ with r values of 0.25m, from 0.3m to 1m with a 0.1m interval, 1.5m and 2m. The relation between coordinates (x, y, z) and (r, θ, φ) is shown in Figure 2 - 13. In practice, a typical human brain superficial source located around a shell from 0.07 m to 0.08 m, corresponding to distances of about 2 cm – 3 cm from

the sensors to the brain activity dipoles. Thus the distances of 0.07 m – 0.08 m from head model origin to the simulated dipoles should be considered seriously. For external dipoles, all the dipoles should be considered because of the complicated interference noise condition. As $L_{in} > 10$ will cause overfitting problem, we consider $L_{in} \leq 10$ in this step.

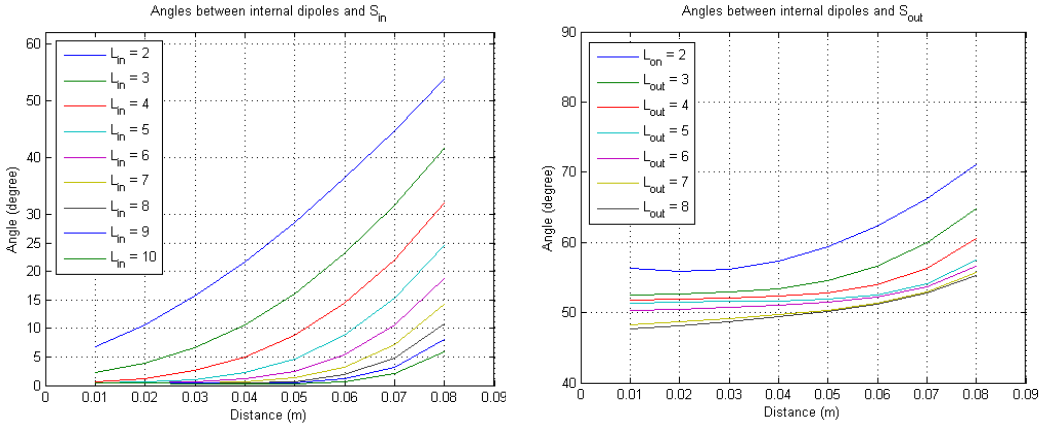

Figure 2 - 14 Angles between simulated internal current dipoles and spherical harmonic bases.

Angles between simulated internal current dipoles and spherical harmonic bases are showed in Figure 2 - 14. The angles between internal dipoles and bases Sin decrease greatly as L_{in} increases and reached a small value around 5° when $L_{in} = 10$. This also confirms $L_{in} = 10$ is the best parameter for our system, because smaller value of the angle means that internal dipoles can be reconstructed by the bases more accurately with fewer leakages. However, these angles are still greater than the corresponding angles in Nueromag 306 system which adopted both gradiometer and magnetometer. The right plot in Figure 2 - 14 illustrated the angles between internal dipoles and bases $\boldsymbol{S}_{out}$. As we try to avoid $\boldsymbol{S}_{out}$ reconstructing internal sources, the angles in this plot is the bigger the better. Angles vary very little and the average value is about 55°. In optimal case when internal source can be perfectly reconstructed, the angle between internal signal and $\boldsymbol{S}_{in}$ is 0° and the angle between internal signal and Sout is 90°. However in our system, the corresponding angles are 5° and 55° with which the signal leakage will absolutely occurred during the reconstruction.

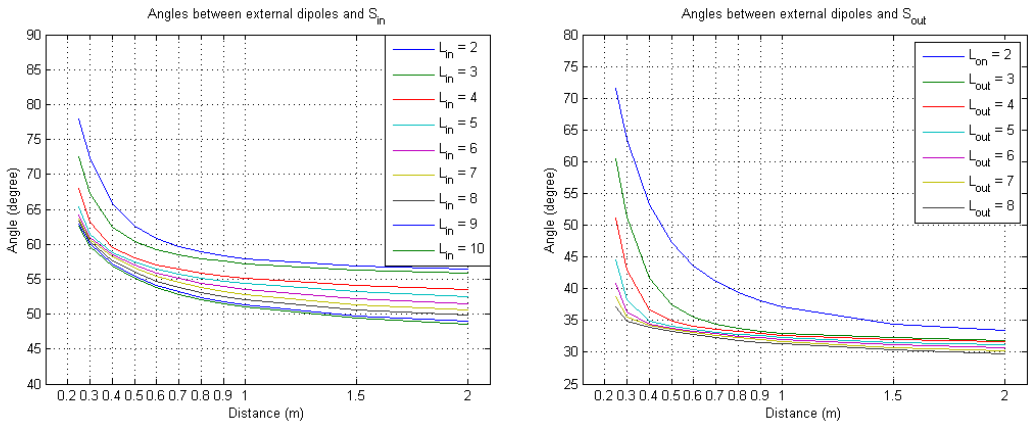

Figure 2 - 15 Angles between simulated external current dipoles and spherical harmonic bases.

The leakage of external signal is much serious as is showed in Figure 2 - 15. In optimal case, the angles between external signals and bases $\boldsymbol{S}_{in}$ and $\boldsymbol{S}_{out}$ should be $90°$ and $0°$, but actually these two angles are around $55°$ and $33°$ respectively. Comparing with the internal signal reconstruction, a more serious leakage will occur during the external signal reconstruction because of the little difference between the two angles. Moreover, intermediate signals which are located in or near sensor space will also cause serious leakage problem. Thus the leakage problem in gradiometer only system contains internal, intermediate and external signal leakages which is a more complicated problem than gradiometer plus magnetometer system.

2.4.3 Insensitivity to correlation limit δ and time-window length

In original tSSS method, there are two important parameters which should be selected very carefully. One of them is δ which is used to control the risk in the selection of common temporal patterns $\boldsymbol{L}$ of $\boldsymbol{X}_{in}$ and $\boldsymbol{X}_{out}$. The selection of δ depended on the noise level of the MEG data, so it is difficult to select a proper value. If δ is too small, only interferences with highest amplitude were rejected, while for a relatively large δ, the risk of removing brain signals would increase. The left two plots in Figure 2 - 16 showed results of original tSSS method using different δ value. As δ increases, more vectors which may hold some internal patterns are selected as common vectors and removed, thus the loss of brain activities around 12 Hz increases as δ increases. In the right two plots which indicated the results of compensation method, there is hardly any difference between different δ values. This concludes

that our compensation method is not sensitive to the value of δ, thus can be easily applied on MEG data different noise level.

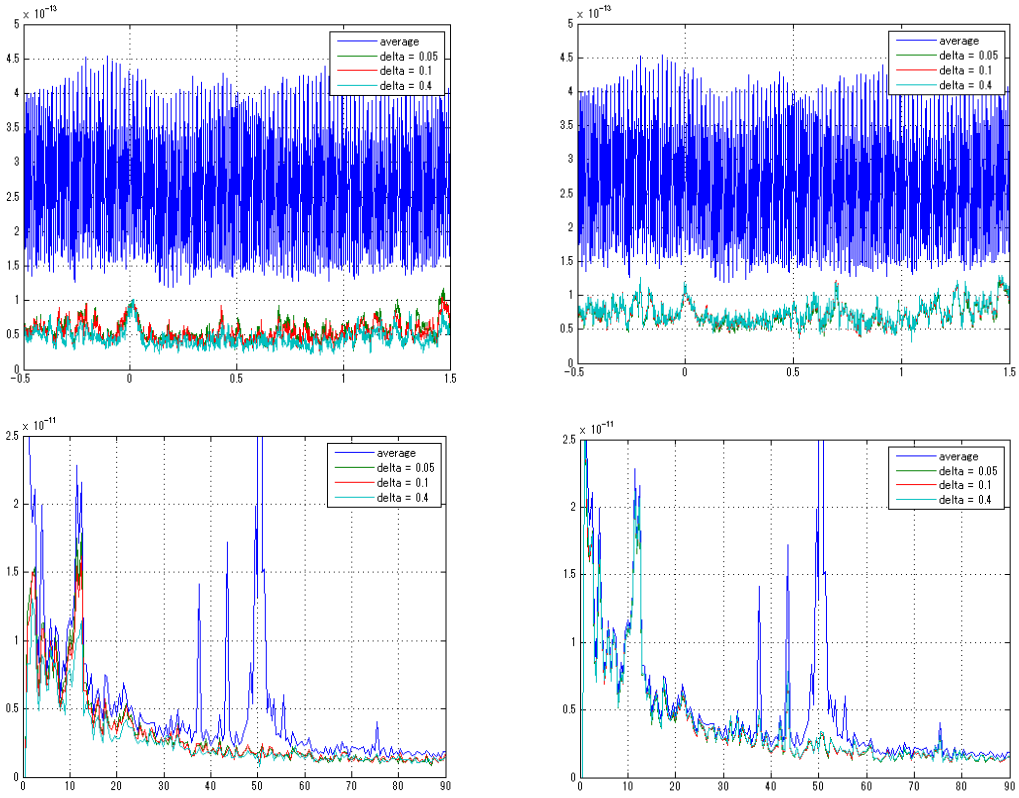

Figure 2 - 16 Results of original and compensation tSSS method with different delta values.

The left two figures illustrate the results of original tSSS method, while the right two figures illustrate the results of compensation tSSS method. Upper two are time-series and lower two are FFT results

The other parameter to which the original tSSS method is sensitive is time window length. As it is mentioned in section 2.2.3, with longer time-window length, the orthogonality is better and the common temporal patterns $\boldsymbol{L}$ is easy to be extracted correctly. However, longer time-window length means larger datasets, which will greatly increase the calculation cost. Moreover, in some experiments, we even can to get a long enough dataset. In this case, compensation tSSS method will be a possible solution which can deal with short time-window data with low calculation cost. Figure 2 - 17 showed the results of original and compensation tSSS method with different time-window length. The left two figures indicated result of original tSSS and the FFT result turns out that with short time-window length, signal loss is more serious than other case. However, in the right two figures, no difference is showed between several

time-window lengths. This concludes that compensation is not sensitive to time-window length and thus can work with small datasets.

For 440 channels data recorded with a sample rate of 1000Hz, the original tSSS calculation time of 1s-long, 2s-long and 4s-long data are 0.153 s, 0.386 s and 1.145 s respectively, while for 1s-long data, compensation tSSS data calculation time is 0.94 s. For 440 channels data recorded with a sample rate of 500Hz, the original tSSS calculation time of 1s-long, 2s-long and 4s-long data are 0.069 s, 0.149 s and 0.378 s respectively, while for 1s-long data, compensation tSSS data calculation time is 0.263 s. Considering the signal loss in compensation tSSS with 1s data is smaller than in original tSSS with 4s data, we concluded that compensation tSSS is an effective noise reduction method for our system.

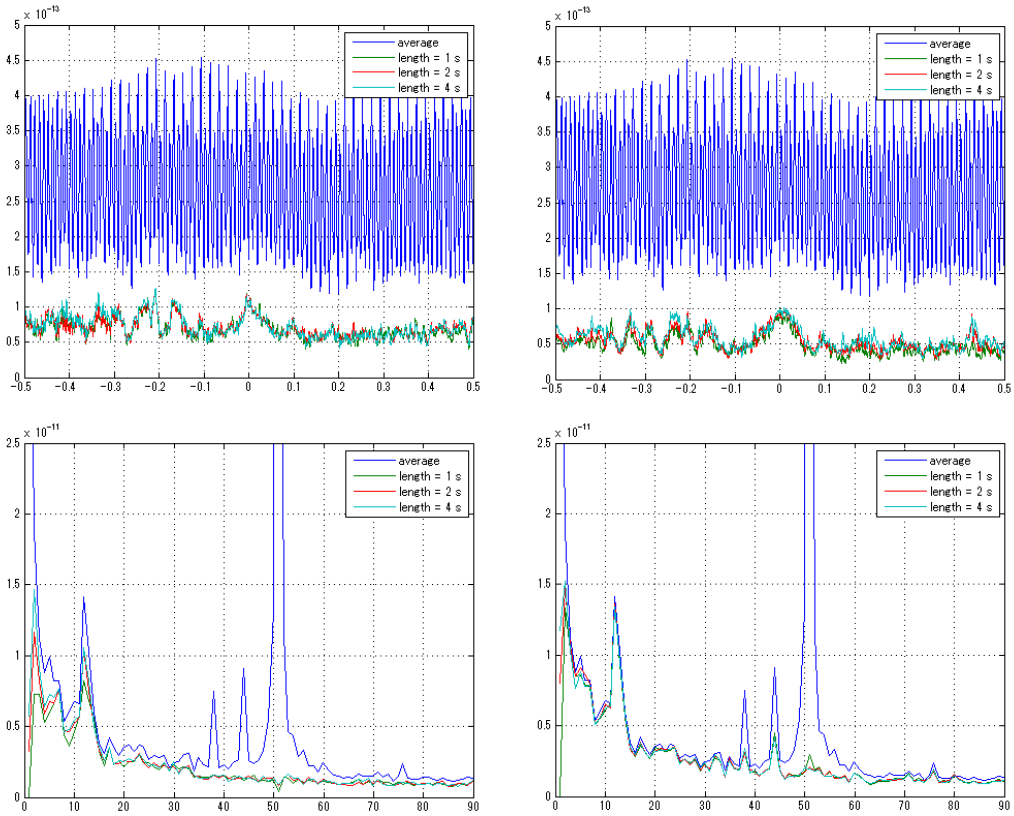

Figure 2 - 17 Results of original and compensation tSSS method with different time-window length.

The left two figures illustrate the results of original tSSS method, while the right two figures illustrate the results of compensation tSSS method. Upper two are time-series and lower two are FFT results.

2.4.4 Parameter *r* for source space judgment and the mix of signals

The only parameter which will affect the performance of compensation tSSS is the ratio for source space judgment which is given by equation 2 - 21. In optimal case, when vector is internal pattern, *r* should be much greater than 1, because the leakage reconstructed by external bases is obviously smaller than the remain part reconstructed by internal bases. On the other hand, when vector is external pattern, *r* should be much smaller than 1. However, in actual case, MEG data also contains some random noises such as sensor noise. These noises will affect the calculation of common patterns and mix internal and external patterns partly. In this case, the considered vector would contain some internal as well as some external patterns and thus make the *r* value approach to 1. In this case, it is difficult to discriminate internal and external patterns. Usually we set the threshold to 1 and it worked well in most of the conditions. All the simulation results in this chapter are calculated with a threshold of 1. But when noise level is high, it is difficult to separate internal patterns from external patterns with threshold 1. Thus it is better to adopt a smaller threshold in order to avoid recognizing internal patterns as noise. Although noise is not completely removed in this case, most of the brain activity can be preserved.

Compensation tSSS method considers the specialty of gradiometer only system and designs a special process to solve the leakage problem. In all of computer simulation, phantom simulation and the simulation with real brain signals, compensation tSSS method works well. Hardly any brain activity in the reconstruction is removed and interference noise is suppressed greatly. Compared with SSS and tSSS method, our compensation method provides very small reconstruction error and dipole fitting error. This suggests that the compensation tSSS is a valuable noise reduction method for single trial analysis in our gradiometer only system.

Chapter 3 Continuous motion related features and trajectory prediction

In this chapter, we present a feature selection method for continuous motion trajectory prediction and confirm the efficiency of compensation tSSS method in continuous motion prediction. We introduced a 1-D continuous motion task using a tool bar, and investigated whether and how the spectrum of brain activities is correlated with the continuous limb motion. From the correlation results, frequency ranges with relatively high correlation values were determined. Also, different channel selection models and time-windows selection models were adopted and the performances were evaluated by multivariate linear regression prediction. The successful prediction results indicated that even non-invasive methods can achieve accurate continuous limb motion prediction performance that is comparable to invasive methods.

3.1 Introduction

Prediction of motion trajectory using brain signals is important for controlling prosthetic devices. The spiking activity of neurons in primary motor cortex has already been proved to be highly correlated with limb movements. Recent findings employing non-invasive recording methods suggested that limb movements could also be decoded by summed results of brain activity. However, such cases mainly employed highly BCI-trained subjects or did not predict so accurately comparing with the invasive case. Thus, it has been assumed that only invasive method could decode kinematic parameters accurately.

To control external devices, prediction of motion trajectory using a subject's brain activity during arm movements is necessary. Several researchers have recently presented findings on precise movement prediction by employing brain activity measurements from invasive methods, such as implanted microelectrode arrays (Wessberg et al., 2000) and electrocorticography (ECoG) (Schalk et al., 2007). Non-invasive methods, such as electroencephalography (EEG) or magnetoencephalography (MEG), have also been introduced to acquire data for movement prediction (Georgopoulos et al., 2005). In many of the previous techniques, large datasets were necessary for the prediction (Georgopoulos et al., 2005; Schalk et al., 2007). This causes a very high load for real-time calculation, especially for continuous training procedures.

In the current study, we extracted the most suitable feature for the prediction of movement trajectory from MEG responses. Particularly, we verified an inconsistency in the frequency feature as follows: earlier MEG studies found that the responses which were filtered at a low frequency range (2-5 Hz) showed high coherence with motion trajectory (Jerbi et al., 2007), while previous ECoG and EEG studies reported that μ-wave (9-14Hz) contains the most motion information. Here we selected frequency bands, channels and time-windows based on the correlation with the subject's arm movement and found that the μ-wave around the motor area is highly correlated with the subject's arm motion. By employing these selected features, a multivariate regression method was carried out, and a high quality prediction was achieved.

3.2 Experiment

3.2.1 Visual stimulus

Visual stimuli for the guidance of arm movement were written in Matlab using the Psychophysics Toolbox extensions (Brainard, 1997; Pelli, 1997) and presented on

a screen positioned at about 1.2 m in front of the subject. The background is black with a fixation mark '+' presented in the center of the screen during the experiment procedure. A green circle is located 2 cm under the fixation mark. The experiment contains 15 blocks, and each block contains a moving session and 10 s rest time before the moving session. During the moving session, the green circle moved left and right periodically at 0.25 Hz on the background and its position scarifies the sine wave of time. In every moving session, 11 moving cycles are performed as is shown in Figure 3 - 2.

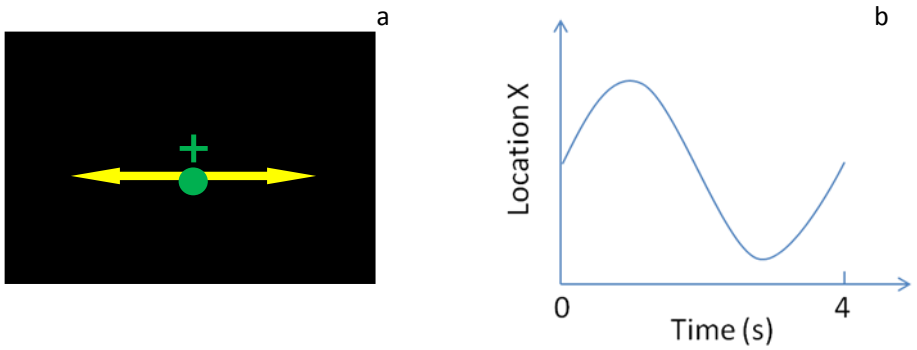

Figure 3 - 1 Visual stimuli used in the experiment.

(a) The screen and visual stimuli used in the experiment. Green '+' mark indicates the fixation point and green ball is the visual guidance. Green ball moves left and right periodically as the yellow arrows show. (b) Green ball's horizontal position to time in one cycle (epoch). Location X indicated the position of the ball. Here the start position at 0 second is the center of the screen. The ball first moves left which presented an increasing X value.

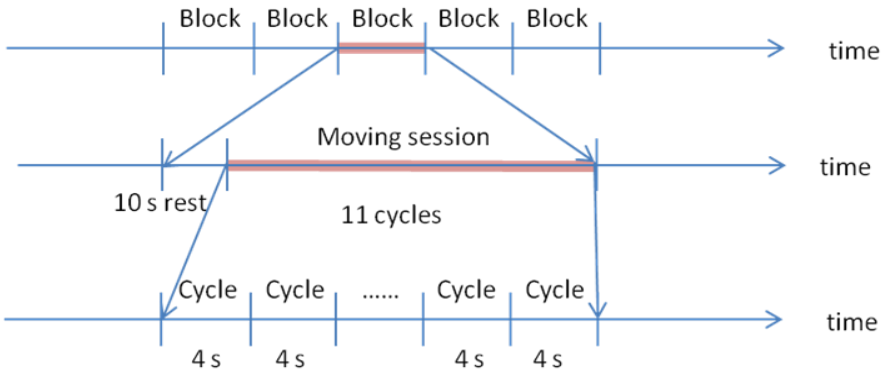

Figure 3 - 2 The task scheme performed in this experiment.

In the experiment, 15 epochs were performed. Each epoch contained a rest and a moving session. In each moving session, there are 11 moving cycles as shown in Figure 3 - 1 .

3.2.2 Experiment task

In this experiment, four right-handed male volunteers were employed. All these subjects are healthy and they have no experience of using brain computer interface (BCI). Subjects were asked to sit on the chair in MEG system and continuously manipulate a bar-shaped tool with their right hands. They were instructed to move the bar to follow the green circle while maintaining fixation on the '+' mark in the center of the screen. Eye blinking was asked to be controlled during the moving session.

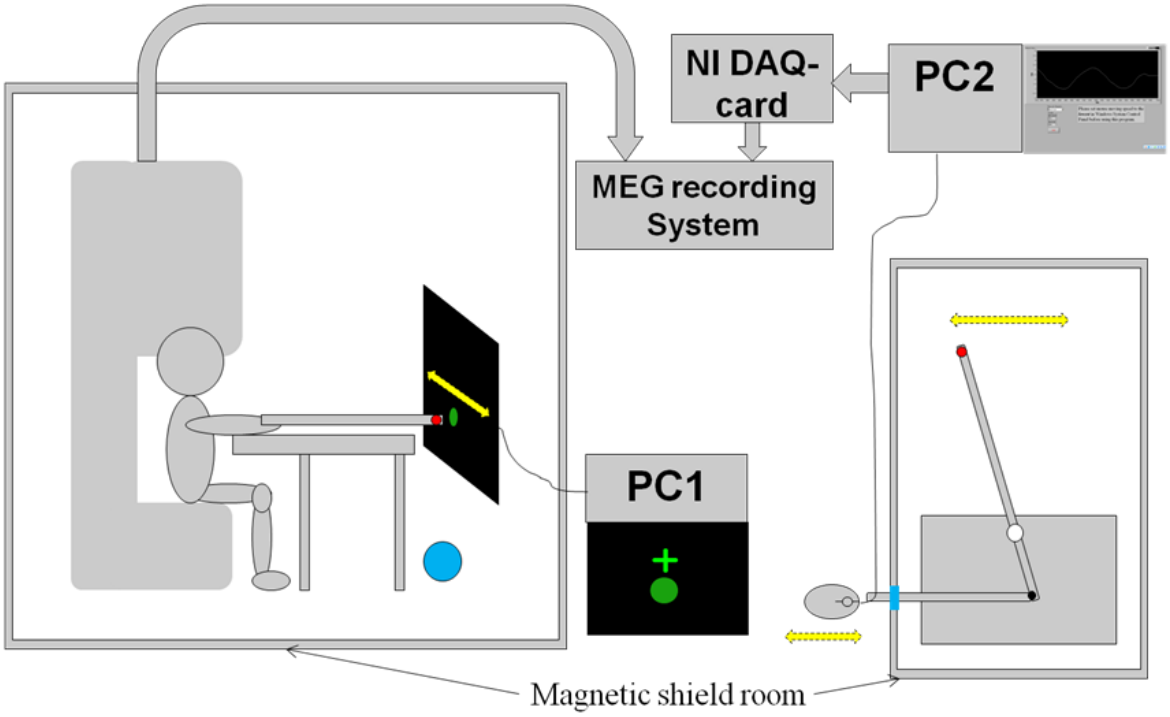

Figure 3 - 3 The experimental setups used in the task.

The left box illustrates the side view of experimental set ups including the magnetic shield room. The stimulus is generated by a Matlab script running on PC1 and projected to the screen in front of subject by a projector. The grey arrow indicates the data stream. The right box is the view from subject, which mainly indicates the motion position transferring system made of wood. In right figure, the red point is the motion position we want to record. The yellow arrows indicate the moving directions. The white point is a support point and the black point is the conjunction point. On the wall of magnetic shield room, a hole shown in light blue used to let a wooden stick pass through. A mouse connected to PC2 is tied on the stick, therefore the position of red point can be transferred to the mouse. PC2 runs a self-programmed Labview script in order to record the mouse motion and output it to MEG recording system.

Experiment set ups are illustrated in Figure 3 - 3. In order to reduce noises from electric devices, we transferred the motion position of the toolbar to the outside of magnetically shielded room and recorded the motion position using a mouse outside the magnetically shielded room. We developed a motion transfer system made of wood by ourselves. This system connects user's toolbar and the mouse with two wooden sticks. These sticks are connected at the end points and formed a lever. Then the large scale toolbar motion could be transferred to a small scale motion which can be accepted by mouse. This transferring procedure is shown in the right side of Figure 3 - 3.

3.2.3 Recordings

Movement of the near-screen end of the tool bar is considered to be consistent with arm movement. We recorded motion position of toolbar with the mouse connected to PC2 as is shown in Figure 3 - 3. In our experiment, we wish to investigate the relation between motion position and MEG signals, thus we have to record MEG signals and motion position simultaneously. In our MEG measurement system, mouse signal is not acceptable, so we developed a program using Labview software (National Instruments Corporation, Texas) in order to record and convert mouse positions into voltage signals for MEG system.

This self-made program adopted a DAQ card USB-6008 produced by National Instruments. This program running on PC2 can record real-time mouse positions as pixels on the screen, transfer them linearly into voltage values in 0 ~ 5 V and output them with a rate of 160 sample points per second. The output was connected to the external input port of MEG system and was simultaneously recorded by the MEG system. This program is one block of feedback brain science experiment system which was used to participate the 2010 National Instrument Application Contest and won a participant prize.

Both motion position and MEG data were collected using a 440 channel whole-head MEG system (Yokogawa, PQ2440R, Tokyo, Japan) at a sampling rate of 1000 Hz with an analog filter of 0.3-200 Hz.

3.3 Data analysis

3.3.1 Preprocessing

Because raw MEG signals are contaminated by electromagnetic noise interference, the spatiotemporal signal space separation (tSSS) method (Taulu and Simola, 2006; Taulu and Kajola, 2009) was applied to the raw MEG data before further analysis. tSSS is a spatial filtering method based on spherical harmonic functions and Maxwell

equations, which express MEG measurements as a linear combination of spherical harmonic functions. MEG signals can be split into brain signals and external interferences, which correspond to the inner and outer part of signals in the MEG sensor space, respectively. This procedure is proven to be effective in removing external electromagnetic noise without affecting useful brain signals (Taulu and Simola, 2006; Taulu and Kajola, 2009). It should be noted that tSSS is not time consuming, which is essential for online processing in the future.

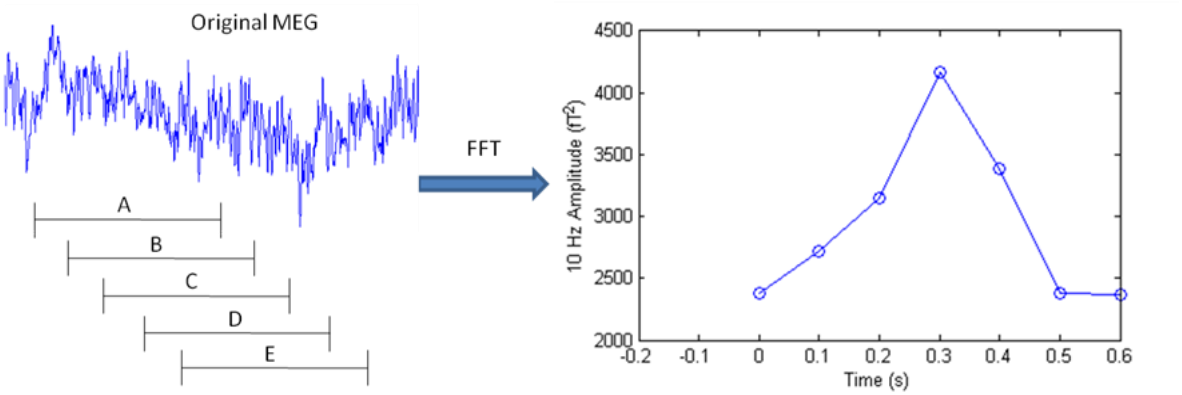

Figure 3 - 4 Schematic illustration of spectral amplitude calculation.
In the left figure, blue line indicates the original MEG data. A~E are 0.5 s time-windows sliding at a 0.1 s time interval. FFT is applied on the windowed MEG data and the right figure shows calculated spectral amplitude at 10 Hz as an example. Here the 10 Hz FFT results of time-window A~E correspond to data at 0~0.4 s in the right figure.

Different to most previous non-invasive researches, we considered and investigated motion-related features using single trial MEG data sets, without any averaging process. After applying tSSS, both MEG and arm location data were first segmented into non-overlapping 4-second epochs, each of which corresponded to 1 cycle of movement. Then, a time-frequency analysis with a 0.5 s Hanning-window was carried out at an interval of 0.1 s to get the time course of the spectral amplitudes of MEG, as is shown in Figure 3 - 4. From this process, spectral amplitudes on each frequency bands (form 1 Hz to 100 Hz, with interval of 1 Hz) were calculated and the sample rate is 10 Hz because of the 0.1 s moving window interval. In the following frequency selection, the correlation between the spectral amplitudes below 100 Hz, not the filtered time-series data, and arm movement trajectory down-sampled to 10 Hz was calculated. For the selection of channel and time-window width, not only single trial (cycle) data but also the data averaged across 5 epochs (cycles) were considered to study the improvement of prediction by increasing signal to noise ratio (SNR).

3.3.2 Multivariate linear regression and cross validation test

In the prediction of continuous motion, a multivariate regression method was applied to the processed MEG data.

$$Y(t) = \beta_0 + \sum_{\tau=1}^{p} \beta_\tau X(t-\tau) + \varepsilon(t), \qquad t = 1, \cdots, n, \qquad 3\text{-}1$$

where $Y(t)$ is the motion position at time t, and $X(t-\tau)$ is the spectral amplitude of pre-processed MEG at time $t-\tau$. Recorded MEG data were split into training and test data, and coefficients β_τ obtained from the training data were used for the prediction of the test data. We selected the best model by comparing the correlation values (r) between actual and predicted motion trajectories for the three models. To differentiate this correlation from the one mentioned in following 3.3.3.1 (correlation between spectral amplitudes and actual motion trajectories), we replace the word 'correlation' with 'prediction performance (r)'.

In order to test the stableness of the prediction, we performed a cross-validation test. We divided data set of 100 trials data into 5 segments, with 20 trials data in each segment. For each segment, 2-fold cross validation was conducted by using the first half (10 trials) as training/test and the second half (10 trials) as test/trainig, which is similar to previous research (Georgopoulos et al., 2005). Thus we performed the training-test procedure for 10 times and averaged the prediction performances. We have also tested 10-fold cross-validation using all 100 trials data, but the prediction results are much lower. This indicates that sequential data (~40 s for 10 trials data) are necessary for the motion prediction.

3.3.3 Feature selection

3.3.3.1 Frequency selection

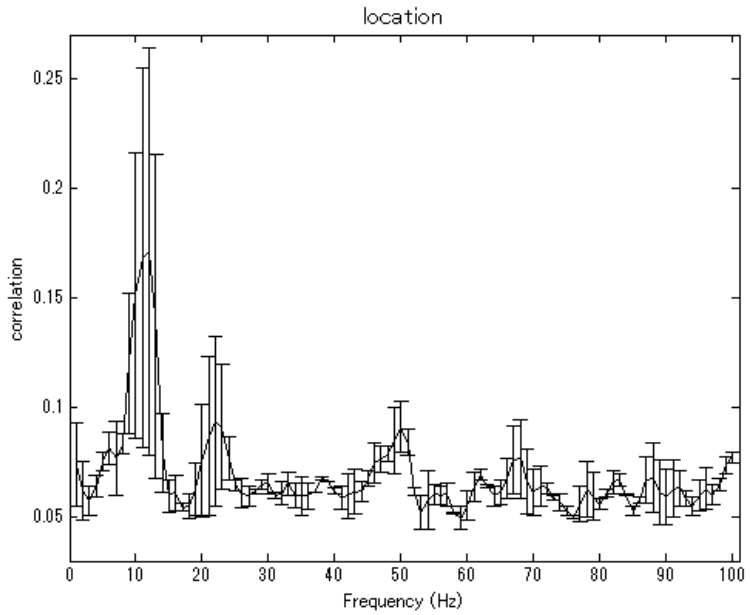

Figure 3 - 5 Correlation between actual motion position and spectral amplitudes at each frequency below 100 Hz, averaged across four subjects. MEG data from sensors over motor cortex are selected.

The black line in the center shows the average correlation value across four subjects. The error bar indicates the standard error of correlation of all four subjects.

To determine the frequency bands that are useful for the prediction of arm movement, we studied the relationship between motion and the spectral amplitude of the sensors near motor cortex. For each channel near motor cortex, we calculated the correlation between the time course of the spectral amplitude at each frequency band (1-100 Hz) and motion information, which included motion position, velocity and acceleration. Figure 3 - 5 shows the correlation at each frequency from 1-100 Hz, averaged across subjects. Here we focused on low-frequency bands (1-30 Hz), in which spectral patterns are common for all subjects. A small peak was found around 50 Hz, but we didn't consider this peak because the peak was found only in Subject A. Subsequently, statistical measurements across the channels located near motor cortex were used to extract motion related features. The spectral amplitude signals that correlated with actual movement were selected, and data in the selected frequency bands were employed during the following analysis. From the final prediction performances, the most appropriate frequency band was confirmed.

3.3.3.2 Channel selection

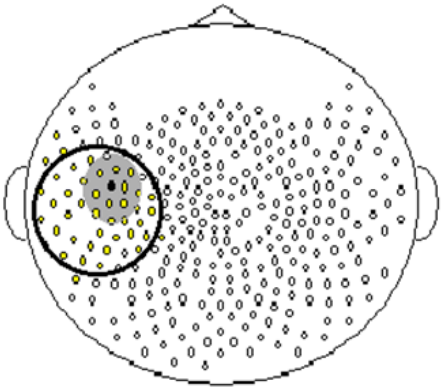

Figure 3 - 6 Example of channels in the three models.

Model I includes only one channel with maximum correlation value to motion parameters. It is indicated by the black dot located in the center of left hemisphere. Model II involves channels in the grey area. Model III contains channels indicated with yellow color inside the black circle.

Channels located near the contralateral motor cortex (left hemisphere as the subjects performed the task with their right hands) were selected because brain responses related to motion position mainly originate there. Three models of channel selection were employed for both single-trial and 5-epoch-average data: Model I used a single channel with the highest correlation value; Model II consisted of 14 channels around the highest correlation channel; and Model III involved 43 channels near motor cortex. The spectral time courses averaged across the selected channels were low-pass filtered at 1 Hz and used for the prediction. Here, in Model II, the correlation value between spectral amplitudes of channel in Model I and its surrounding channels were calculated first. Then surrounding channels with correlation value over 0.7 were selected as the channels used in Model II. In Model III, channels with index number of 128~191 were considered as channels near motor cortex. Finally, we used only the axial gradiometer among them and removed all bad channels which have large noises or strange signals.

3.3.3.3 Time-window selection

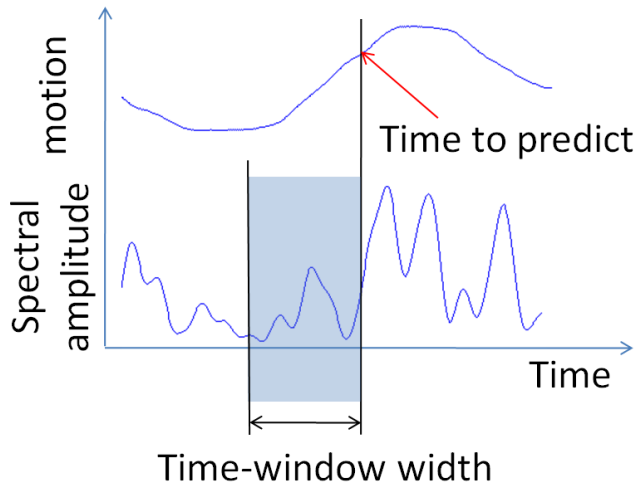

Figure 3 - 7 Model of time-window selection.

The red arrow points the motion data to predict. The area with light blue color shows the time-window used in prediction. Note the spectral amplitude is the averaged data of selected frequency bands across selected channels.

Most researches used MEG signals several hundred milliseconds just before motion to be predict. However, in periodic continuous motion, the mechanism might change to some extent, thus we have to investigate and determine the proper time-window width by ourselves. To achieve the best prediction, different time-window widths (one sample point as one feature) and training dataset numbers were considered in the regression coefficient training procedure. From the training result, the coefficients β_τ could be determined and by applying them to the test data set, the prediction performance could be calculated. The appropriate time-window width providing the best prediction could be determined by considering the prediction performance on test data set.

3.3.4 Comparison of predictions using tSSS and compensation tSSS

In Chapter 2, we discussed the effectiveness of compensation tSSS method for our system. In order to verify this fact in real application, we also applied this method here instead of tSSS method, and compared the differences of the prediction results.

In this procedure, instead of tSSS, compensation tSSS method was first applied on

raw MEG data before other preprocessing. After this, all the data processing procedure of these two cases are similar.

After the prediction of both these two cases, the statistics of prediction performances are listed and the differences of these two cases are discussed.

3.4 Results

3.4.1 Frequency selection (Spectral feature)

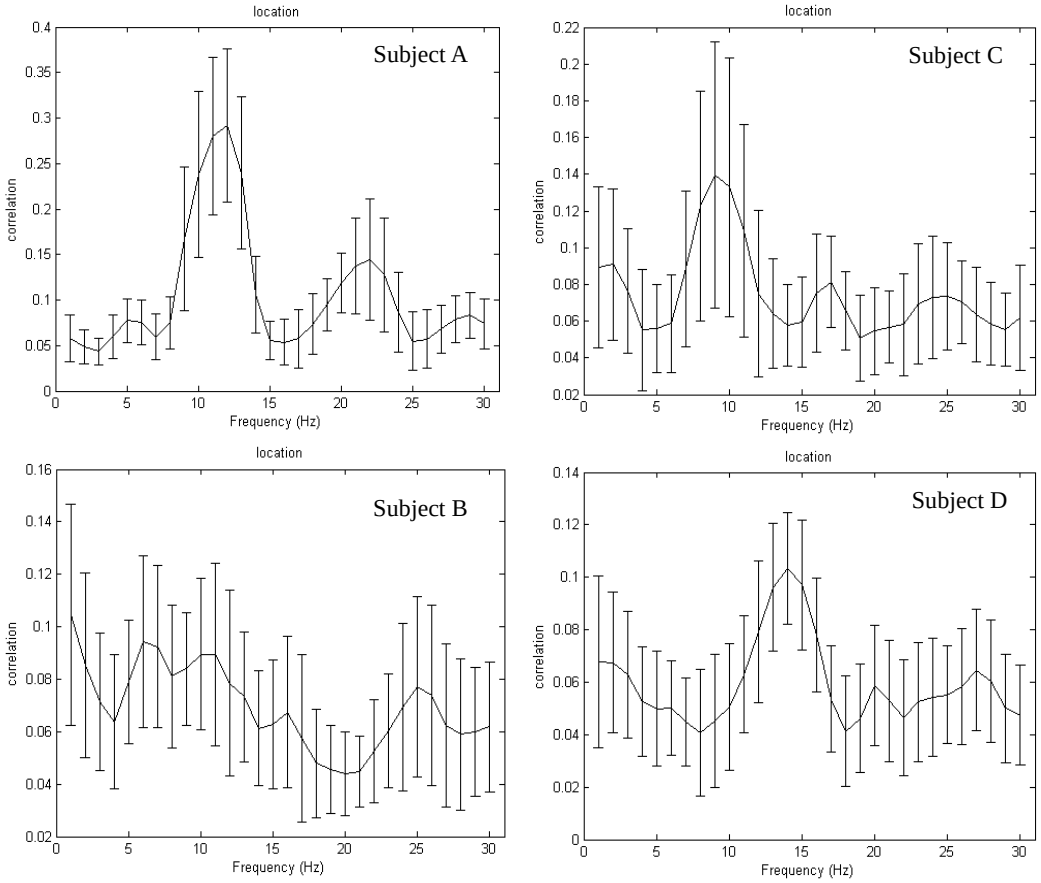

Figure 3 - 8 Correlation between actual motion and the spectral amplitudes of MEG from sensors over motor cortex, for each subject.

In each figure, the black line is the average correlation value of selected channels over motor cortex. The error bar is the standard error value of selected channels. Here, we focus on low frequency band and show frequency below 30 Hz.

Figure 3 - 8 shows examples of the correlation between motion position and spectral amplitudes of MEG measured from sensors near the motor cortex. Three subjects (A, C, D) showed a correlation result with three peaks: two prominent peaks

around 9-14 Hz and 20-26 Hz and a small peak around 3-7 Hz (subjects A and D). This finding indicates that these frequency bands contain a relatively large amount of information about motion position. Moreover, these frequency bands correspond to μ-wave (9-14 Hz), β-wave (20-26) and δ-rhythm (3-7 Hz), which are all frequency bands related to motion. This is similar to the previous studies with ECoG (Miller et al., 2007; Schalk et al., 2007) and EEG (Wolpaw and McFarland, 2004). One subject (B) showed less prominent peaks, but the peak frequencies were similar to the other subjects.

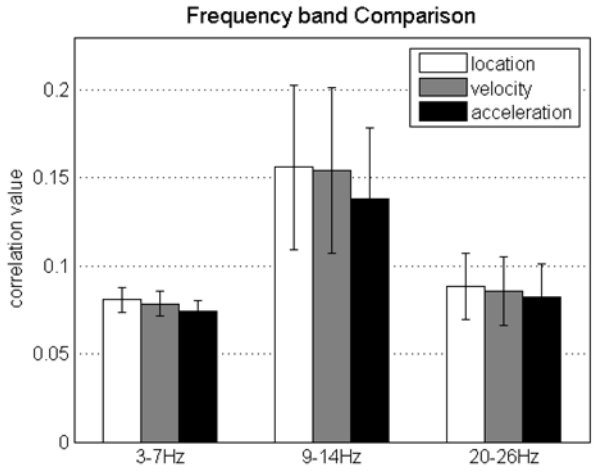

Figure 3 - 9 Correlation between motion parameters (motion position, velocity and acceleration) and the spectral amplitudes of different frequency bands, averaged across four subjects.

White, gray and black color bars indicate results of motion position, velocity and acceleration respectively. 3-7 Hz, 9-14 Hz and 20-26 Hz indicate correlation results between motion parameters and spectral amplitudes of corresponding frequency bands. The error bars are the standard errors of four subjects.

Figure 3 - 9 illustrates the correlation between motion parameters (motion position, velocity and acceleration) and spectral amplitudes, averaged across all subjects. Error bars indicate the standard error across subjects. In two-way repeated measures ANOVA results, a significant main effect of frequency band was shown ($F(2, 6) = 6.17$, $p < 0.05$). The multiple comparison results showed that frequency band 9-14 Hz has a significant higher correlation value than frequency band 20-26 Hz ($p < 0.05$). No significant difference between frequency band 9-14 Hz and 3-7 Hz ($p > 0.05$). Considering many previous researches have confirmed that μ-wave played an important role the motion prediction (Wolpaw and McFarland, 2004; Schalk et al.,

2007), we choose frequency band 9-14 Hz rather than 3-7 Hz as our frequency feature.

3.4.2 Channel selection (Spatial feature)

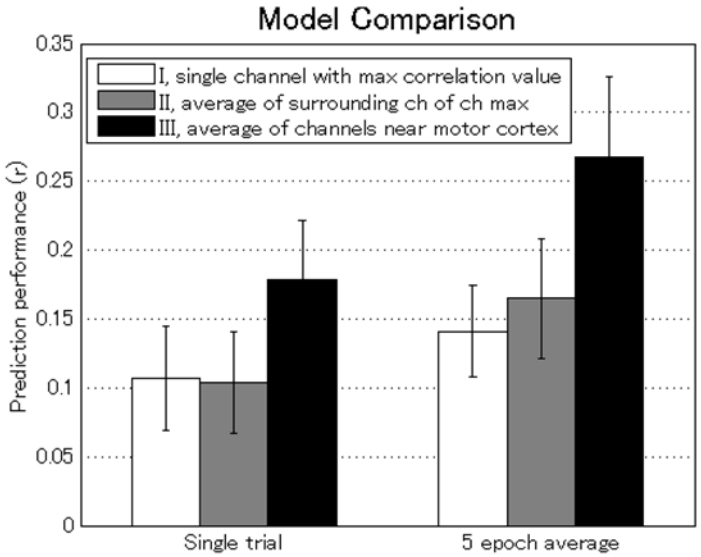

Figure 3 - 10 Prediction performances of the three models.

White, grey and black color bars correspond to prediction performance using Model I, II and III. In x axis, 'single trial' means single trial MEG data used in the prediction and '5 epoch average' indicates 5 epoch averaged MEG data used in the prediction. The error bar is standard error of results of four subjects.

After this analysis, we selected the 'max channel' with the highest correlation value at 9-14 Hz in the contralateral motor cortex (the black dot in left hemisphere shown in Figure 3 - 6). Motion location was predicted by using the 9-14 Hz power data from the following models: Model I, max channel only; Model II, averaged across channels around the max channel; and Model III, averaged across channels near motor cortex. Figure 3 - 10 shows the prediction performance comparison of the three models. Error bars indicate the standard error across subjects. Here, both single-trial and 5-averaged-epoch condition suggested that model III showed the highest prediction performance. A two-way repeated measures ANOVA found a significant main effect of channel selection model ($F(2,6) = 10.5$, $p < 0.05$), and the multiple comparison results showed that prediction performance of model III was significantly different compared to the other two ($p < 0.05$). Thus, the average over all motor channels was found to provide the best prediction performance.

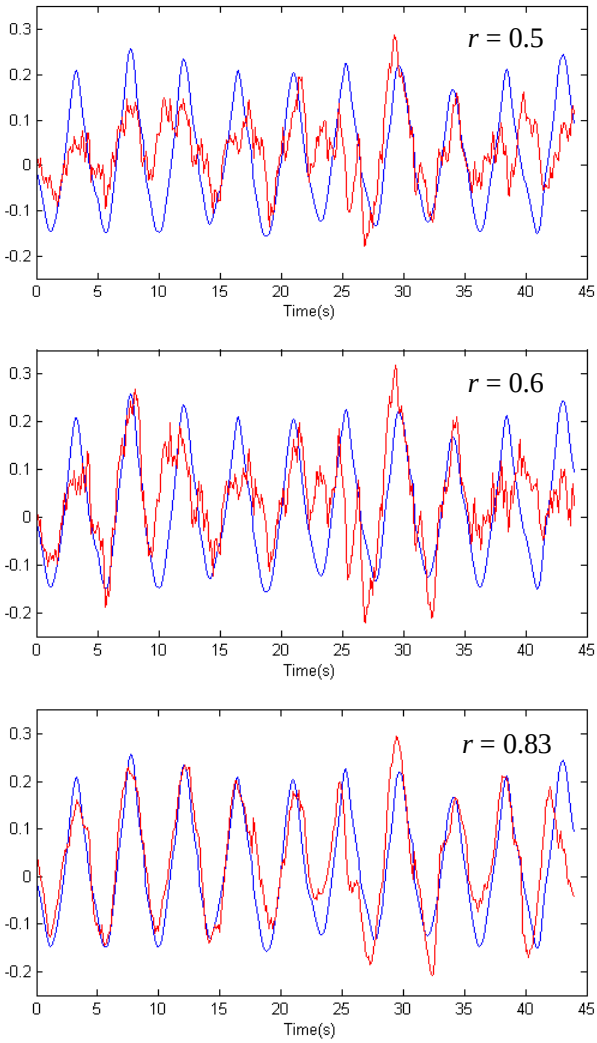

Figure 3 - 11 Typical examples of actual (blue) and predicted (red) motion trajectories with different prediction performances (*r*), for Subject A.

Figure 3 - 11 shows an example of the actual motion trajectory and its prediction with the three different channel selections. Graphs in the upper, middle and lower panels show the result of Model I, II and III, respectively, for subject A. From upper to lower graph, the prediction performance increases. When the prediction performance is 0.5, the predicted motion trajectory is noisy and different to real motion trajectory sometimes. When it improves to 0.6, the predicted line is less noisy and much similar to real one. When it improves to 0.83 as is shown in the lower graph, the predicted line is very smooth, suggesting very little noise, and the predicted and real motion trajectory are very similar.

3.4.3 Time-window selection (Temporal feature)

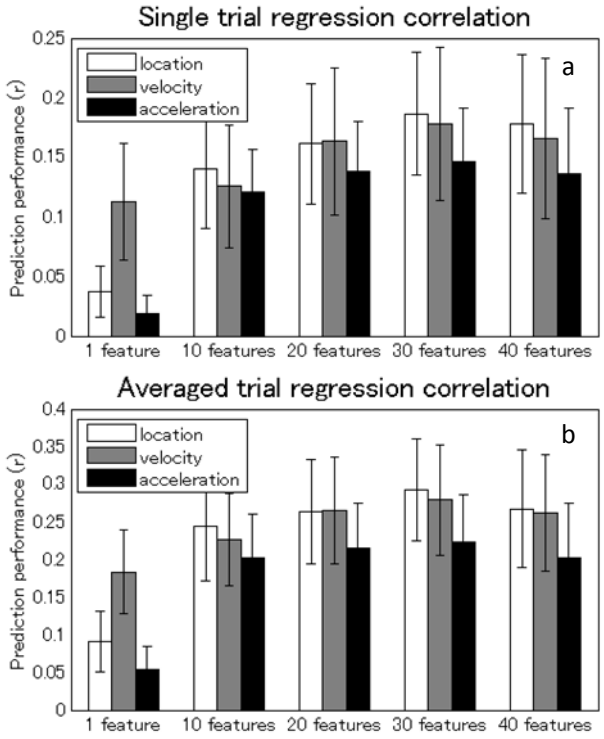

Figure 3 - 12 Prediction Performances using different feature numbers.

The upper graph illustrates prediction performance statistics using single trial MEG data. The lower graph illustrates prediction performance statistics using 5 epoch average MEG data. White, grey and black color bars are results of motion position, velocity and acceleration respectively. In x axis, 1 feature means the time-window width is 0.1s, 10 features means a 1s time-window width, and so on. Error bars are standard errors of four subjects.

The performances of regression prediction are displayed in Figure 3 - 12 (**a**, results of single trial data; **b**, results of average data across 5 epochs). Error bars indicate the standard error across subjects. In both predictions using single trial data and using averaged data from 5 epochs, the statistics of all subjects' prediction performances are illustrated in Figure 3 - 12. For both single trial and averaged data conditions, prediction performances showed similar tendency, improved with the feature number and saturated at about 30 features (30 sample points) regardless of motion location, velocity or acceleration. Thus in the following prediction, we used 30 features for the prediction of location. As the prediction procedures are similar to all these three types of motion, we focused on the motion trajectory prediction without

talking about velocity and acceleration prediction in detail.

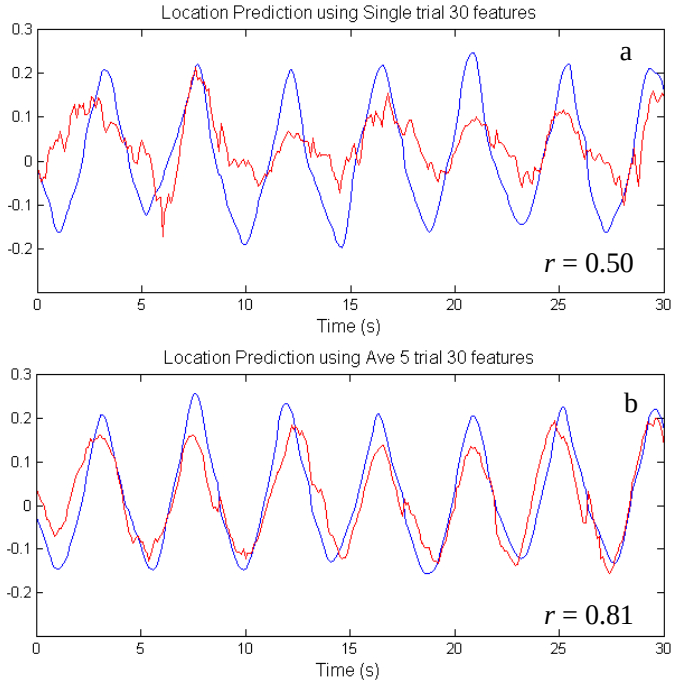

Figure 3 - 13 Examples of actual (blue) and predicted (red) motion trajectory using 30 features

a. prediction and real motion trajectories using 30 features of single trial MEG data. The prediction performance value is 0.50. b. prediction and real motion trajectories using 30 features of 5 epoch average MEG data. The prediction performance value is 0.81. Frequency band selection and channel selection are the same as discussed in the former two sections.

By employing these feature numbers in the prediction procedure, examples of movement trajectory prediction for a typical subject A are illustrated in Figure 3 - 13 (**a**, result using single trial data; **b**, result using 5 epochs averaged data.). Blue lines indicate actual motion trajectories while red lines indicate predicted motion trajectories. In subject A's results, 5 epochs averaged data provides a higher prediction performance than single trial data, indicating data with higher SNR could predict motion better. Considering the prediction performances of all subjects, the prediction performances showed similar result that averaged data (average $r = 0.36$, $p < 0.001$) provides a higher prediction performance than single trial data (average $r = 0.23$, $p < 0.001$).

3.4.4 Training data set determination

The training data set size also affects prediction performance. When training data set is small, we have the overfitting problem in which the model becomes relatively complex as there is not enough effective information. We considered different size of training data set from 1 trail to 20 trials for selected model mentioned in previous sections. The results in Figure 3 – 14 showed that the performance saturates at around 10 trials so that we adopted the training data size of 10 trials.

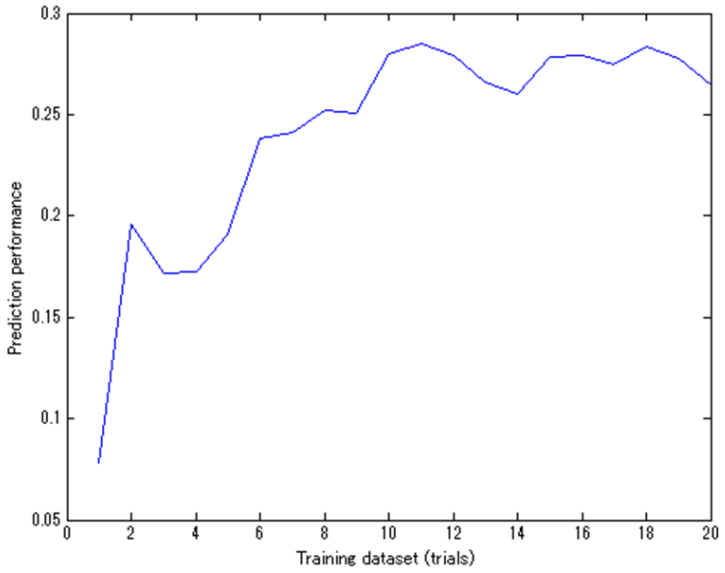

Figure 3 - 14 Prediction performance with different training data sets.

3.4.5 Comparison of tSSS and compensation tSSS

Table 3 - 1 lists the best prediction performance using feature selection methods mentioned in former sections. All processes are the same except the noise reduction method in preprocessing procedure. Two aspects are considered: single trial or 5 epoch average MEG data sets; tSSS or compensation tSSS method as noise reduction method before preprocessing. For single trial data case, the prediction performance of tSSS is 0.23 ± 0.14 (mean ± standard deviation (SD), across all subjects) which is a rather poor value, while the one of compensation tSSS is 0.32 ± 0.14 which is an acceptable performance. For 5 epoch average data case, the prediction performance of tSSS is 0.36 ± 0.40 which is a good prediction performance, while the one of compensation tSSS is 0.59 ± 0.27 which is much better than tSSS. Two-way repeated measures ANOVA found a significant main effect of noise reduction method ($F(1,3)$ =

22.3, $p < 0.05$), indicating that prediction using compensation tSSS method performed significantly better than that using tSSS method. This result confirmed that compensation tSSS method could provide a higher signal to noise ratio than tSSS method on our MEG system, thus motion related information is easier to be extracted. In the ANOVA results, no significant main effect of average method was found ($F(1, 3) = 3.92$, $p > 0.05$), indicating that prediction using averaged data has no significant difference to single trial data. This may because of the variety of prediction performances of all subjects on current data sets.

Table 3 - 1 Comparison of prediction performance results using tSSS and compensation tSSS method. Results of both single trial and 5 epoch average cases of all subjects are listed below (mean ±SD).

Data	**tSSS**	**Compensation tSSS**
Single trial	0.23 ± 0.14	0.32 ± 0.14
5 epoch average	0.36 ± 0.40	0.59 ± 0.27

The prediction result examples are illustrated in Figure 3 - 15. After performing tSSS method, the prediction performance using selected features is 0.16 (subject A). In upper graph of Figure 3 - 15, hardly any motion pattern is well predicted in the first half part of the motion, in the second half of the motion, only sometimes predicted motion trajectory is similar to real motion. While using compensation tSSS method, the prediction performance improved to 0.3. In the comparison of predicted and real motion trajectories, the first half does not change comparing to tSSS case. However in the second half, predicted motion is very similar to real motion which suggesting a good prediction. Thus from both the statistics of prediction performance and predicted motion trajectories, the results of compensation tSSS are better than tSSS method.

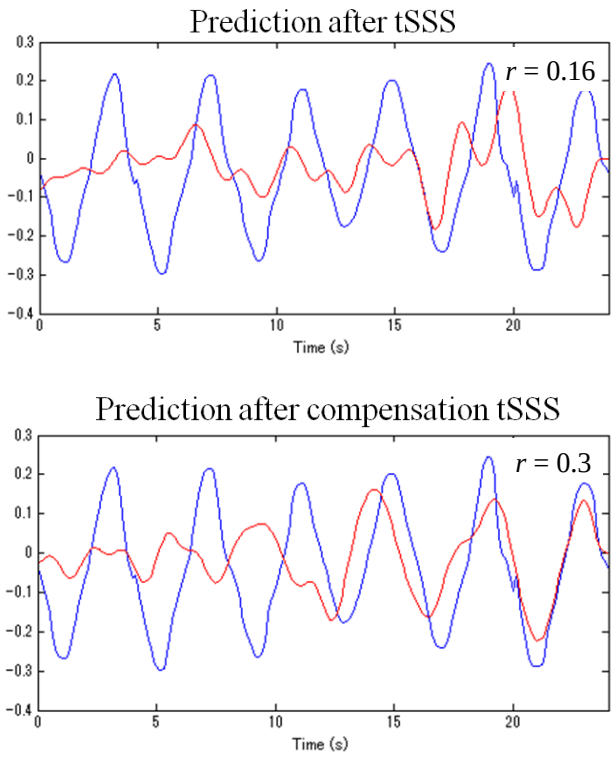

Figure 3 - 15 Prediction results of subject C using single trial MEG data after applying tSSS or compensation tSSS method.

Upper graph is result using tSSS method before preprocessing. Lower graph is result using compensation tSSS method as noise reduction method. Blue line and red line are corresponding to real and predicted motion positions. *r* in the right upper position of each graph is prediction performance which suggesting the similarity of predicted and real motion position.

3.5 Discussion

3.5.1 Overfitting in feature selection

In channel selection, we tested three models with changing the number of channels, but it should be noted that the data are averaged across sensors, and the feature number is fixed across the three models. Here we tested channels over contralateral motor cortex instead of all the channels. This is because we were trying to improve prediction performance by using the features related to the real motion. Specifically, we tried not to use signals related to visual motion processing by restricting the sensors to those around motor cortex. We used previous knowledge that contralateral motor cortex is activated during motion. Since subjects used right hand, channels around left motor cortex are considered. The analysis basically shows that

increasing the number of channels around the motor cortex improved prediction performance. This is because signal to noise ratio is increased by increasing the number of sensors averaged.

In time-window selection, five models were tested with changing the number of used features. As is shown in Figure 3-12a, the prediction performance of motion position, velocity and acceleration using single trials data peaks at around the feature number of 30. The same tendency was observed in the averaged data case, as is shown in Figure 3-12b. The reason for the decrease in prediction performance for the feature number of 40 is that the model focuses not on general pattern but on the too much detail of training data. The feature number which has the highest prediction performance provides the proper time-window length which indicates a model with suitable complexity. Thus we used the time-window size of 30 to solve the overfitting problem.

3.5.2 Motion related features

Earlier studies found that MEG responses filtered at low frequency ranges (2-5 Hz) showed high coherence with motion trajectory (Jerbi et al., 2007). In the current study, we considered the spectral amplitude rather than the filtered MEG signals and found that not only a similar frequency band (3-7 Hz) but also two additional frequency bands (9-14 Hz and 20-26 Hz) were correlated with motion trajectory. Our results suggested that μ-wave (9-14 Hz) contains the most motion information for every subject, which is consistent with previous ECoG and EEG studies (Wolpaw and Mcfarland, 1994). Although an EEG study employing trained subjects reported that 20-26 Hz activity was also useful for motion prediction (Wolpaw et al., 2003; Wolpaw and McFarland, 2004; Mellinger et al., 2007; Yuan et al., 2010), the prediction of motion trajectory using this frequency band was not successful in our case. This might result from the fact that we used untrained subjects, but further investigations are necessary. The peak at the low frequency band (3-7 Hz) demonstrated that non-invasive MEG findings, by considering spectral amplitude, are consistent with a former ECoG study (Miller et al., 2007).

The most appropriate number of features was found to be 30 for all of location, velocity and acceleration, which correspond to 3 s data because the spectrum amplitude was calculated using a 0.1 s sliding time-window. We concluded that for continuous motion, long duration brain activities at 9-14 Hz might contain more information and provide better predication than short duration activities. Contrary to our results, a previous MEG study predicted joystick trajectory by using only 20 ms MEG data before the motion. Although we applied very different features, our prediction was comparable to their prediction but with significantly fewer features (4960 features vs. 30 features). Therefore, our method could greatly reduce the

calculation cost in regression training and reduce the risk of overfitting problem, which is vital for real-time closed-loop prediction.

In compensation tSSS case, the prediction performances are higher than tSSS case for all subjects, both on single trial and 5 epoch average data sets. This suggests that using compensation tSSS method, our feature selection method worked better under current MEG measurement condition. Comparing with tSSS method, compensation tSSS could not only further remove external noises, but also recover useful brain activity patterns. Thus the noise levels are lower and brain activities are larger in compensation tSSS results than in tSSS results. It is the lower noise level and the larger brain activity that improved the SNR. With more information of motion patterns, the prediction performance could surely be improved. This result further confirmed that compensation tSSS method is a more efficient noise reduction method than tSSS method for our gradiometer only MEG system. Regardless to noise level (single trial or 5 epoch data), compensation tSSS could improve the prediction performances, which indicated compensation tSSS method could work well under different noise levels.

The current study demonstrated that μ-wave of MEG contains information that is necessary for the prediction of arm trajectory. By extracting μ-wave brain activity around the motor cortex, we could reduce the effect of the contaminating environmental noise and improve the trajectory prediction performance. Although the single trial prediction performance is not so good, the prediction performance using 5 epochs average data demonstrated the possibility of a high-quality non-invasive BCI.

Chapter 4 Subject-dependent features in continuous motion

In Chapter 3, we revealed the motion related MEG features and achieved good prediction on 5 epoch averaged data. In Chapter 4, we reconsidered the experiment in Chapter 3 and investigated correlation between motion trajectory and MEG spectral amplitudes below 100 Hz for each subject. Compared with the fixed frequency band (9~14 Hz) used in Chapter 3, subject-dependent frequency band based on the correlation between spectral amplitude and motion offered a better prediction performance. The combination of subject-dependent two or three frequency bands further improved the prediction performance, and we could achieve a good single-trial prediction (r = 0.47) with few features. These results suggest that non-invasive study can predict as efficient as invasive studies.

4.1 Introduction

Continuous motion predictions have already been performed by several non-invasive studies and most of them used time-series (Georgopoulos et al., 2005) or pre-determined frequency bands (Wolpaw and McFarland, 2004). These researches mainly focused on the prediction itself and lacked the analysis of extracting more proper features. Thus the feature number in non-invasive case was always large and prediction training was time consuming. Furthermore, prediction using a large feature number has a high risk of causing overfitting problem. In this case, although we could get a good prediction on training data sets, the prediction on long time testing data set will not be stable. In Chapter 3, we have developed a feature selection method based on correlation values between motion and spectral amplitudes and performed a good continuous motion trajectory prediction. However, these predictions were well performed on only the 5 epoch average data for most of the subjects. Even using compensation tSSS method, the prediction value is only acceptable, but not well enough in the single trial data case. One reason is that fixed frequency range is not proper for every subject because of the differences between subjects. The other reason is that although the selected feature is highly motion related, other motion related frequency ranges may exist depending on different subjects. These problems need to be further considered to improve prediction performance.

In this chapter, we investigate correlation between motion position and spectral amplitude below 100 Hz again and focus on different features for each subject. Here, subject-dependent features lay in several frequency bands ranged from low frequency δ to high γ bands were extracted by our feature selection method and were applied in motion prediction. Also, we try to combine several subject-dependant features to further improve the single trial prediction performance. By using combination of subject-dependent features, efficient single trial prediction is achieved.

4.2 Method

4.2.1 Participants

Four right-handed male volunteers participated in the experiment after given informed consent about their risks and tasks in the experiment. All these subjects are healthy and they have no experience of using brain computer interface (BCI) devices. Just before the experiment, every subject practiced tasks and how to use the toolbar for about 15 minutes.

4.2.2 Task design

We used the same task design as mentioned in Chapter 3. Totally 11 motion sessions were included in the whole task and 10 seconds resting sessions were added between each two motion sessions for performing eye blinking. Below a fixation mark '+' in the center of screen, a green ball continuously moving left and right at 0.25 Hz was presented during the motion session. Subjects were instructed to move the bar to follow the green circle while maintaining fixation on the '+' mark in the center of the screen.

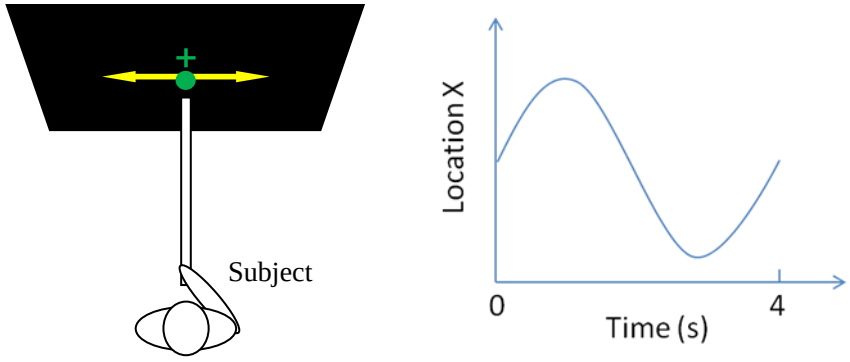

Figure 4 - 1 The experimental set up used in the task.
The left figure illustrates the experimental design. The right figure indicates the position of green ball shown on the screen.

4.2.3 Motion trajectory and MEG recording

Brain magnetic fields were recorded by a whole-head MEG system comprising 440 gradiometers (Yokogawa, PQ2440R, Tokyo, Japan) located in a magnetically shielded room. The sampling rate was 1000 Hz, and the signals were bandpass filtered between 0.3 and 200 Hz before digitalizing and recording.

Continuous motion information was transferred to a mouse outside the magnetic shielded room by a self-made transferring system made of wood. We programmed an application using Labview software (National Instruments Corporation, Texas, USA) to record mouse information and output it into MEG system as voltage signals. This voltage motion information was then recorded simultaneously by our MEG system with a sample rate of 1000 Hz.

4.2.4 Data analysis

In this experiment, we focused on frequency features, thus we kept channel selection and time-window selection method the same as is mentioned in Chapter 3. All the results are calculated after applying tSSS method if it is not specified as using compensation tSSS. For frequency characteristics, we reconsidered correlation between continuous motion and spectral amplitudes of MEG. In order to extract more motion related features, spectral amplitudes at each frequency below 100 Hz were investigated in this experiment. For each subject, several frequency bands with relatively high correlation values were selected and regarded as subject-dependant motion related features. These subject dependant features were then adopted in the following continuous motion trajectory prediction.

Then, we considered three motion related feature selection models: (1) fixed frequency band (9~14 Hz) mentioned in the former chapter; (2) main subject-dependent frequency band around 9~14 Hz; (3) combination of several subject-dependent frequency bands. For each subject, spectral amplitudes in these three models were averaged across channels near motor cortex, and 3s-long spectral amplitude data (30 features for each frequency band) was used in the multivariate linear regression method to predict motion trajectory. The multivariate regression formula is shown as follows:

$$Y(t) = \beta_0 + \sum_{i=1}^{N} \sum_{\tau=1}^{p} \beta_{i,\tau} X_i(t-\tau), \qquad t = 1, \dots, 30, \qquad 4\text{-}1$$

where $Y(t)$ is motion position at moment t, $X_i(t-\tau)$ is the τ-th feature in the i-th frequency range and $\beta_{i,\tau}$ is the regression coefficient of feature $X_i(t-\tau)$.

In this experiment, we adopted single trial data as the test dataset and performed the prediction of different models. Here, we performed a cross-validation test similar to the one mentioned in chapter 3 and the prediction performances were evaluated by the correlation between real and predicted motion trajectories.

4.2.5 Comparison of predictions using tSSS and compensation tSSS

Similar to Chapter 3, both tSSS method and compensation tSSS method were applied on raw MEG data before feature selection and prediction. Other processing are exactly the same. To testify the effectiveness of subject-dependant feature selection method, the results in this chapter were compared to the prediction results in Chapter 3 using fixed frequency band. Also, the results here are compared between

tSSS and compensation tSSS cases in order to check the effectiveness of compensation tSSS method and the stableness of the subject-dependant feature selection method.

4.3 Results

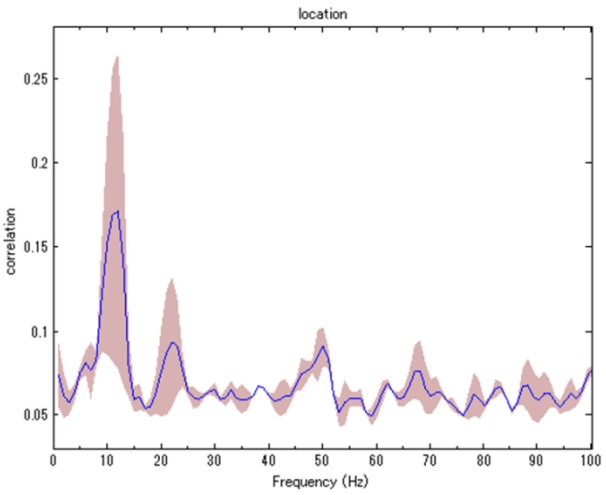

Figure 4 - 2 Statistics of correlation values between continuous motion position and spectral amplitudes of MEG data over motor cortex, averaged across all subjects.

The blue line in the plot is the average correlation value across 4 subjects and the dark red area shows the standard error of the correlation value. The correlation values are first calculated for each frequency and for each channel over motor cortex, and then averaged across channels.

The averaged correlation values across all subjects were shown in Figure 4 - 2. Several peaks which are related to motion position can be recognized from this figure. These peaks range from μ-rhythm, β-rhythm to several γ-bands. Among them, μ-rhythm around 9~14 Hz is a common frequency band with the highest correlation values, which is mentioned in the former chapter. The β-rhythm around 18~24 Hz is also a common frequency band with high correlation value as is mentioned before. Moreover, several γ-bands such as 45~50 Hz and 65~70 Hz presented a relatively high correlation value in the averaged plot. As these frequency bands are not common features of all subjects, they might play an important role in the subject-dependent prediction.

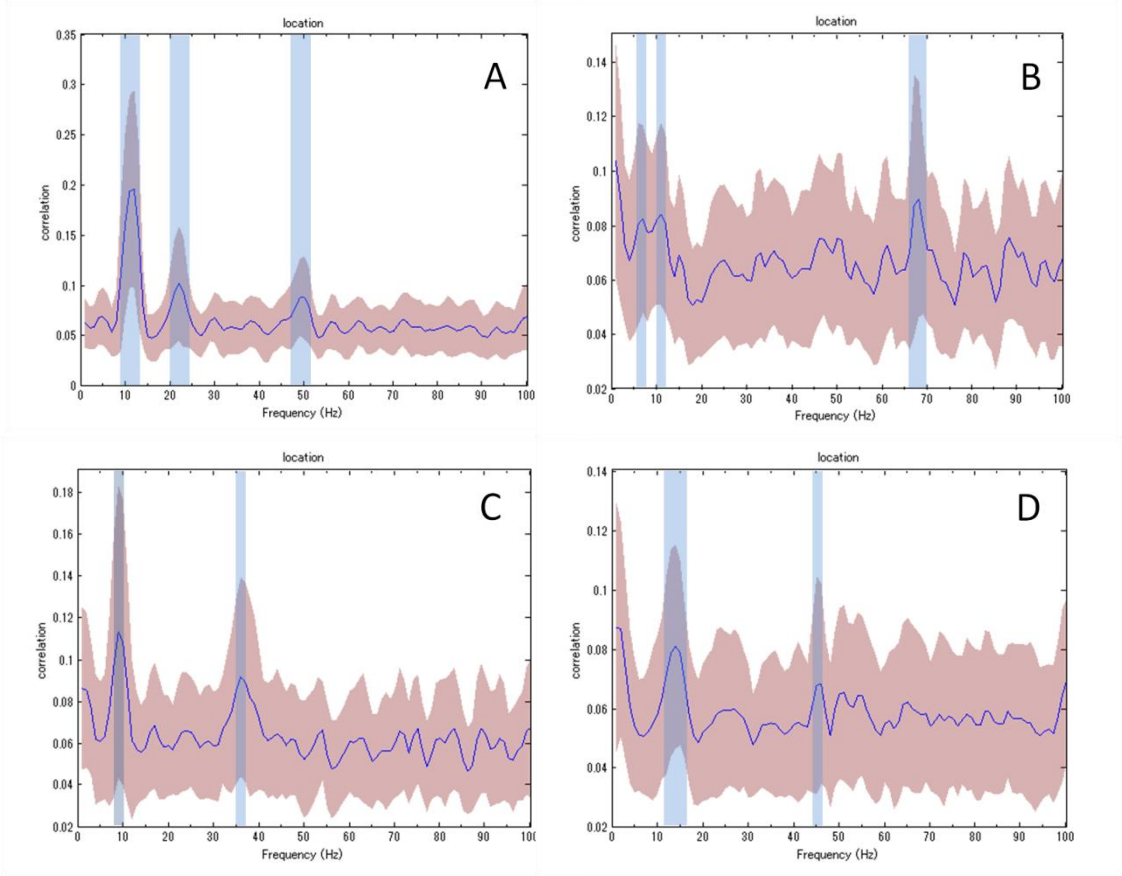

Figure 4 - 3 Statistics of correlation values between continuous motion positions and spectral amplitudes of MEG data over motor cortex, listed for each subject.

Labels A, B, C and D indicated correlation results of different subjects. For each frequency and each channel over motor cortex, correlation value is calculated. The blue line in every plot is the average correlation value across channels and the dark red area shows the standard difference of the correlation value. The light blue area indicates the frequency ranges which have relatively high correlation value. These frequency ranges are 9~13 Hz, 20~24 Hz, 47~50 Hz for subject A; 5~7 Hz, 10~12 Hz, 66~70 Hz for subject B; 8~10 Hz, 35~37 Hz for subject C; 11~16 Hz, 44~45 Hz for subject D.

The correlation results below 100 Hz of all subjects were investigated and shown in Figure 4 - 3. For subject A and B, three frequency ranges with relatively high correlation value were selected while for subject C and D, only two frequency ranges were selected. The detailed ranges of these motion related frequency are described in the description of Figure 4 - 3 and we call them subject-dependant frequency ranges. From the figures, we could confirm again that μ- rhythm frequency bands (9~14Hz) presented a much higher correlation value than other selected frequency bands. Thus,

we recognized μ-rhythm as the main motion related frequency features. However, μ-rhythm frequency ranges varied a little around 9~14 Hz for different subject, and we called them the main subject-dependant frequency ranges. From Figure 4 - 3, we could determine that main subject-dependant frequency ranges are 9~13 Hz, 10~12 Hz, 8~10 Hz and 11~16 Hz for subject A-D respectively.

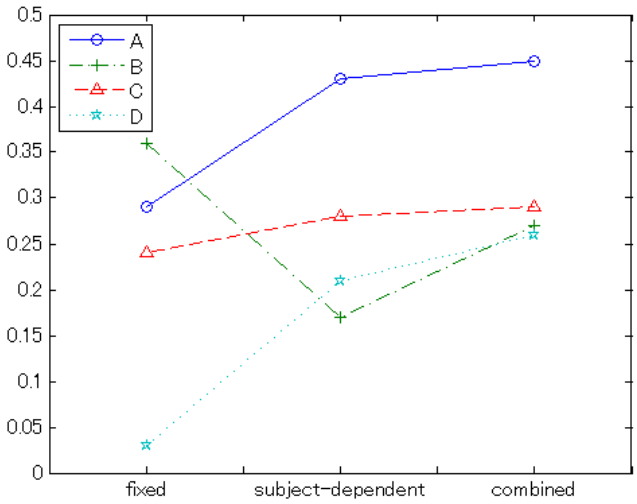

Figure 4 - 4 Prediction performances using different feature selection models on single trial data. MEG data was preprocessed using tSSS method.

Labels 'fixed', 'subject depended' and 'combined' in x axis indicate results using model 1: fixed frequency band (9~14 Hz), 2: main subject-dependent frequency range around 9~14 Hz; 3: combination of several subject-dependent frequency ranges respectively. Blue, green, red and light blue lines in the plots represent prediction performances of subjects A-D respectively.

Using multivariate linear regression method, we predicted continuous motion trajectory and evaluated performances on different models. In prediction results adopting tSSS preprocessed single trial data, two subjects (A and D) presented much better performances using main subject-dependent feature than pre-defined fixed feature, while the other two subjects presented a minor increased (subject C) or decreased (subject B) performances. When features of several subject-dependent frequency ranges are combined, prediction performances of all subjects improved comparing to main subject-dependent feature. Considering the total effects, subject A, C and D showed an improvement between combined subject-dependant and fixed feature models.

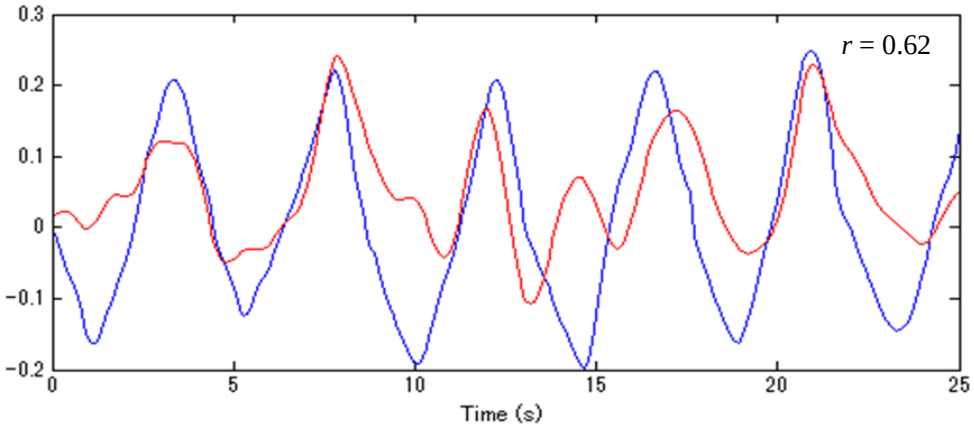

Figure 4 - 5 Single trial prediction results using combination of several subject-dependant features, for subject A.

Y axis indicates motion position in meters. Blue line is the actual motion position and red line is the predicted motion position. Prediction performance is evaluated by the correlation between actual and predicted motion position, and is shown in the upper left corner as $r = 0.62$.

Predicted motion position using tSSS preprocessed single trial MEG data is shown in Figure 4 - 5. Comparing predicted to actual motion trajectories, we found out that similar motion tendency is shown in the whole 25 s motion process. The correlation value $r = 0.62$ also indicated that this single trial prediction is successful.

In the data analysis using compensation tSSS as noise reduction method, correlation values showed similar results for each subject while varied slightly. By using the same subject-dependant feature selection method, mainly the same frequency bands were chosen as selected frequency features (8~14 Hz, 20~24 Hz, 44~46 Hz for subject A; 10~14 Hz, 5~8 Hz, 66~69 Hz for subject B; 7~11 Hz, 45~47 Hz, 54~56 Hz for subject C; 12~18 Hz, 28~30 Hz, 45~47 Hz, 53~54 Hz for subject D).

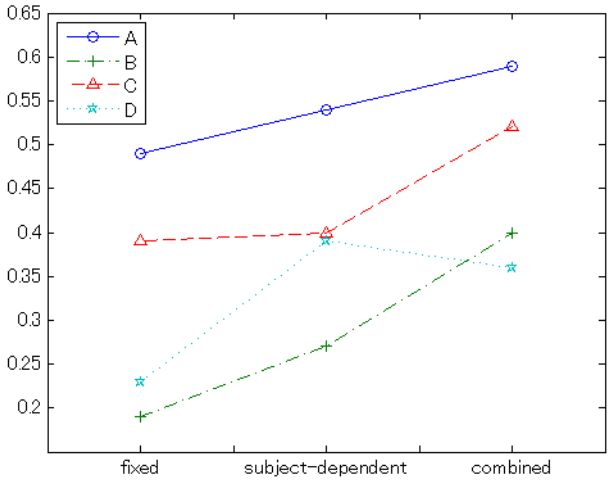

Figure 4 - 6 Comparison of prediction performances using different feature selection models on single trial data. MEG data was preprocessed using compensation tSSS method.

Labels 'fixed', 'subject depended' and 'combined' in x axis indicate results using model 1: fixed frequency band (9~14 Hz), 2: main subject-dependent frequency range around 9~14 Hz; 3: combination of several subject-dependent frequency ranges respectively. Blue, green, red and light blue lines in the plots represent prediction performances of subjects A-D respectively.

The prediction performances using compensation tSSS preprocessed single-trial data are illustrated in Figure 4 - 6. For all the subjects, the prediction performance value improves as the model changes from pre-defined fixed frequency feature to subject-depended frequency feature. When several subject-dependent frequency features are combined, subject A, B and C showed great improvements while subject D is an exception that prediction performance decreased slightly. However, comparing combined feature model to fixed feature model, the improvement is still significant for all the subjects, which indicates an effectiveness of combined subject-dependent frequency feature model under compensation tSSS condition.

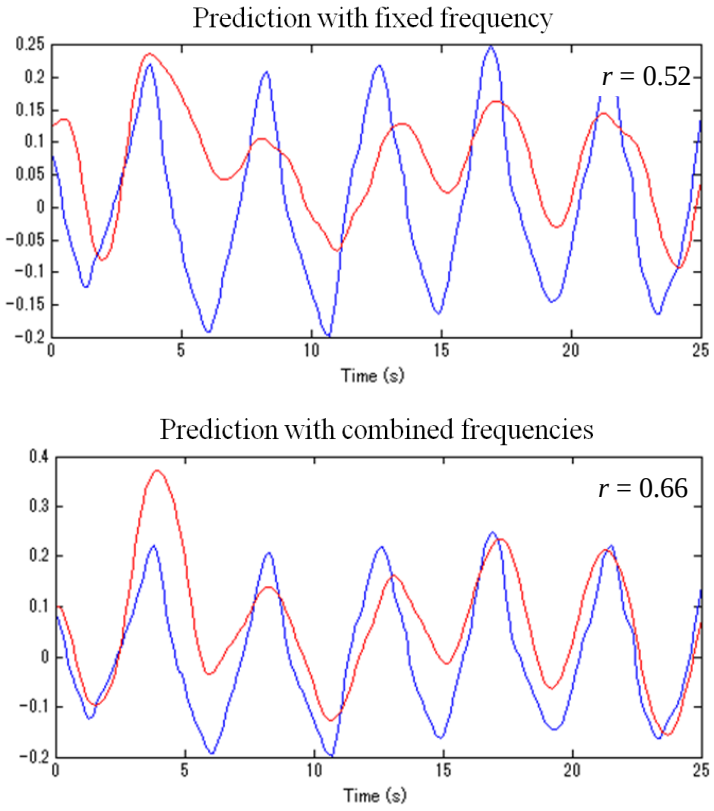

Figure 4 - 7 Single trial compensation tSSS prediction results using fixed frequency feature and combination of several subject-dependant features, for subject A.

Upper graph indicates prediction result using fixed frequency features; lower graph shows prediction result using combination of several subject-dependant features. Y axis indicated motion position in meters. Blue line is the actual motion position and red line is the predicted motion position. Prediction performance is evaluated by the correlation between actual and predicted motion position, and is shown in the upper left corner as *r* value.

The prediction results using compensation tSSS are shown in Figure 4 - 7. In the upper graph, prediction performance is $r = 0.52$, which is a relatively high value. The waveform pattern of predicted motion trajectory is briefly the same with actual motion. In the lower graph, prediction performance using combination of several subject-dependant features is $r = 0.66$, which is a good prediction performance. Comparing to the upper graph, predicted motion trajectory using combined model is much more similar to actual motion and nearly all the motion pattern peaks and tendency are well depicted.

4.4 Discussion

4.4.1 Overfitting in model selection

In this task, we used subject-dependent frequency feature selection instead of using all the spectrums to avoid overfitting problem. By selecting motion-related features, effective information is extracted from the large amount of spectral data, thus prediction will not focus on irrelevant noise and other brain activities. Here we used the combination of several subject-depended frequency bands as feature selection method and obtained the best prediction performance than the other models. When we tested the combination of frequency bands that are not subject-dependent, the performance got worse because of the overfitting problem. Although the feature number increased in such cases, the prediction performance rather got worse. This indicated that performance improvement by using subject-dependent frequency bands does not come from the increased number of features, but from the extraction of effective information, which is precisely our purpose.

4.4.2 Model comparison

Both the averaged and subject-dependant correlation values indicated that μ-rhythm (around 9~14 Hz) is the common and best motion related frequency range. This is consistent with not only our former study, but also some previous EEG studies. Also, we found out that low frequency δ rhythm (5~7 Hz) or β rhythm (18~24 Hz) is related to continuous motion in some subject's data, which is similar to previous continuous MEG and EEG studies. Moreover, several high frequency γ bands (30~50 Hz, 60~70 Hz) were also revealed as motion related frequency ranges. This has been presented by some non-invasive discrete motion studies and invasive continuous motion studies, but has not been reported by continuous non-invasive studies.

In the comparison of three different frequency selection models, improvement of prediction performance varied a lot from subject to subject. This variance might come from different distribution of motion related frequency ranges and different signal to noise ratio (SNR).

Table 4 - 1 listed the prediction performances of different models using different noise reduction methods. The prediction performance results indicated that subject-depended features predict continuous motion more efficiently than pre-defined fixed features. Subject A, C and D represented an improvement in tSSS preprocessed data. This revealed that motor related signal differed slightly from person to person. An exception is subject B. Considering the correlation plot of subject B, correlation peak around fixed frequency band 9~14 Hz is not as clear and high as other subjects and thus the subject-dependant frequency band 10~12 Hz is not

a proper main subject-dependant frequency range for subject B, which lead to very little improvement. However, in the prediction performance using compensation tSSS, this problem is fixed and all subjects presented an improvement, which further confirms motor related subject-dependent feature is more proper for motion prediction.

Table 4 - 1 Prediction improvement between different models for each subject.

Model 1, 2 and 3 indicated fixed frequency range model, main subject-dependant frequency range model and combination of several subject dependant frequency range model respectively. Symbol '○' means improvement on both original tSSS and compensation tSSS data. Symbol 't' means only improvement on original tSSS data, while symbol 'c'means only improvement on compensation tSSS datga.

Subject	Model 1 to 2	Model 2 to 3	Model 1 to 3
A	○	○	○
B	c	○	c
C	○	○	○
D	○	t	○

In the comparison of main subject-dependant model and combination model, almost all the subjects showed significant improvement in both tSSS and compensation tSSS data, which revealed the efficiency of combination model. Subject D represented a slight decreased prediction performance in compensation tSSS data and the possible reason is that current selected frequency features did not contain enough motion information and other undiscovered motion related frequency band may exist.

In both tSSS and compensation tSSS data prediction results, it turned out that a much better prediction performance was achieved by using the combination of subject dependant frequency model than using fixed frequency feature model. The only exception is subject B who showed significant improvement only on compensation tSSS data. This might be the reason that the main subject-dependent frequency band (10 – 12 Hz) has the same correlation level to frequency band 5 – 7 Hz and mixed with each other, thus it is not a really main subject-dependent frequency band for subject B.

The significant improvement of prediction performance in combined feature model confirmed that continuous motion was not only related to μ (9~14 Hz) and β rhythm (18~24 Hz), but also related to low frequency δ rhythm (5~7 Hz) and some part of high frequency γ bands (30~50 Hz, 60~70 Hz), which is similar to previous ECoG and MEG discrete motion study (Waldert et al., 2008). Moreover, the high

prediction performance value in this study is comparably high with previous study using averaged data. This confirmed that our subject-dependant frequency feature selection method is efficient in single trial prediction of continuous motion.

The statistics of prediction performances were also considered. Prediction performances were first averaged for each subject and each condition (model and noise reduction method). Then, the statistical results of all subjects were calculated and listed in Table 4 - 2. A two-way repeated measures ANOVA found a significant main effect of noise reduction method ($F(1,3) = 12.2$, $p < 0.05$), indicating that prediction using our compensation tSSS performed significantly better than that using the conventional tSSS. There was also a significant main effect of the model ($F(2, 6) = 5.6$, $p < 0.05$), and the multiple comparison results showed that prediction performances of model 3 was significantly higher than model 1 ($p < 0.05$) and model 2 ($p < 0.05$). The interaction between noise reduction method and model was not significant.

Table 4 - 2 Comparison of prediction performance results using tSSS and compensation tSSS method, fixed model, main subject-dependant model and combined model. The result is shown as mean ± SD.

Single-trial data	**tSSS**	**Compensation tSSS**
Fixed frequency	0.23 ± 0.14	0.32 ± 0.14
Main subject-dependant frequency	0.27 ± 0.11	0.40 ± 0.10
Combination of subject-dependant frequencies	0.31 ± 0.08	0.47 ± 0.10

From this study, we concluded that using subject-dependant feature selection method, single-trial MEG data could also predict continuous motion as well as some invasive studies with fewer features.

Chapter 5 Robustness of motion-related feature selection

In Chapter 5, we tested different motion cycles and devices to study the robustness of our motion trajectory projection. In task 1, we performed an experiment with motion similar to chapter 3 using a different device (trackball). The prediction result confirmed that our feature selection method could work equally well on different devices which indicated a robustness of different devices. In task 2, we considered a different motion cycle without visual guidance and confirmed the efficiency of our feature selection method on different motion cycle. This indicated a robustness of different motion. As there is no visual guidance in this task, the selected features are absolutely from motion brain activities. We then applied source localization technique, and confirmed that the frequency features selected by our feature selection method were motion related activities originating from motor cortex and sensorimotor cortex.

5.1 Introduction

Currently, there are many studies focused on continuous motion prediction. However, most of them are invasive studies on monkeys who have been implanted microelectrode arrays. These studies contained from one dimensional to three dimensional motions as well as the real-time robotic arm controls. By using the firing spikes of certain area of motor cortex, a direction tuning between arm motion directions and firing rate was discovered as a convincing motion related mechanism. Therefore perfect continuous motion prediction can be achieved and this kind of prediction is robust. However, as invasive recording is risky, very few human invasive studies on continuous motion were reported.

Because invasive study is difficult to apply on human, recent years, some non-invasive studies started to focus on continuous motion of human. These studies mainly used MEG or EEG recordings and tried to perform a good prediction on kinematic parameters. However, most of them simply presented a good prediction performance with a huge quantity of data set, and did not provide any motion related feature or mechanisms. Therefore, whether these predictions are robust on other kinds of motion or devices is still unknown. Also, whether the information they used are really related to motion or some other responses is still not fully investigated yet.

In the former study, we proposed an efficient subject-dependant feature selection method which could provide good prediction performance using single trial data recorded by non-invasive MEG. As these features are selected from the correlation between brain activities and motion parameters, they are highly possible to be motion related features. However, without contour map or source analysis, it is not so convincing. Therefore, in this chapter, we first performed different tasks to testify the robustness of our method, then considered the spatial patterns and source level activities to investigate our selected features are motion related or not.

In this study, different external device (track ball) or motion cycle is adopted in task 1 or task 2 in order to test the robustness of different device and motion type. By comparing the prediction performance of former and current experiments, the robustness on different devices and motion type is confirmed, indicating our subject-dependant feature selection method could be used under different conditions. In chapter 3, we investigated motion task with visual stimulus. Although we adopted MEG signals over motor cortex, whether the selected features used in prediction come from motion intention or visual response is still unclear. Thus, task 2 is designed as a voluntary motion task without any visual stimulus guidance in order to find out the truth. In source analysis of task 2, we firstly considered the correlation between motion position and spectral amplitude and then illustrated the contour map of different frequency bands with high correlation values to indicate the source area of selected frequency features. Finally, we further discussed the source position of

continuous motion by beamformer source determination using Fieldtrip toolbox on Matlab. From beamformer source analysis, it is confirmed that these frequency band features came from motor cortex in some subject, which provided the evidence for feature selection in motion prediction.

5.2 Method

5.2.1 Participants

Three volunteers are participated in the experiment after giving informed consents about the safety of experimental devices, our duty of confidentiality concerning private matters, and the task design of our experiment, etc. All subjects were novices (not experts) at track ball control.

5.2.2 Task design

5.2.2.1 Task 1

Participants were seated upright on the chair in MEG system, watching a 50*50 cm area on a screen located at an eye distance of 1.2 m, resulting in a maximum visual angle of 12 ° from the central direction.

Visual stimuli for the guidance of continuous motion were generated using Psychtoolbox (Brainard, 1997; Pelli, 1997) and presented on the screen. The background is black with a green fixation mark '+' presented in the center of the screen during all the experiment procedure. A green ball is located 2 cm under the fixation mark. The experiment contains 15 moving sessions with 10 s rest time between two moving sessions, as is described in chapter 3. During the moving session, the green ball moved left and right periodically every 4 seconds on the background and its position scarifies the sine wave to time. In every moving session, 11 moving cycles is performed. During the following task, instead the end point of toolbar, a red ball smaller than the green ball stimulus is used as feedback. The motion of the red ball is exactly the same as the horizontal motion of trackball.

Recordings were performed in the session lasting about 15 minutes. In the moving session, participants were asked to using a track ball (Logitech® Trackman® Marble®) to control the cursor on the screen and follow the moving ball. Here we used track ball instead of tool bar because track ball is easy to use and could provide a smooth continuous motion while tool bar is hard to move and the motion is not strictly continuous and periodical. By following the periodically moving ball, we assumed that subjects could perform similar continuous motion in every moving cycle.

5.2.2.2 Task 2

Voluntary motions with similar motion pattern are performed in task 2. With the purpose of avoiding the effect of visual stimulus, no moving visual stimulus guidance is adopted in this task. Instead, a '+' mark is provided in the center of the screen as an onset guidance. The position of the '+' mark does not change during the whole experiment procedure and is used as a fixation point. The task contained 100 trials without any interval. In each trial, there are one rest session and one move session, both lasted for 3 seconds. The color changing of the '+' mark is used as the guidance of session onset. When the color of '+' mark changes from green to white, the rest session starts and the color keeps white during the 3 seconds rest session. When the color of '+' mark changes from white to green, the move session starts and the color keeps green during the 3 seconds move session. The scheme is illustrated in Figure 5 - 1.

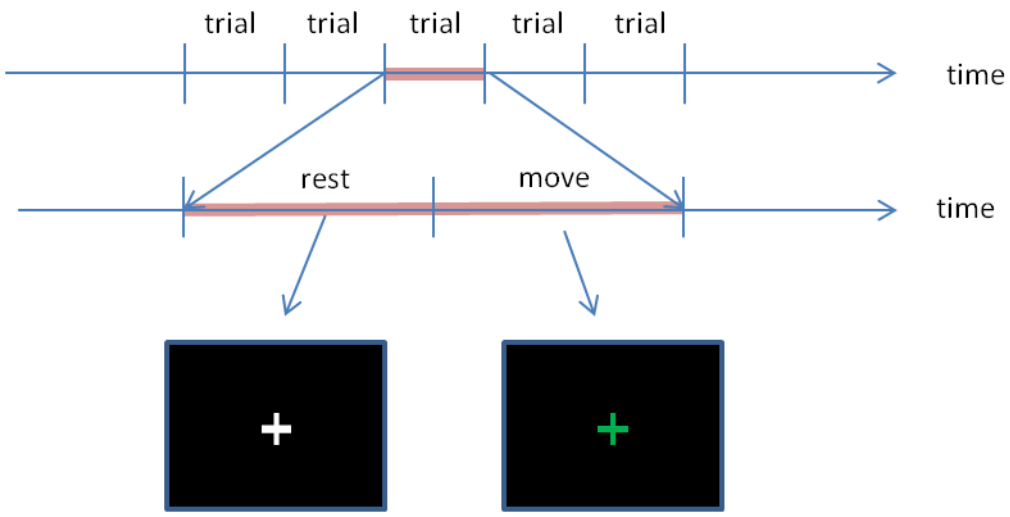

Figure 5 - 1 Experiment scheme of Task 2.

Two graphs in the bottom are the screen shown to subjects during rest or move session. The screen contents do not change during each session.

Because there is no visual stimulus guidance during the task, subjects were asked to practice 3 seconds periodical continuous left-right motion using a visual guidance mentioned in task 1 for over 15 minutes just before the task in order to remember the motion pattern and perform similar motion in each move session. During the task, subjects were asked to fix their eye on the fixation point to avoid eye movement during both rest and move sessions. Subjects were told to keep their eye open without any movement of their hand during the rest session, and start moving when the '+'

mark turned green and perform smooth left-right motion they have just remembered. No feedback was provided during the task in order to avoid effect of visual stimulus. Eye blinking was asked to be controlled during the move session.

5.2.3 Continuous motion and MEG recording

MEG was recorded in a magnetically shielded room using a whole-held system (Yokogawa, PQ2440R, Tokyo, Japan) comprising 440 first-order gradiometers. Data were sampled at a rate of 1000 Hz with a band pass filter from 0.3 Hz to 200 Hz.

Head position was recorded before the experiment for each subject using localization coils that were fixed at the forehead as prefrontal points and at left and right ear as preauricular points, forming a head-relative coordinate system. From the coil signals present in the recordings, it was possible to compute the head's relative position and orientation off-line using goodness of fitting of each coil's amplitude distribution to a magnetic dipole forward model. This was done by source dipole determination method provided by PC software MegLaboratory 2.003D (Yokogawa, Tokyo, Japan).

Continuous motion position which was provided by track ball was recognized from the mouse position on PC. Then the visual stimuli program presented mouse position in the form of a smaller red ball on the screen as a feedback in task 1 (no visual feedback is provided in task 2). Meanwhile, the program also adopted the Matlab data acquisition toolbox to output motion positions immediately using NI (National Instruments Corporation, Texas) DAQ card (USB-6008) in both task 1 and task 2. The output motion positions were recorded simultaneously with MEG signals by MEG system.

5.2.4 Data analysis

5.2.4.1 Task 1

As raw MEG signals are contaminated by electromagnetic noise interference, compensation tSSS method which is designed for our MEG system in chapter 2 was applied to the raw MEG data before further analysis. Then, both MEG signals and track ball motion position data were split into non-overlapping 4-second epochs, each of which corresponded to 1 cycle of movement. After that, similar spectrum calculation and subject-dependent feature selection to chapter 4 was adopted to extract several motion related features for prediction. Spatial and temporal feature selection models were also fixed following the result mentioned in chapter 3. With selected features, prediction was performed using multivariate linear regression method, as is mentioned in equation 4 - 1. Finally, statistics of prediction performance of all

subjects were calculated and compared in order to testify the robustness.

5.2.4.2 Task 2

Similar to Task 1, before further data analysis, compensation tSSS method was applied in order to remove external noises. Then, motion onset was determined from motion position data with a threshold of 5% of the maximum position from the center. According to the motion onset in each move session, both MEG and motion position data from track ball were split into non-overlapping 6-second epochs, each of which corresponded to 1 trail (3-second data before motion onset is rest session and 3-second data after motion onset is move session). Then, time-frequency analysis and feature selection similar to task 1 were performed. Subject-dependant features were selected for each subject and used in the following motion trajectory prediction. From statistic analysis, the robustness of feature selection method is tested.

In order to find out the origin of subject-dependent features, we investigated the spatial patterns and source positions on these selected frequency bands. As the SNR is still not high enough for contour map illustration, we assumed that motor responses are similar in each cycle and investigated the patterns by averaging certain frequency band powers of single trial signals. The relative power is calculated by considering average power in the rest session as baseline and dividing average power in the move session by it. Then we presented contour map of the relative power of certain frequency bands by using the function of Fieldtrip toolbox (developed by Centre for Cognitive Neuroimaging of the Donders Institute for Brain, Cognition and Behaviour together with collaborating institutes).

In contrast to evoked response analysis of contour map, we imaged the brain sources underlying the sensor measurements from statistics of single-trial data which contained not only data averaging but also covariance. Thus we preserved trial-specific temporal information which is crucial to the study of the spatiotemporal properties of motor encoding. The neural current density distribution of certain frequency bands was estimated by applying dynamic imaging of coherent sources (DICS), which calculated the power normalized with an estimate of the spatially inhomogeneous noise. This was implemented with beamforming analysis in Fieldtrip toolbox.

5.3 Results

5.3.1 Results of Task 1

The correlation value between motion parameter and spectral amplitudes is considered as is mentioned in former chapters. In the correlation plots, high

correlation value indicates much motion information contained in the corresponding frequency band, thus these frequency bands are selected as subject-dependant frequency features. As is shown in Figure 5 - 2, subject-dependent frequency bands are 9-15 Hz, 20-24 Hz and 49-53 Hz for subject A; 8-12 Hz for subject D; 6-10 Hz, 15-19Hz, 25-39Hz and 48-52 Hz for subject E. The similar prediction is performed as mentioned in chapter 4 using combination of all listed subject-dependant features. The prediction performance in task 1 is 0.45 ± 0.25 (mean ± SD, across all subjects), which is the same prediction level to tasks using tool bar. This indicates that our subject-dependent feature selection method is robust on different external devices.

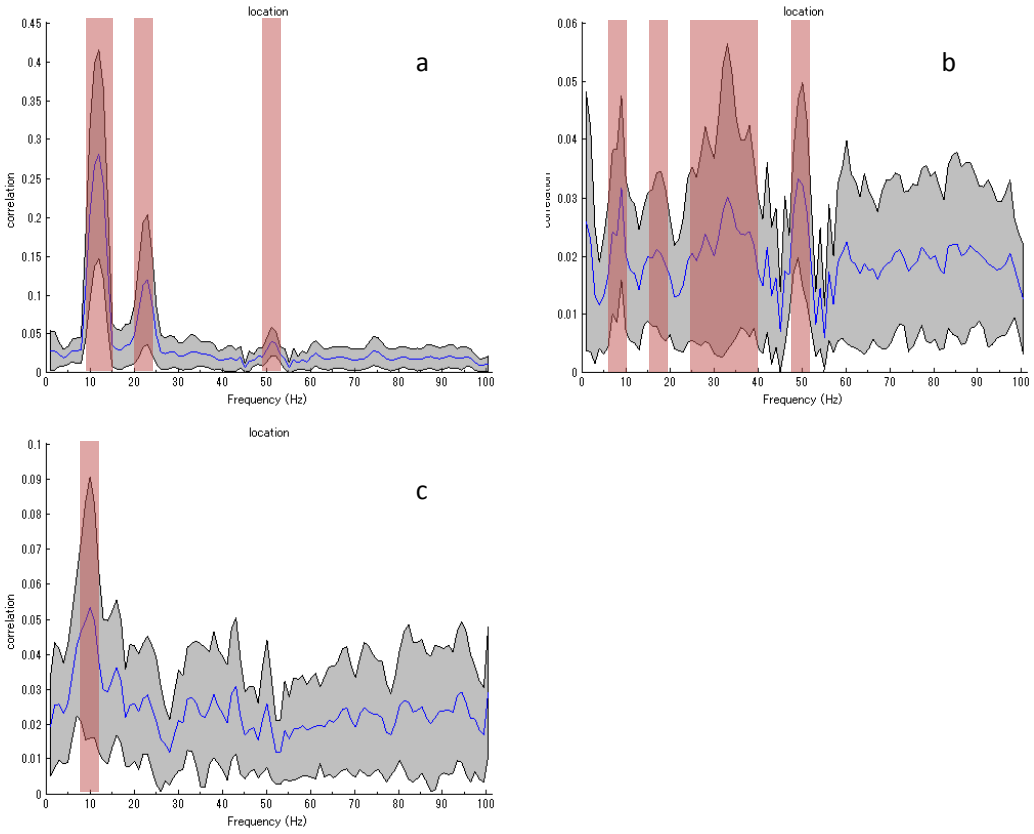

Figure 5 - 2 Correlation between motion position and spectral amplitudes using the method mentioned in chapter 3.

Graphs a, b and c indicate the results of subject A, D and E, respectively. The red areas indicate subject-dependant motion related frequency ranges.

5.3.2 Results of Task 2

Figure 5 - 3, Figure 5 - 4 and Figure 5 - 5 illustrate the correlation value between motion parameter and spectral amplitudes, the contour map and source estimation of subject-dependant motion related features of each subject in task 2. In the correlation

plots, high correlation value indicates much motion information which is contained in the corresponding frequency band. In the contour map of certain frequency band, we used the relative power of each frequency band which is calculated by absolute powers in move session dividing by absolute powers in rest session, as the following :

$$V = \frac{Power_{move} - Power_{rest}}{Power_{rest}}$$

Here the source pattern (red color) in contour map presented increasing values of the powers in move session comparing to the baseline (powers in rest session), while the sink pattern (blue color) presented decreasing values of the power in certain frequency band such as μ-wave or β-wave.

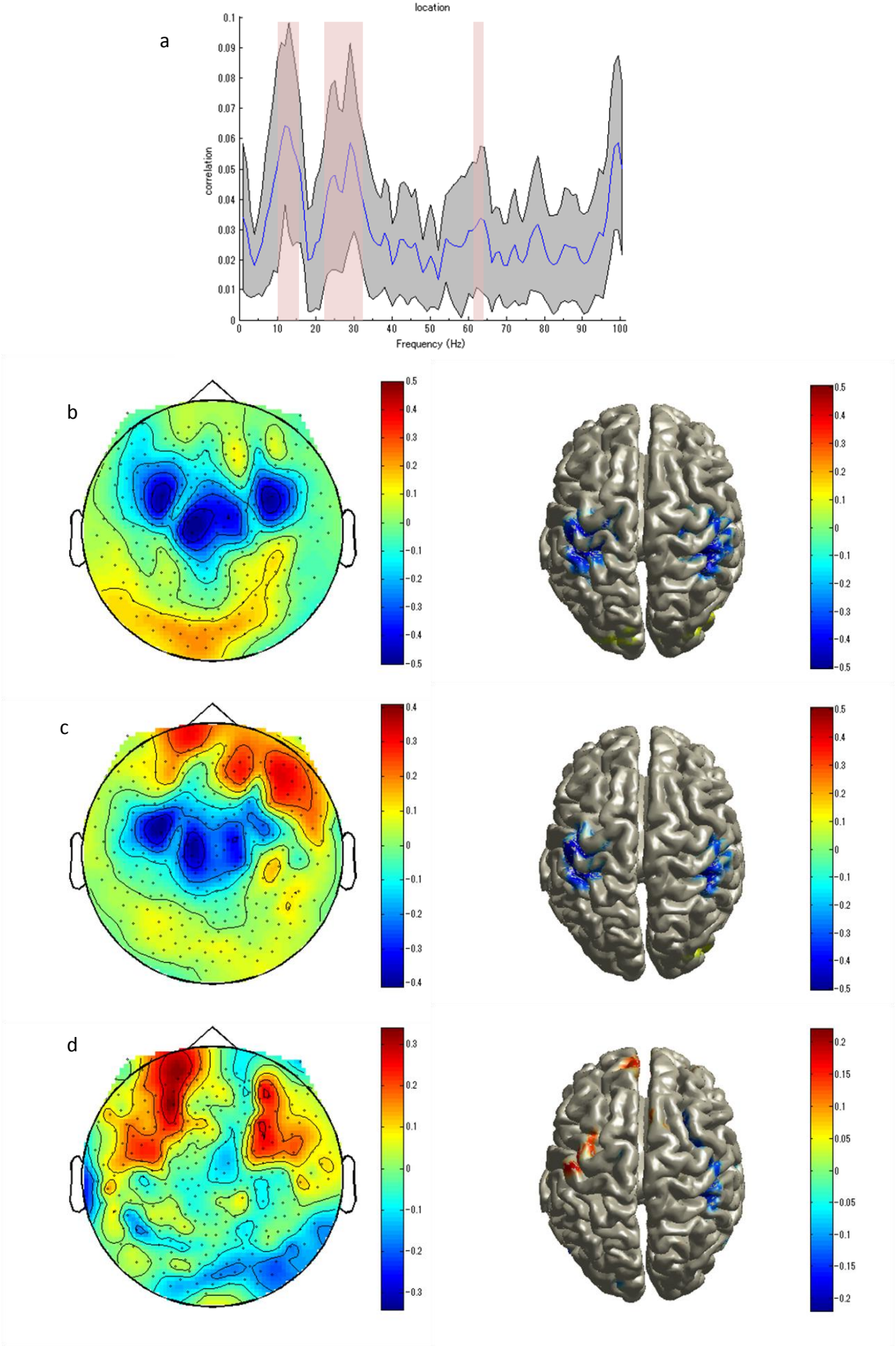

Figure 5 - 3 Correlation plot and contour map of relative power of Subject D.

Relative power is the division of power in move session by power in rest session. Different colors in color bar indicated the intensity of the source.

(a) Correlation between motion position and spectral amplitudes using the method mentioned in chapter 3. The red area indicates subject-dependant motion related frequency range (10-16 Hz, 22-32 Hz, 61-63 Hz).

(b) Contour map and source estimation of relative power in the selected frequency band 10-16 Hz.

(c) Contour map and source estimation of relative power in the selected frequency band 22-32 Hz.

(d) Contour map and source estimation of relative power in the selected frequency band 61-63 Hz.

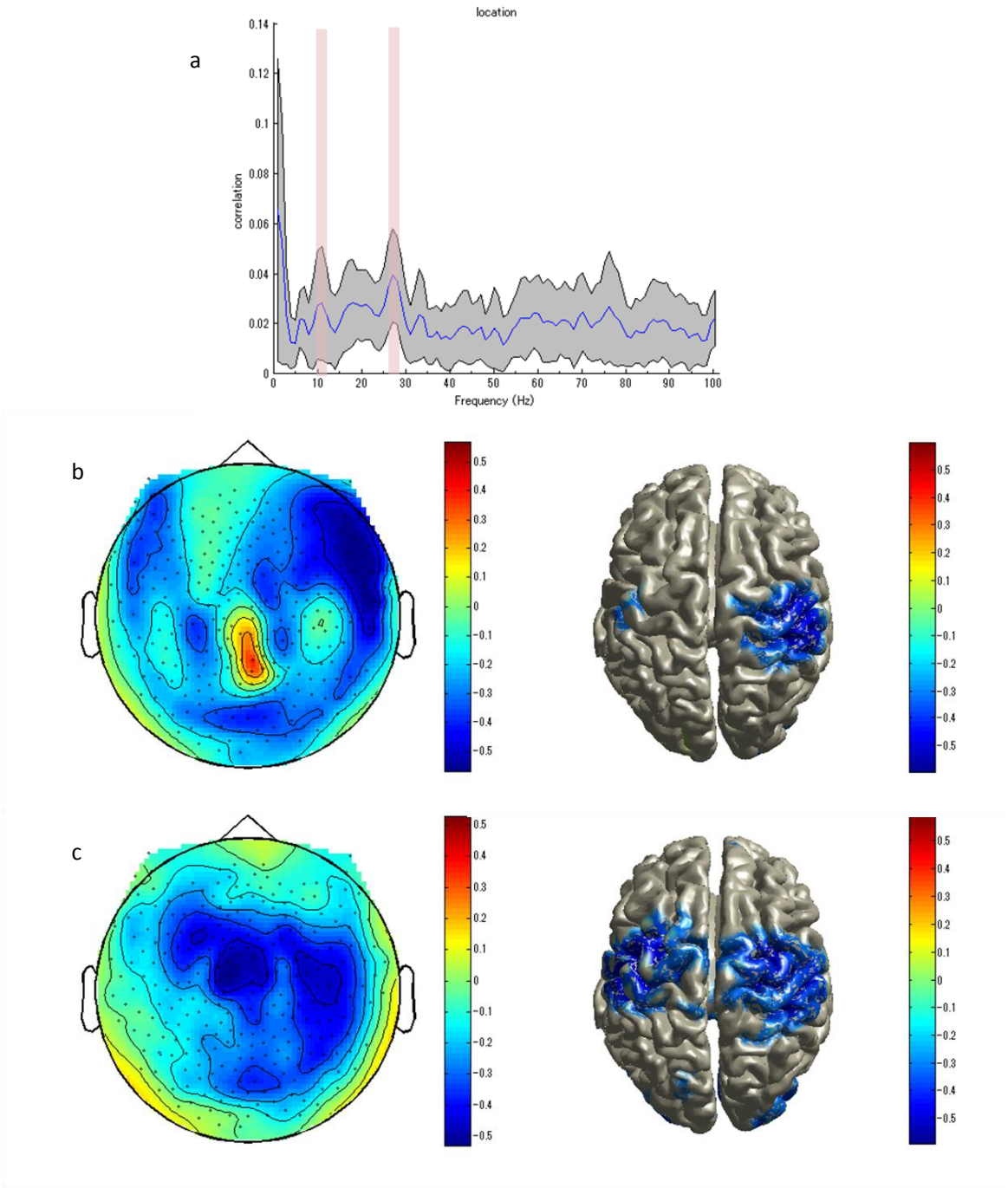

Figure 5 - 4 Correlation plot and contour map of relative power of Subject E.

Relative power is the division of power in move session by power in rest session. Different colors in color bar indicated the intensity of the source.

(a) Correlation between motion position and spectral amplitudes using the method mentioned in chapter 3. The red area indicates subject-dependant motion related frequency range (9-12 Hz, 27-28 Hz).

(b) Contour map and source estimation of relative power in the selected frequency band 9-12 Hz.

(c) Contour map and source estimation of relative power in the selected frequency band 27-28 Hz.

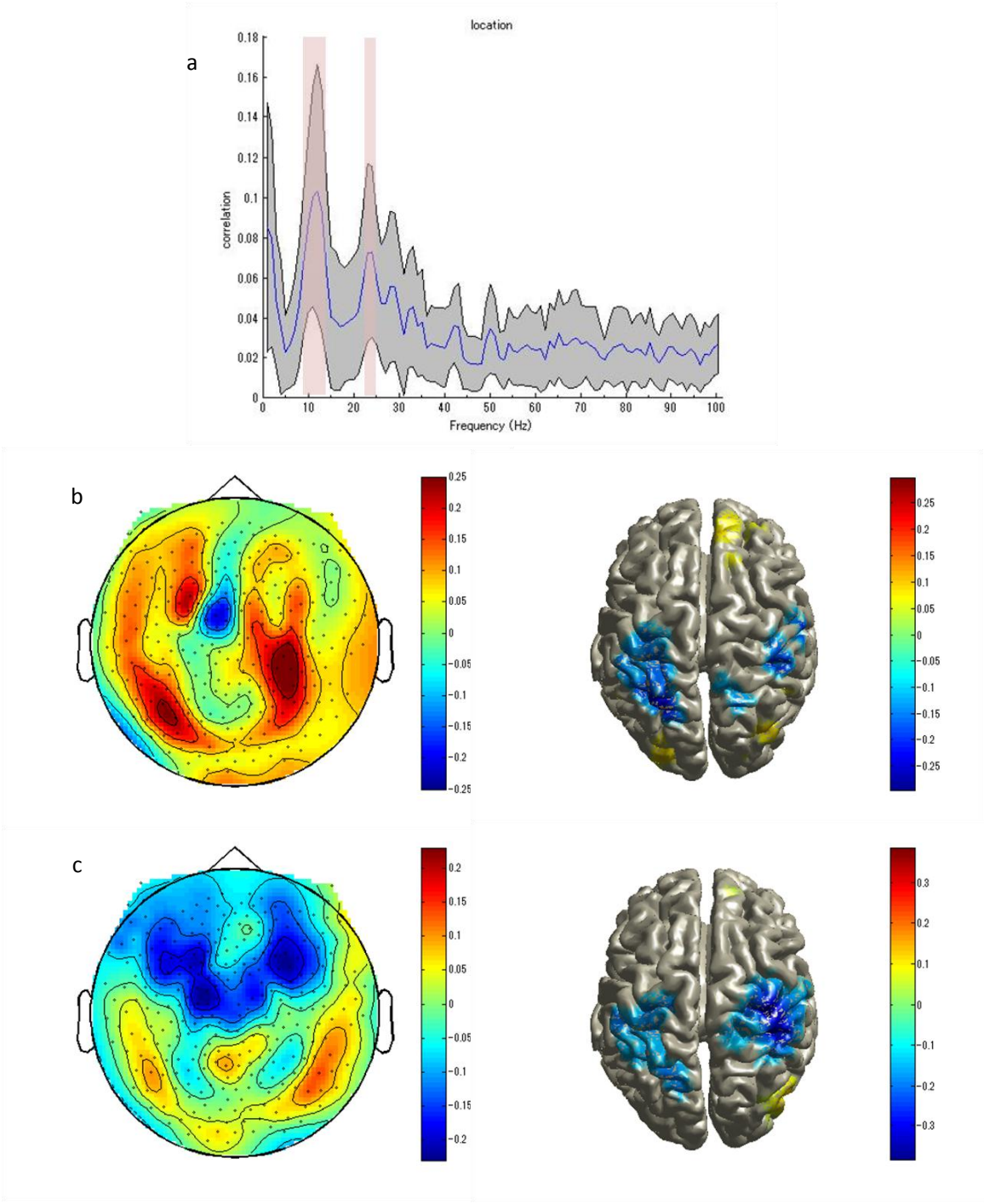

Figure 5 - 5 Correlation plot and contour map of relative power of Subject E.

Relative power is the division of power in move session by power in rest session. Different colors in color bar indicated the intensity of the source.

(a) Correlation between motion position and spectral amplitudes using the method mentioned in chapter 3. The red area indicates subject-dependant motion related frequency range (9-14 Hz, 22-25 Hz).

(b) Contour map and source estimation of relative power in the selected frequency band 9-14 Hz.

(c) Contour map and source estimation of relative power in the selected frequency band 22-25 Hz.

In the correlation plot of subject D shown in Figure 5 - 3a, several frequency bands (10-16 Hz, 22-32 Hz, 61-63 Hz) showed obvious peaks. Among them, 10-16 Hz power spectral amplitude showed the highest correlation value and thus was regarded as the main subject-dependant frequency feature. Considering the fact that signals around 100 Hz might be the affection of power line noises, we do not include this frequency band. Therefore, contour map in 10-16 Hz, 22-32 Hz and 61-63 Hz was shown in Figure 5 - 3a, b and c. From the contour map shown in Figure 5 - 3b, the channels over motor cortex in left hemisphere, which is corresponding to the contralateral side of the moving hand, presented two peaks. The color is deep blue, which means a great decrease of μ-wave during the motion comparing to the rest. Over the right motor cortex which is corresponding to the ipsilateral side of the moving hand, the contour map also showed two peaks. Although the peaks are smaller than the ones in the left and even some parts of the peaks are mixed with peaks in the left hemisphere, we could still recognize them and they also turned to be a smaller decrease in power than the peaks over left motor cortex. This suggested a major motion reaction in contralateral cortex. These results are similar to previous knowledge. The two peaks in right motor cortex indicated that ipsilateral motor cortex also works during the continuous motion. From the brain surface map, we could further specify that these patterns come from motor cortex and sensorimotor cortex which play an important role in motion. In Figure 5 - 3c, the contour map showed two decrease peaks of 22-32 Hz in the left motor cortex, which suggested a decrease of β-wave in contralateral side of moving hand during the motion. The brain surface map presented the sources located in both hemispheres which indicated the ipsolateral side is also related to continuous motion. In the results of 61-63 Hz, although there is no obvious peak of the γ-wave signal in contour map, we could still find a clear source located in the contralateral motor and sensorimotor cortex in the brain surface map. This is because beamformer analysis in source analysis considers varieties in different trial, thus it is much more accurate and reliable than contour map.

Figure 5 - 4a illustrates the correlation plot of subject E. It turned out to be no major peaks but two minor peaks (9-12 Hz, 27-28 Hz). 9-12 Hz is just a μ-wave signal and thus is recognized as main subject-dependant frequency band. The contour maps of these two frequency bands do not present any clear two peak pattern in both left and right motor cortex. Instead, a large area over both left and right hemisphere including the motor cortex shows a decrease pattern during the move session. In brain surface maps, although the decreased sources located in a relatively larger area than subject D, these activated areas are still in motor and sensorimotor cortex. This indicates μ-wave and β-wave which decrease during the motion of hand are really motion related activities, which is similar to both previous knowledge and subject D.

In results of subject A indicated in Figure 5 - 5, one major peak and one minor

peak turned out to be related to motion. 9-14 Hz is the major peak and thus is recognized as main subject-dependant peak. In 9-14 Hz, the contour map presents no clear two peaks pattern, however, areas over left motor cortex indeed reveals a decrease μ-wave pattern in brain surface map. In 22-25 Hz, the areas over both left and right motor cortex presents decrease patterns and the decrease peak over left motor cortex has a larger change which suggests that the main β-wave brain activity occurred in the contralateral side of moving hand.

In task 2, the prediction performance is 0.43 ± 0.02 (mean ± SD, across all subjects), which is the similar prediction level to 4 second motion cycle tasks. This indicates that our subject-dependent feature selection method is robust on different motion types.

5.4 Discussion

The average prediction performances of task 1 and task 2 are 0.45 and 0.43, which are similar levels to task using tool bar. This indicates that the motion mechanisms are the same using tool bar and using track ball. In task 2, although different motion cycle is considered, the prediction performance does not change. This demonstrates that our subject dependant feature selection method can work equally well for different motion types. Thus our subject-dependant feature selection method is robust on different kinds of motion and is a reliable method for continuous motion prediction.

In former tasks and task 1 in this chapter, visual guidance is used. Although the features are selected from channels over motor cortex by using correlation between brain activities and motion parameters, it is still possible that these features are affected by other brain activities such as visual response. In task 2, no moving visual stimulus is applied and thus the visual response related to motion does not exist. In this case, the subject-dependent features are surely motion related features come from motor cortex. Moreover, the similar level prediction performance in task 2 also provides evidence that our prediction does not affected by brain activities other than motor response.

From contour map and source analysis results of all subjects in task 2, we cand find out that motor responses in both left and right motor cortex appear simultaneously in most of the subject dependent frequency bands. This is similar to previous knowledge that during hand motion, although the contralateral motor cortex dominates this process, the ipsilateral motor cortex also participates in the control. This reveals that during continuous motion process, bilateral motor cortex collaborates with each other to achieve the motion task. Thus if channels over motor cortex in both sides are used in the feature selection, more motion related information is included and prediction performance may improve again.

For subject D, the contour map and source responses in left motor cortex have greater power than the right ones, which is consistent to the contralateral domination theory. However for subject E, case is opposite that the right motor cortex has a greater power than the left. For subject A, the contour map shows a contralateral dominated pattern while the source analysis presents an opposite result. The possible reason of the inconsistency of all subjects is the problem of average process in data analysis, as we have assumed in the design of the experiment that all the continuous motion cycles in moving session are the same. Actually, continuous motions vary a little bit and this leads to the peak cancellation during the average process.

In contour maps of task 2, almost all the patterns in μ-wave, β-wave and γ-wave are shown exactly over motor cortex, and source analysis results further confirm this fact. This reveals that the selected feature frequency bands are indeed motor related activities. From the relative power results, we can confirm that these patterns are decrease patterns in μ-wave and β-wave, increase patterns in γ-wave, which are exactly the same to previous researches of discrete motion (Waldert et al., 2008).

Low frequency band 3-7 Hz is regarded as minor common peak in chapter 3, which is similar to previous researches. In this chapter, although this frequency band is not extracted by our subject-dependent feature selection method, all subjects present a clear motor related pattern in the contour map. This suggests that in low frequency band 3-7 Hz, another mechanism about continuous motion still remains unrevealed. Considering this frequency band is a common frequency band, it might be a possible way to further improve the single trial prediction performances.

Chapter 6 Conclusion

The chapter 6 summarized all the experiments in this thesis and discussed the effects and problems of them. Then, we talked about possible improvements of the motion prediction based on current results. Finally, we described the plans that we will work on in the future as the extension of our past researches.

6.1 Summary and discussion

In this thesis, we firstly discussed the interference noise condition and explained the signal loss problem of tSSS on our system. We demonstrated a compensation step in the original tSSS method and argued its value by both simulation data and raw MEG data. This effectively suppressed the noise without MEG signal loss and to some extent solved most of the SNR problem in single trial data analysis. Moreover, this method worked better with higher noise levels and therefore can be used in some simple magnetically or non-magnetically shielded room cases.

Then we aimed designing a valuable feature selection method for single trial continuous motion prediction. In chapter 3, we investigated continuous motion related features from spectral, spatial, and temporal aspects; and applied adaptive and non-adaptive feature selection methods to extract the optimal features of these three aspects. It is confirmed by 5 epoch average data prediction that these features contained more motion information than MEG raw data and thus can provide a more efficient prediction, which is represented by fewer features and higher prediction performance.

In contrast to using 5 epoch average data, in chapter 4 we used single-trial data for prediction. We employed the knowledge of spatial and temporal features in chapter 3, and reconsidered the spectral features for each subject. In the single trial prediction, it turned out that by combining several subject-dependent frequency bands, a successful prediction can be achieved with single trial MEG data. We concluded that the subject-dependent spectral feature selection method is more powerful and is suitable for single trial motion prediction.

In both chapter 3 and chapter 4, we applied tSSS and compensation tSSS as preprocessing noise reduction methods. The higher prediction performance of compensation tSSS confirmed again that this method is optimal for our gradiometer only MEG system because of the improvement in signal-to-noise ratio.

Contour map and source analysis in chapter 5 revealed the sources of selected frequency features. The results provided some evidence that motion related features selected by our method come mainly from motor and sensorimotor cortices but not visual responses, and thus should be motion-related features.

From all tasks in this thesis, we could obtain statistics of prediction performances of continuous motion under different experiment conditions, as is shown in Table 6 - 1. Considering the feature selection method, we found out that combined subject-dependent model is definitely better than fixed frequency model.

By using combined feature selection model, for different devices such as toolbar or trackball, the motion mechanism changes little although they involve wrist motion and finger motion respectively. Also, in task 2 in chapter 5, we performed a continuous motion with different motion cycle. The averaged prediction performance

confirmed that different cycle length does not affect the prediction results. This indicates that current feature selection method extracts the intention of left-right continuous motion, thus is robust on different kinds of motion and valuable for actual continuous motion prediction.

Both experiments with and without visual stimulus are discussed in this thesis. In tasks with visual stimulus, although the selected features over motor cortex provided a good prediction, little possibility that prediction is affected by visual response exists. In task without visual stimulus, visual response aroused by moving stimulus is absent and thus the selected features for prediction are therefore definitely related to motor commands.

Table 6 - 1 Comparison of motion condition and prediction performances in all tasks

Feature selection	**Device**	**Cycle**	**Visual stimulus**	**Number of Subject**	**Average *r***
Fixed frequency	Toolbar	4 s	Yes	4	0.32±0.14
Combined subject-dependent	Toolbar	4 s	Yes	4	0.47±0.10
Combined subject-dependent	Trackball	4 s	Yes	3	0.45±0.25
Combined subject-dependent	Trackball	3 s	No	3	0.43±0.02

Our study revealed detailed characteristics of motion related activities which are consistent to ECoG and EEG studies. It also provided guidance in selecting features and achieved a successful single trial motion prediction. The high quality prediction demonstrated that a non-invasive measurement predicts motion comparably well as in invasive measurement such as ECoG. As is shown in Figure 6 - 1, our prediction performance is better than some of the MEG studies with fewer features. Thus, the prediction of arm movement trajectory in our study provides the possibility to control external prosthetic devices.

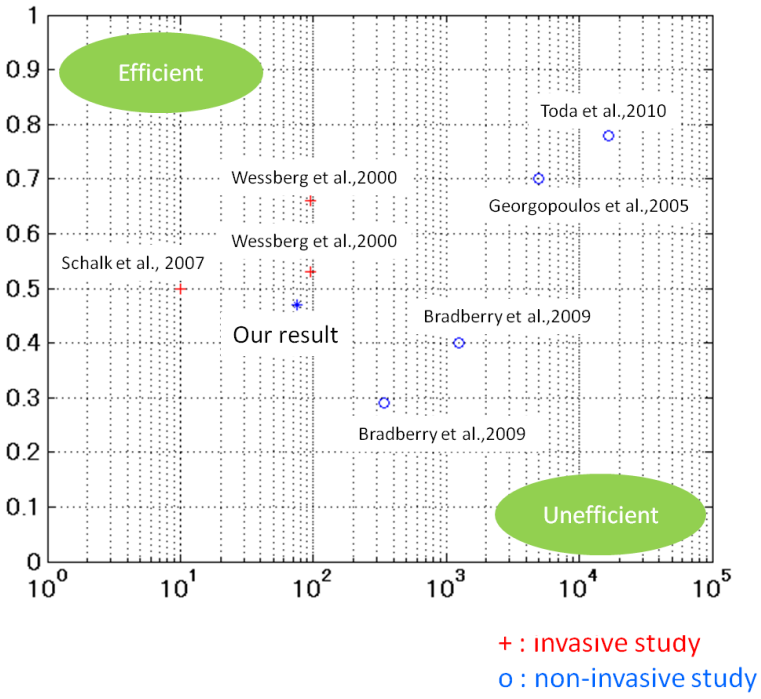

Figure 6 - 1 Comparison of continuous motion prediction.

Red '+' mark indicates invasive study (Schalk et al., 2007 used ECoG, Wessberg et al., 2000 used implanted microelectrode arrays). Blue 'o' mark indicates non-invasive study (Bradberry et al., 2009 and Georgopoulos et al., 2005 used MEG, Toda et al., 2010 used both MEG and fMRI). X axis is feature numbers used in the experiment and Y axis is prediction performance. The left top side means an efficient prediction while the right bottom side means an inefficient prediction.

6.2 Possible improvement and future work

We noted that the motion related feature selection method is effective even on single trial data. However, it is less stable than predictions using invasive methods and can not achieve sufficient results on some subjects. One reason is that current feature selection is mainly based on the correlation between motion parameters and spectral amplitude of brain activities, while other mechanisms (Todorov, 2000) or relationships such as other frequency bands mentioned in chapter 5 or direction tuning in some invasive studies might exist and remain undiscovered. This led to the deficiency in motion related features which might cause unsuccessful motion prediction. Currently, some research (Todorov, 2000) has built models of different motion parameters theoretically. Also, in the invasive studies using implanted microelectrode arrays (Paninski et al., 2004) or ECoG, direction tuning is proved to be a sophisticated algorithm for motion prediction. However, these methods are difficult

to apply in non-invasive studies. In our case, although the motion is continuous, the motion intention might not be a continuous process. This leads to the difficulty about making a conjunction between motion and intention. In chapter 5, we used averaging method as well as source determination method and successfully presented clear motor patterns. This is also a possible way to determine mechanisms such as direction tuning.

Most current continuous motion predictions including ours used the multivariate linear regression method as the prediction algorithm. This method is a simple method and is easily applied. Meanwhile, other complicated methods such as sparse regression (Sato, 2001) were also employed in some research, and these methods are regarded as more valuable for prediction. Improvement of prediction method will enable much higher performance increases.

Current research is done at the sensor level. Although we have done some sensor (channel) selection, it was rather simple. More complicated channel selections have been implemented in some previous research and proved to be helpful. Moreover, some research (Toda et al., 2011) discussed continuous motion prediction in source level and demonstrated progress. Such kind of improvement can also improve prediction performance.

In the future, we wish to build a model that connects motion and intention on non-invasive cases, based on our previously mentioned theoretical model and try to develop a more stable prediction. Also, we hope to adopt a more efficient channel selection or use the source current in motor cortex for prediction. With a sophisticated regression method, we definitely believe the prediction performance can be further improved.

Acknowledgements

I would like to express my deepest gratitude to Prof. Tsunehiro Takeda, my supervisor, for full supports for my research activities in the three years doctoral study. He gave me the important environment for recording MEG for the scientific research and his comments and suggestions were of inestimable value for my study. The present study cannot be completed without his supports.

Next, I greatly appreciate Dr. Kaoru Amano for providing me many suggestions on my experiment design and data analysis. His comments made enormous contribution to my work. He is ones of the pioneers in brain research and I studied the research styles and attitude during working with him, this is really helpful in my life.

Then, I am deeply grateful to Dr. Masanori Shimono. He guided me to start my first experiment and helped me to make the experiment device mentioned in Chapter 3. Without his help, I could not finish this experiment in such a short time. Also, I learnt many ideas in the discussion with him.

I also appreciate Mr. Yutaka Uno, who discussed the problem in tSSS with me. The discussion with him often arouse me many fruitful ideas. Also, he provided me many supports in my daily life in Japan.

Mr. Daisuke Narushima and other students in Biological Complexity Laboratory often assisted me in performing MEG experiments and provided helps in the daily life. I also appreciate them for their warmhearted supports.

At last, I would like to express the best thank to my family. They gave me very huge kind support to concentrate in research in the long student life.

Bibliography

Papers

Qi L, Amano K, Shimono M, Takeda T.
MEG feature selection for motion prediction.
The Journal of Japan Biomagnetism and Bioelectromagnetics Society, (in press)

Conference papers

Qi, L, Amano, K. Shimono, M. Takeda, T.
Motion trajectory prediction using MEG spectral amplitudes.
25th annual meeting of Japan biomagnetism and bioelectromagneticd society (2010).

Qi, L. Amano, K. and Takeda, T.
MEG feature selection in movement trajectory prediction (Conference Abstract).
17th International Conference on Biomagnetism (2010).

Qi, L. Amano, K. Shimono, M. Takeda, T.
MEG feature selection in movement trajectory prediction.
24th annual meeting of Japan biomagnetism and bioelectromagneticd society (2009).

Others:

Qi, L.
フィードバックを用いた脳科学実験システム (Participation Prize).
National Instruments Application Contest (2010).

References

Adachi Y, Shimogawara M, Higuchi M, Haruta Y, Ochiai M (2001) Reduction of non-periodic environmental magnetic noise in MEG measurement by continuously adjusted least squares method. Ieee Transactions on Applied Superconductivity 11:669-672.

Ahissar E, Nagarajan S, Ahissar M, Protopapas A, Mahncke H, Merzenich MM (2001) Speech comprehension is correlated with temporal response patterns recorded from auditory cortex. Proceedings of the National Academy of Sciences of the United States of America 98:13367-13372.

Ahmar N, Simon J (2005) MEG adaptive noise suppression using fast LMS. In: IEEE EMBS Conference on Neural Engineering, pp 29-32.

Barbati G, Porcaro C, Zappasodi F, Rossini PM, Tecchio F (2004) Optimization of an independent component analysis approach for artifact identification and removal in magnetoencephalographic signals. Clinical Neurophysiology 115:1220-1232.

Bogdan M, Schroder M, Rosenstiel W (2003) Artificial neural net based signal processing for interaction with peripheral nervous system. In: Neural Engineering, 2003. Conference Proceedings. First International IEEE EMBS Conference on, pp 134-137.

Bradberry T, Rong F, Contreras-Vidal J (2009) Decoding center-out hand velocity from MEG signals during visuomotor adaptation. Neuroimage:1691-1700.

Bradberry T, Gentili R, Contreras-Vidal J (2010) Reconstructing Three-Dimensional Hand Movements from Noninvasive Electroencephalographic Signals. Journal of Neuroscience:3432-3437.

Brainard D (1997) The psychophysics toolbox. Spatial Vision:433-436.

Brodmann K (1909) Vergleichende Lokalisationslehre der Grosshirnrinde in ihren Prinzipien dargestellt auf Grund des Zellenbaues: Barth Leipzig.

Carmena JM, Lebedev MA, Crist RE, O'Doherty JE, Santucci DM, Dimitrov DF, Patil PG, Henriquez CS, Nicolelis MA (2003) Learning to control a brain-machine interface for reaching and grasping by primates. PLoS Biology 1:E42.

Cohen D (1968) Magnetoencephalography: evidence of magnetic fields produced by alpha-rhythm currents. Science 161:784-786.

Cohen D (1972) Magnetoencephalography: detection of the brain's electrical activity with a superconducting magnetometer. Science 175:664-666.

de Cheveigné A, Simon JZ (2007) Denoising based on time-shift PCA. Journal of Neuroscience Methods 165:297-305.

Drung D, Assmann C, Beyer J, Kirste A, Peters M, Ruede F, Schurig T (2007) Highly sensitive and easy-to-use SQUID sensors. Ieee Transactions on Applied Superconductivity 17:699-704.

Fetz EE (1969) Operant conditioning of cortical unit activity. Science 163:955-958.

Gazzaniga MS, Ivry RB, Mangun GR (2002) Cognitive neuroscience : the biology of the mind, 2nd Edition. New York: W. W. Norton.

Georgopoulos AP, Langheim FJ, Leuthold AC, Merkle AN (2005) Magnetoencephalographic signals predict movement trajectory in space. Experimental Brain Research 167:132-135.

Georgopoulos AP, Lurito JT, Petrides M, Schwartz AB, Massey JT (1989) Mental rotation of the neuronal population vector. Science 243:234-236.

Geyer S, Matelli M, Luppino G, Zilles K (2000) Functional neuroanatomy of the primate isocortical motor system. Anatomy and Embryology 202:443-474.

Golub GH, Van Loan CF (1996) Matrix computations, 3rd Edition. Baltimore ; London: Johns Hopkins University Press.

Gross J, Kujala J, Hamalainen M, Timmermann L, Schnitzler A, Salmelin R (2001) Dynamic imaging of coherent sources: Studying neural interactions in the human brain. Proceedings of the National Academy of Sciences of the United States of America 98:694-699.

Hamalainen M, Hari R, Ilmoniemi RJ, Knuutila J, Lounasmaa OV (1993) Magnetoencephalography—theory, instrumentation, and applications to noninvasive studies of the working human brain. Reviews of Modern Physics 65:413-497.

He SQ, Dum RP, Strick PL (1993) Topographic organization of corticospinal projections from the frontal lobe: motor areas on the lateral surface of the

hemisphere. The Journal of Neuroscience 13:952-980.

He SQ, Dum RP, Strick PL (1995) Topographic organization of corticospinal projections from the frontal lobe: motor areas on the medial surface of the hemisphere. The Journal of Neuroscience 15:3284-3306.

Hochberg LR, Serruya MD, Friehs GM, Mukand JA, Saleh M, Caplan AH, Branner A, Chen D, Penn RD, Donoghue JP (2006) Neuronal ensemble control of prosthetic devices by a human with tetraplegia. Nature 442:164-171.

Huber D, Petreanu L, Ghitani N, Ranade S, Hromádka T, Mainen Z, Svoboda K (2008) Sparse optical microstimulation in barrel cortex drives learned behaviour in freely moving mice. Nature 451:61-64.

Ikeda A, Yazawa S, Kunieda T, Ohara S, Terada K, Mikuni N, Nagamine T, Taki W, Kimura J, Shibasaki H (1999) Cognitive motor control in human pre-supplementary motor area studied by subdural recording of discrimination/selection-related potentials. Brain 122:915-931.

Jerbi K, Lachaux JP, N'Diaye K, Pantazis D, Leahy RM, Garnero L, Baillet S (2007) Coherent neural representation of hand speed in humans revealed by MEG imaging. Proceedings of the National Academy of Sciences of the United States of America 104:7676-7681.

Kayser J, Tenke CE (2003) Optimizing PCA methodology for ERP component identification and measurement: theoretical rationale and empirical evaluation. Clinical Neurophysiology 114:2307-2325.

Kayser J, Tenke CE (2006) Principal components analysis of Laplacian waveforms as a generic method for identifying ERP generator patterns: I. Evaluation with auditory oddball tasks. Clinical Neurophysiology 117:348-368.

Kennedy PR, Bakay RA (1998) Restoration of neural output from a paralyzed patient by a direct brain connection. Neuroreport 9:1707-1711.

Lebedev MA, Nicolelis MA (2006) Brain-machine interfaces: past, present and future. Trends in Neurosciences 29:536-546.

Lebedev MA, Carmena JM, O'Doherty JE, Zacksenhouse M, Henriquez CS, Principe JC, Nicolelis MA (2005) Cortical ensemble adaptation to represent velocity of an artificial actuator controlled by a brain-machine interface. Journal of Neuroscience 25:4681-4693.

Luppino G, Matelli M, Rizzolatti G (1990) Cortico-cortical connections of two electrophysiologically identified arm representations in the mesial agranular frontal cortex. Experimental Brain Research 82:214-218.

Makeig S, Bell A, Jung T, Sejnowski T (1996) Independent component analysis of electroencephalographic data. Advances in neural information processing systems:145-151.

Matelli M, Luppino G, Rizzolatti G (1985) Patterns of cytochrome oxidase activity in the frontal agranular cortex of the macaque monkey. Behavioural Brain Research 18:125-136.

Matelli M, Luppino G, Rizzolatti G (1991) Architecture of superior and mesial area 6 and the adjacent cingulate cortex in the macaque monkey. The Journal of Comparative Neurology 311:445-462.

Matsumoto R, Nair DR, LaPresto E, Bingaman W, Shibasaki H, Lüders HO (2007) Functional connectivity in human cortical motor system: a cortico-cortical evoked potential study. Brain 130:181-197.

Matsumoto R, Ikeda A, Ohara S, Matsuhashi M, Baba K, Yamane F, Hori T, Mihara T, Nagamine T, Shibasaki H (2003) Motor-related functional subdivisions of human lateral premotor cortex: epicortical recording in conditional visuomotor task. Clinical Neurophysiology 114:1102-1115.

Mellinger J, Schalk G, Braun C, Preissl H, Rosenstiel W, Birbaumer N, Kübler A (2007) An MEG-based brain-computer interface (BCI). Neuroimage 36:581-593.

Miller KJ, Leuthardt EC, Schalk G, Rao RP, Anderson NR, Moran DW, Miller JW, Ojemann JG (2007) Spectral changes in cortical surface potentials during motor movement. Journal of Neuroscience 27:2424-2432.

Miyawaki Y, Uchida H, Yamashita O, Sato MA, Morito Y, Tanabe HC, Sadato N, Kamitani Y (2008) Visual image reconstruction from human brain activity using a combination of multiscale local image decoders. Neuron 60:915-929.

Musallam S, Corneil BD, Greger B, Scherberger H, Andersen RA (2004) Cognitive control signals for neural prosthetics. Science 305:258-262.

Okada Y (1983) Neurogenesis of evoked magnetic fields. New York: Plenum Press.

Paninski L, Fellows MR, Hatsopoulos NG, Donoghue JP (2004) Spatiotemporal

tuning of motor cortical neurons for hand position and velocity. Journal of Neurophysiology 91:515-532.

Parra LC, Spence CD, Gerson AD, Sajda P (2005) Recipes for the linear analysis of EEG. Neuroimage 28:326-341.

Pascual-Marqui R (1999) Review of methods for solving the EEG inverse problem. International Journal of Bioelectromagnetism 1:75-86.

Paxinos G, Mai J (2004) The human nervous system: Elsevier Academic Press.

Pelli D (1997) The VideoToolbox software for visual psychophysics: Transforming numbers into movies. Spatial Vision:437-442.

Picard N, Strick PL (1996) Motor areas of the medial wall: a review of their location and functional activation. Cerebral Cortex 6:342-353.

Picard N, Strick PL (2001) Imaging the premotor areas. Current Opinion in Neurobiology 11:663-672.

Pistohl T, Ball T, Schulze-Bonhage A, Aertsen A, Mehring C (2008) Prediction of arm movement trajectories from ECoG-recordings in humans. Journal of Neuroscience Methods:105-114.

Ranson SW (1920) Anatomy of the Nervous System: WB Saunders.

Santucci DM, Kralik JD, Lebedev MA, Nicolelis MA (2005) Frontal and parietal cortical ensembles predict single-trial muscle activity during reaching movements in primates. European Journal of Neuroscience 22:1529-1540.

Sato M (2001) Online model selection based on the variational bayes. Neural Computation:1649-1681.

Schalk G, Kubánek J, Miller KJ, Anderson NR, Leuthardt EC, Ojemann JG, Limbrick D, Moran D, Gerhardt LA, Wolpaw JR (2007) Decoding two-dimensional movement trajectories using electrocorticographic signals in humans. Journal of Neural Engineering 4:264-275.

Scherg M (1990) Fundamentals of dipole source potential analysis. Advances in Audiology 6:40-69.

Schmidt EM, McIntosh JS, Durelli L, Bak MJ (1978) Fine control of operantly conditioned firing patterns of cortical neurons. Experimental Neurology 61:349-369.

Schwartz AB, Cui XT, Weber DJ, Moran DW (2006) Brain-controlled interfaces: movement restoration with neural prosthetics. Neuron 52:205-220.

Sekihara K, Hild KE, Nagarajan SS (2006) A novel adaptive beamformer for MEG source reconstruction effective when large background brain activities exist. Ieee Transactions on Biomedical Engineering 53:1755-1764.

Sekihara K, Nagarajan S, Poeppel D, Miyashita Y (2001) Reconstructing spatio-temporal activities of neural sources from magnetoencephalographic data using a vector beamformer. In: Acoustics, Speech, and Signal Processing, pp 2021-2024: IEEE.

Serruya M, Donoghue J Design principles of a neuromotor prosthetic device. Neuroprosthetics: Theory and Practice:1158-1196.

Serruya MD, Hatsopoulos NG, Paninski L, Fellows MR, Donoghue JP (2002) Instant neural control of a movement signal. Nature 416:141-142.

Sitaram R, Caria A, Veit R, Gaber T, Rota G, Kuebler A, Birbaumer N (2007) FMRI brain-computer interface: a tool for neuroscientific research and treatment. Computational Intelligence and Neuroscience:25487.

Spencer KM, Dien J, Donchin E (2001) Spatiotemporal analysis of the late ERP responses to deviant stimuli. Psychophysiology 38:343-358.

Stanley GB, Li FF, Dan Y (1999) Reconstruction of natural scenes from ensemble responses in the lateral geniculate nucleus. Journal of Neuroscience 19:8036-8042.

Taheri BA, Knight RT, Smith RL (1994) A dry electrode for EEG recording. Electroencephalography and Clinical Neurophysiology 90:376-383.

Taulu S (2008) Processing of Weak Magnetic Multichannel Signals: The Signal Space Separation Method. In: Faculty of Information and Natural Sciences, p 23. Espoo, Finland: Helsinki University of Technology.

Taulu S, Kajola M (2005) Presentation of electromagnetic multichannel data: The signal space separation method. Journal of Applied Physics 97:124905-124910.

Taulu S, Simola J (2006) Spatiotemporal signal space separation method for rejecting nearby interference in MEG measurements. Physics in Medicine and Biology 51:1759-1768.

Taulu S, Kajola M (2009) Presentation of electromagnetic multichannel data: The signal space separation method. Journal of Applied Physics 97:124905.

Taulu S, Simola J, Kajola M (2005) Applications of the signal space separation method. Ieee Transactions on Signal Processing 53:3359-3372.

Taylor DM, Tillery SI, Schwartz AB (2002) Direct cortical control of 3D neuroprosthetic devices. Science 296:1829-1832.

Tesche CD, Uusitalo MA, Ilmoniemi RJ, Huotilainen M, Kajola M, Salonen O (1995) Signal-space projections of MEG data characterize both distributed and well-localized neuronal sources. Electroencephalography and Clinical Neurophysiology 95:189-200.

Toda A, Imamizu H, Kawato M, Sato MA (2011) Reconstruction of two-dimensional movement trajectories from selected magnetoencephalography cortical currents by combined sparse Bayesian methods. Neuroimage 54:892-905.

Todorov E (2000) Direct cortical control of muscle activation in voluntary arm movements: a model. Nature Neuroscience 3:391-398.

Uusitalo MA, Ilmoniemi RJ (1997) Signal-space projection method for separating MEG or EEG into components. Medical & Biological Engineering & Computing 35:135-140.

Van Veen BD, van Drongelen W, Yuchtman M, Suzuki A (1997) Localization of brain electrical activity via linearly constrained minimum variance spatial filtering. IEEE Transactions on Biomedical Engineering 44:867-880.

Vidal JJ (1973) Toward direct brain-computer communication. Annual Review of Biophysics & Bioengineering 2:157-180.

Vidal JJ (1977) Real-time detection of brain events in EEG. Proceedings of the Ieee:633-641.

Vigário R, Jousmäki V, Hämäläinen M, Hari R, Oja E, Oja E (1998) Independent component analysis for identification of artifacts in magnetoencephalographic recordings. In, p 229: The MIT Press.

Volegov P, Matlachov A, Mosher J, Espy MA, Kraus RH (2004) Noise-free magnetoencephalography recordings of brain function. Physics in Medicine & Biology 49:2117-2128.

Vrba J, Robinson SE (2001) Signal processing in magnetoencephalography. Methods 25:249-271.

Waldert S, Preissl H, Demandt E, Braun C, Birbaumer N, Aertsen A, Mehring C (2008) Hand movement direction decoded from MEG and EEG. Journal of Neuroscience 28:1000-1008.

Wessberg J, Stambaugh CR, Kralik JD, Beck PD, Laubach M, Chapin JK, Kim J, Biggs SJ, Srinivasan MA, Nicolelis MA (2000) Real-time prediction of hand trajectory by ensembles of cortical neurons in primates. Nature 408:361-365.

Wolpaw JR, Mcfarland DJ (1994) Multichannel EEG-based brain-computer communication. Electroencephalography and Clinical Neurophysiology:444-449.

Wolpaw JR, McFarland DJ (2004) Control of a two-dimensional movement signal by a noninvasive brain-computer interface in humans. Proceedings of the National Academy of Sciences of the United States of America 101:17849-17854.

Wolpaw JR, McFarland DJ, Vaughan TM, Schalk G (2003) The Wadsworth Center brain-computer interface (BCI) research and revelopment program. Ieee Transactions on Neural Systems and Rehabilitation Engineering:204-207.

Wolpaw JR, Birbaumer N, McFarland DJ, Pfurtscheller G, Vaughan TM (2002) Brain-computer interfaces for communication and control. Clinical Neurophysiology 113:767-791.

Yuan H, Perdoni C, He B (2010) Relationship between speed and EEG activity during imagined and executed hand movements. Journal of Neural Engineering 7:26001.

Zimmerma.Je, Thiene P, Harding JT (1970) Design and Operation of Stable rf - Biased Superconducting Point - Contact Quantum Devices, and a Note on the Properties of Perfectly Clean Metal Contacts. Journal of Applied Physics 41:1572-1580.